

**BOND STRENGTH AND ANISOTROPIC PERFORMANCE
OF CONSTRUCTION AND DEMOLITION WASTE-BASED
GEOPOLYMER AND CEMENTITIOUS COMPOSITES FOR
3D ADDITIVE MANUFACTURING**

**ÜÇ BOYUTLU EKLEMELİ İMALATA UYGUN İNŞAAT VE
YIKINTI ATIKLARI İÇEREN JEOPOLİMER VE ÇİMENTO
BAĞLAYICILI KOMPOZİTLERİN BAĞ DAYANIMI VE
ANİZOTROPİK ÖZELLİKLERİ**

HAMZA ÖZKILIÇ

PROF. DR. MUSTAFA ŞAHMARAN

Supervisor

Submitted to
Graduate School of Science and Engineering of Hacettepe University
as a Partial Fulfillment to the Requirements
for be Award of the Degree of **Doctor of Philosophy**
in Civil Engineering

2024

ABSTRACT

BOND STRENGTH AND ANISOTROPIC PERFORMANCE OF CONSTRUCTION AND DEMOLITION WASTE-BASED GEPOLYMER AND CEMENTITIOUS COMPOSITES FOR 3D ADDITIVE MANUFACTURING

Hamza ÖZKILIÇ

Doctor of Philosophy, Department of Civil Engineering

Supervisor: Prof. Dr. Mustafa ŞAHMARAN

January 2024, 129 pages

The construction industry has immense economic, technological and environmental influence worldwide. Within this sector, conventional concrete relies heavily on Portland cement (PC) as its primary binder, leading to a surge in global PC consumption. Heightened awareness of the carbon footprint linked to cement usage has spurred substantial research into alternative binding systems like geopolymers. The recent growth in the construction sector has generated a substantial upsurge in construction and demolition waste (CDW), imposing a notable environmental burden. Besides technology and material-oriented research, operational advancements are also emerging. Notably, three-dimensional additive manufacturing (3D-AM) offers various advantages, including reduced labor costs, mold-free production and the ability to create non-standard geometric products. This thesis centers on assessing operational and material-related factors, aiming to integrate innovative, environmentally friendly construction materials derived from CDW into 3D-AM for sustainable construction. In this context, this study is planned to address a literature gap concerning anisotropy, printing time intervals, material aging and manufacturing methodologies' influence on 3D-printed structures' mechanical performance. It

simultaneously conducts several tests to comprehensively evaluate the mechanical performance of printed cementitious systems under diverse conditions. Initially, the study evaluates anisotropy in samples produced at different time intervals using two different mixtures through compression tests conducted from various directions. Subsequently, it assesses bond strength changes via triplet shear and direct tensile tests on samples produced at different time intervals. Lastly, the study observes the effect of varying material ages on strength using diagonal tension and triplet shear tests. The study's findings are anticipated to make a substantial contribution to current technology by offering comprehensive insights into the impact of operational and material-related parameters on the mechanical performance of printed structures.

Keywords: Additive manufacturing, geopolymer, construction and demolition waste, anisotropy, bond strength, printing time interval, material aging time.

ÖZET

ÜÇ BOYUTLU EKLEMELİ İMALATA UYGUN İNŞAAT VE YIKINTI ATIKLARI İÇEREN JEOPOLİMER VE ÇİMENTO BAĞLAYICILI KOMPOZİTLERİN BAĞ DAYANIMI VE ANİZOTROPİK ÖZELLİKLERİ

Hamza ÖZKILIÇ

Doktora, İnşaat Mühendisliği Bölümü

Tez Danışmanı: Prof. Dr. Mustafa ŞAHMARAN

Ocak 2024, 129 sayfa

İnşaat sektörünün küresel olarak muazzam bir ekonomik, teknolojik ve çevresel etkisi vardır. Sektörün en önemli parametrelerinden biri olan geleneksel betonda, temel bağlayıcı olarak global ölçekte tüketimi hızla artan Portland çimentosu (PÇ) kullanılmaktadır. Çimento kullanımına bağlı olarak karbon ayak izinin daha iyi anlaşılması, son yıllarda jeopolimerler gibi alternatif bağlayıcı sistemleri üzerine kapsamlı araştırmaların yapılmasına yol açmıştır. Son yıllarda inşaat sektöründe meydana gelen hızlı büyüme ise üretilen inşaat ve yıkıntı atıklarında (İYA) muazzam bir artışa neden olarak çevre üzerinde önemli bir yük oluşmasına neden olmuştur. Bunun yanında gelişen teknoloji ile malzeme ile ilgili yapılan araştırmalara ek olarak operasyonel olarak da gelişmeler meydana gelmektedir. Bu minvalde üç boyutlu eklemeli imalat (3B-Eİ) yöntemi ile işçilik maliyetin azalması, kalıpsız üretim yapılması, geometrik olarak standart dışı ürünlerin de elde edilebilmesi gibi birçok avantaj söz konusu olabilmektedir. Bu çalışma ile, inşaat ve yıkım çalışmaları sonucu elde edilen atık malzemeler kullanılarak geliştirilen yenilikçi, alternatif, ekolojik yapı malzemelerinin sürdürülebilirlik çerçevesinde 3B-Eİ ile birleştirilebilmesi için operasyonel ve malzeme

odaklı parametrelerin etkisi üzerine odaklanılmıştır. Bu bağlamda literatürde anizotropinin, baskı zaman aralıklarının, malzeme yaşlanması ve üretim metodolojisinin 3D baskılı yapıların mekanik performansı üzerindeki etkisine ilişkin çalışmaların eksikliği göz önüne alındığında, bu çalışma planlanmıştır. Bu çalışma, baskılı çimentolu sistemlerin çeşitli koşullar altında mekanik performansını değerlendirmek için çeşitli testlerin aynı anda gerçekleştirilmesi bakımından yenidir. Bu kapsamda öncelikle iki farklı karışım kullanılarak farklı zaman aralıklı olarak üretilen numunelerin farklı yönlerden yükleme yapılmak suretiyle basınç testi uygulanarak anizotropi performansı değerlendirilmiştir. Sonrasında, yine farklı zaman aralıklı olarak üretilen numunelerin üçlü kesme ve doğrudan çekme testi ile bağ dayanımı değişimi tespit edilmiştir. Son olarak diyagonal çekme ve üçlü kesme testi ile farklı malzeme yaşlarının dayanıma etkisi gözlenmiştir. Bu çalışmanın bulgularının, operasyonel ve malzeme odaklı parametrelerin baskılı yapıların mekanik performansı üzerindeki etkisi hakkında kapsamlı bilgiler sağladığı için mevcut teknolojiye önemli bir katkı sağlayacağına inanılmaktadır.

Anahtar Kelimeler: Eklemeli imalat, jeopolimer, inşaat ve yıkıntı atığı, anizotropi, bağ dayanımı, baskı zaman aralığı, malzeme yaşlanma süresi.

ACKNOWLEDGEMENT

Foremost, I would like to extend my sincere gratitude to my supervisor, Mustafa ŞAHMARAN, for his invaluable guidance and unwavering support throughout this endeavor. He provided consistent support during my thesis, sharing his extensive experience and knowledge. It has been an honor to be his student.

Also, I would like to express my gratitude to Prof. Dr. İsmail Özgür YAMAN, Prof. Dr. İlhami DEMİR, Assoc. Prof. Dr. Gürkan YILDIRIM and Assoc. Prof. Dr. Mustafa Kerem KOÇKAR for their participation as members of my thesis jury.

I extend my heartfelt appreciation to all members of the Hacettepe University Advanced Concrete Research Laboratory for their unwavering support. Special thanks go to my friends Hüseyin İLCAN and Ehsan AMINIPOUR for their invaluable contributions.

Finally, I would like to thank my parents for their boundless support, encouragement and enduring love.

HAMZA ÖZKILIÇ

January 2024, Ankara

TABLE OF CONTENTS

ABSTRACT	i
ÖZET	iii
ACKNOWLEDGEMENT	v
TABLE OF CONTENTS	vi
LIST OF FIGURES	viii
LIST OF TABLES	xi
SYMBOLS AND ABBREVIATIONS	xii
1. INTRODUCTION	1
1.1. Problem Definition	1
1.2. Scope and Objectives	4
1.3. Thesis Outline	4
2. LITERATURE REVIEW	6
2.1. 3D Technology	6
2.1.1. 3D Concrete Printing	6
2.1.2. Effect of 3D-Printing on Strength	12
2.2. Geopolymers	23
2.3. Interlayer Bond Strength	47
2.3.1. Macroscale Characterization	47
2.3.2. Microscale Characterization	48
3. EXPERIMENTAL PROGRAM	51
3.1. WPC-Based Mixture	51
3.1.1. Materials	51
3.1.2. Mixture Proportion and Preparation	52
3.2. CDW-Based Geopolymer Mixture	54
3.2.1. Materials	54
3.2.2. Mixture Proportion and Preparation	60
3.3. Specimen Preparation	61
3.4. Testing Methods	66
3.4.1. Compression Test	66
3.4.2. Direct Tensile Test	68

3.4.3. Triplet Shear Test	70
3.4.4. Diagonal Tension Test.....	73
4. RESULTS AND DISCUSSIONS	77
4.1. WPC-Based Mixture	77
4.1.1. Compressive Strength.....	77
4.1.2. Bond Strength.....	80
4.1.3. Manufacturing Methodology	85
4.2. CDW-Based Geopolymer Mixture.....	87
4.2.1. Compressive Strength.....	87
4.2.2. Bond Strength.....	90
4.2.3. Manufacturing Methodology	97
4.2.4. Correlation in Test Results	100
4.3. Comparison of Cementitious Composites and CDW-Based Geopolymer.....	102
5. CONCLUSION	109
6. REFERENCES	112
APPENDIX	127
Thesis Originality Report	127
CURRICULUM VITAE	128

LIST OF FIGURES

Figure 2.1.	Latest instances of sizable 3D-AM constructions (Robayo-Salazar et al., 2023)	8
Figure 2.2.	Approach for developing and enhancing cementitious material for 3D printing (redrawn after Robayo-Salazar et al., 2023).....	11
Figure 2.3.	Loading directions for a 3D-printed layers and filaments.	14
Figure 2.4.	Formation of polymeric Si-O-Al-O bonds (Chanh et al., 2008).....	24
Figure 3.1.	Pan-type mixer (a) and pump (b) used in the study.	54
Figure 3.2.	Jaw crusher (a) and ball mills machines (b) used in the study.....	55
Figure 3.3.	Digital and SEM images of the precursors.	56
Figure 3.4.	Particle size distribution of the precursors.	57
Figure 3.5.	Images of RCA (a), powder Ca(OH) ₂ (b) and flaked NaOH (c).	59
Figure 3.6.	Detailed parts of 3D printer (a) and schematic depiction of samples printed in 3D (b).....	62
Figure 3.7.	Real time view of printed samples for different tests (a,b,c,d) and mold-cast samples (e).	64
Figure 3.8.	The freshly printed mixtures and subsequently extracted specimens	66
Figure 3.9.	Schematic depiction of printing time intervals (a), printing directions (b), compressive strength loading details (c) and representative images from experiments (d).....	67
Figure 3.10.	Compressive strength test machine	68
Figure 3.11.	Displacement controlled test machine	69
Figure 3.12.	Schematic depiction of T-shaped (a) and single-hole metal plates (b).....	69
Figure 3.13.	Schematic depiction of direct tensile test (a) and representative images from experiments (b).....	70
Figure 3.14.	Schematic depiction of WPC- and CDW-based specimens printed at different time intervals (a), WPC-based specimens printed at different aging time (b) and CDW-based jeopolymer specimens printed at different aging time (c)	71
Figure 3.15.	Schematic depiction of triplet shear test (a) and representative images from experiments (b,c,d,e).....	73

Figure 3.16. Schematic depiction of WPC- and CDW-based geopolymers printed at different aging times..	74
Figure 3.17. Schematic depiction and image of steel head (a), diagonal tension test (b), preparation of samples (c,d) and testing different samples (e,f,g,h)..	76
Figure 4.1. Loading directions (a) and the results of the compressive strength tests carried out on cementitious specimens printed vertically (b).	79
Figure 4.2. Bond strength of vertical-printed WPC mixtures with varied printing time intervals (VP: Vertical-printed specimen).	81
Figure 4.3. The images depict various aspects of a freshly 3D-printed specimen at the 0-min, including: The progression of crack propagation (a), fragments resulting from the cracks (b) and processed representations of the cracked surface (c).	82
Figure 4.4. The images depict various aspects of a 3D-printed 60-min aged specimen, including: The progression of crack propagation (a), fragments resulting from the cracks (b) and processed representations of the cracked surface (c).	83
Figure 4.5. Average diagonal tension tension and triplet shear test results of white-cemented mortars (HP: Horizontal-printed specimen, VP: Vertical-printed specimen).	85
Figure 4.6. The view of cast (a), vertical- (b) and horizontal-printed (c) specimens under diagonal tension test.	87
Figure 4.7. Compressive strength outcomes of vertical-printed geopolymer mortars with varied printing time intervals and loading directions.	90
Figure 4.8. Bond strength results of vertical-printed geopolymer mortars with varied printing time intervals.	92
Figure 4.9. Representative images showing details of failure modes on specimen of diagonal tension (a,b), triplet shear (c,d) and direct tensile test (e,f).	94
Figure 4.10. Average diagonal tension tension and triplet shear test results of geopolymer mortars (HP: Horizontal-printed specimen, VP: Vertical-printed specimen).	95
Figure 4.11. Representative load-displacement curves for manufacturing methodologies (a) and the view of cast (b), vertical- (c) and horizontal-printed (d) specimens under diagonal tension test .	99

Figure 4.12. Correlation bw compressive strength in different directions and bond strength obtained from both triplet shear and direct tensile test with varied intervals (a) and linear regression results of bond strength and triplet and diagonal tension tests (b) (TS: Triplet Shear, DT:Diagonal Tension)...	101
Figure 4.13. Graphical interpretation of compressive strength test results	104
Figure 4.14. Graphical interpretation of direct tensile and triplet shear test results.....	105
Figure 4.15. Graphical interpretation of diagonal tension and triplet shear test results	108

LIST OF TABLES

Table 2.1. The evaluations of the environmental footprint for manufacturing 1 m ³ PC 32.5 and the innovative CDW-based geopolymer binder (Mir et al., 2022a).	45
Table 3.1. Details regarding to the binder phase.	51
Table 3.2. Admixtures used in this study and their details.	52
Table 3.3. Mixture proportion of WPC-based 3D-printed object.	53
Table 3.4. Composition and density characteristics of CDW-derived source materials.	55
Table 3.5. Detailed informations about Ca(OH) ₂ and NaOH used in this study	59
Table 3.6. Details of geopolymer mortar mixture.	60
Table 4.1. Comparison of compression test results.	103
Table 4.2. Comparison of direct tensile and tripler shear test results (VP: Vertical-printed specimen).	105
Table 4.3. Comparison of diagonal tension and triplet shear test results (HP: Horizontal-printed specimen, VP: Vertical-printed specimen).	107

SYMBOLS AND ABBREVIATIONS

Symbols

°C	Centigrade Degree
%	Percent
Å	Ångström
D	Layer Height-Diameter Ratio
g	Gram
µm	Micrometer
mm	Milimeter
cm	Centimeter
min	Minute(s)
kV	Kilovolt
l	Liter
M	Molarity
D _{max}	Maximum Particle Size
CEM	Cement
MPa	Megapascal
Al	Aluminium
Si	Silicon
Ca	Calcium
OH	Hydroxide
CO ₂	Carbon Dioxide
NaOH	Sodium Hydroxide
KOH	Potassium Hydroxide
Ca(OH) ₂	Calcium Hydroxide
Na ₂ SiO ₃	Sodium Silicate
K ₂ SiO ₃	Potassium Silicate
SiO ₂	Silicon Dioxide
Al ₂ O ₃	Aluminium Oxide
Na ₂ O	Sodium Oxide
C ₆ H ₈ O ₇	Citric Acid

Na_2SO_4	Sodium Sulfate
CaO	Calcium Oxide
Na_2CO_3	Sodium Carbonate
CaCO_3	Calcium Carbonate
NaCl	Sodium Chloride
Fe_2O_3	Ferric Oxide
MgO	Magnesium Oxide
SO_3	Sulfur Trioxide
K_2O	Potassium Oxide
TiO_2	Titanium Dioxide
P_2O_5	Diphosphorus Pentoxide
Cr_2O_3	Chromium (III) Oxide
Mn_2O_3	Trimanganese Trioxide
F_{voi}	Tripler Shear Strength
$F_{\text{i,max}}$	Maximum Shear Load
P_{ult}	Ultimate Load
f_t	Diagonal Tension Strength
p-value	Statistical Measurement Used to Validate a Hypothesis Against Observed Data
R^2	Coefficient of Determination,
$f_{\text{ct,corrected}}$	Direct Tensile Strength at the Chosen Printing Time Interval
C_1	Coefficient for the Direct Tensile Strength Loss Due to Chosen Printing Time Interval
C_2	Coefficient for the Shear Strength Loss due to Chosen Printing Time Interval
τ_{0,t_0}	Direct Tensile Strength at 0-min Batch of Geopolymer

Abbreviations

PC	Portland Cement
CDW	Construction and Demolition Wastes
USA	United States of America

EU-18	European Union Countries
3D	Three-Dimensional
AM	Additive Manufacturing
3D-AM	Three-Dimensional Additive Manufacturing
WPC	White Portland Cement
3D-CP	Three-Dimensional Concrete Printing
ASTM	American Society for Testing Materials
2D	Two-Dimensional
et al.	Et Alia
etc.	Et Cetera
CAD	Computer Aided Design
e.g.	Exempli Gratia
w/c	Water-to-Cement Ratio
w/s	Water-to-Solid Ratio
mm/s	Milimeter per Second
cm/s	Centimeter per Second
b/s	Binder-to-Sand Ratio
w/b	Water-to-Binder Ratio
a/b	Aggregate-to-Binder Ratio
kN/s	Kilonewton per Second
N/s	Newton per Second
XCT	X-ray Computed Tomography
C-S-H	Calcium-Silicate-Hydrate
MIP	Mercury Intrusion Porosimetry
SEM	Scanning Electron Microscopy
GGBFS	Ground Granulated Blast Furnace Slag
FA	Fly Ash
RHA	Rice Husk Ash
SF	Silica Fume
PVA	Polyvinyl Alcohol
N-A-S-H	Sodium-Alumino-Silicate-Hydrate
SEM	Scanning Electron Microscope
XRD	X-ray Diffraction

EDX	Energy-dispersive X-ray
3ITT	Three Interval Thixotropy Test
eq	equivalent
CFC	Chlorofluorocarbon
CTUe	Comparative Toxic Units for Effects on Human Health
EDS	Energy Dispersive Spectrometer
HB	Hollow Brick
RCB	Red Clay Brick
RT	Roof Tile
G	Glass
C	Concrete
LVDT	Linear Variable Differential Transformer
EN	European Norm
QS	Quartz Sand
SP	Superplasticizer
VM	Viscosity Modifier
R	Retarder
SR	Shrinkage Reducer
W	Water
h	Height
A	Area
w_{av}	Average Width
BFS	Blast Furnace Slag
XRF	X-ray Fluorescence
PSD	Particle Size Distribution
RCA	Recycled Concrete Aggregate
TSI	Turkish Standard Institute
C-A-S-H	Calcium-Aluminate-Silicate-Hydrate
HP	Horizontal-Printed
VP	Vertical-Printed

1. INTRODUCTION

1.1. Problem Definition

Concrete stands as the predominant construction material, prized for its affordability, dependability, adaptability and straightforward application. Its annual consumption surpasses 30 billion tons, exceeding the per capita production of any other material (Monteiro, Miller and Horvath, 2017). While concrete is a ubiquitous building material, it presents significant obstacles. Portland Cement (PC), the main binding agent in conventional concrete plays a significant role in environmental concerns, primarily due to its energy-intensive production and resulting greenhouse gas emissions (Sabir, Wild and Bai, 2001). To manufacture a ton of cement, nearly 1.5 tons of primary substances are necessary, leading to the direct emission of 0.55 tons of carbon dioxide (CO₂). Additionally, fuel burning contributes around 0.4 tons of CO₂, resulting in a total emission of 0.8-1 tons of CO₂ (Wei and Cen, 2019). As per Madloul et al. (2011), the cement sector is associated with substantial consumption of fossil fuels, accounting for roughly 12-15% of industrial energy. On a global scale, the production of PC is approximated to produce almost 1.35 billion tons of atmospheric pollutants annually, constituting 6-9% of total atmospheric pollutants releases worldwide. This is primarily attributed to decarbonization of limestone, fuel burning in the kiln and power usage. Estimates that annual PC production will increase by 50% by 2050 increase the severity of the situation (Monteiro, Miller and Horvath, 2017). Moreover, concrete production further impacts the environment by necessitating the consumption of natural resources like clean water, aggregates of various sizes, clay, limestone and gypsum (Cachim, Velosa and Ferraz, 2013). The World Green Building Council (2020) has released recommendations and principles for designing eco-friendly structures and infrastructures. These suggestions involve employing alternative fuels, capturing CO₂, enhancing kiln energy efficiency, incorporating nanoparticles instead of cement and advancing technologies for green concrete products.

Conventional concrete does not last long because of its fragility, which gives rise to a high cracking propensity and increases durability issues. Inadequate durability performance of conventional concrete often results in costly repairs and/or maintenance practices (Şahmaran et al., 2015) and even fulfill destruction and rebuilding of structures, thus generating great quantity of construction and demolition wastes (CDW). Because of surge in worldwide

populace, there has been a rise in civil engineering projects, resulting in a tremendous amount of CDW being produced (Baniyas et al., 2010; Nagapan, Abdul Rahman and Asmi, 2012; Wu, Yu and Shen, 2019). The CDW is recognized as significant contributors to the global generation of solid waste (Wu et al., 2019). The amount of generated CDW was recorded as approximately 10 billion tons annually worldwide and is expected to increase gradually in further years (Wu et al., 2019). Three billion of this is supplied by China (Zheng, et al., 2017), while more than 700 and 800 million tons are produced by the United States of America (USA) and the European Union countries (EU-28) (Wu et al., 2019). In China, the yearly increase in CDW generation is predicted to be billions in the coming years (AECOM, 2018).

The wastes of the buildings destroyed after the disasters are also an important problem that needs to be solved. For example, after the 2 earthquakes that occurred in Kahramanmaraş-Türkiye on February 6, 2023, according to the damage assessments in 11 provinces affected by the earthquakes, a total of 272860 buildings and 817548 independent sections were determined as moderately damaged, heavily damaged, demolished and urgently demolished (Kahramanmaraş and Hatay Earthquake's Report, 2023). These earthquakes and the subsequent destruction necessitate the completion of the urban transformation activities carried out throughout the Türkiye, especially in İstanbul, as soon as possible. The instances underscore the gravity of the CDW issue globally.

The rise in the amount of generated CDW has serious results, such as increases in unregulated waste disposal sites, soil contamination and economic challenges (Duan et al., 2019). To address these challenges, researchers are increasingly favoring the recycling of CDW to develop eco-friendly building materials, thereby reducing reliance on natural resources (McKelvey et al., 2002; Mustafa et al., 2011). The outcome of these endeavors resulted in the high-value-added valorization of CDW-based materials in a new category of binding agents known as geopolymers, which have proven to be promising alternatives to PC-based systems (Allahverdi and Kani, 2009; Torres-Carrasco and Puertas, 2015; Vafaei and Allahverdi, 2017b), in addition to the valorization of those wastes as filler materials in low-tech applications.

Regarding the various crucial aspects of the construction industry, such as faster construction speed, adaptable design and efficient use of materials and energy, the existing technologies have reached their maximum potential. To surpass these limits, it is anticipated that automation will provide a significant improvement. In recent years, a significant and pioneering development in integrating automated technology into the construction sector has been the adoption of three-dimensional additive manufacturing (3D-AM) systems for the built environment. In the current scenario, where construction firms are seeking novel methods to enhance performance and lower costs in building projects, 3D-AM can offer many environmental and economic advantages in proportion to conventional manufacturing methodologies (Bos et al., 2016). The primary advantages that the 3D-AM technique can offer include minimizing errors related to production, reducing production time, decreasing risks associated with occupational safety and lowering costs (Maskuriy et al., 2019). To elaborate further, 3D-AM has a notable edge over traditional techniques in terms of reducing formwork expenses, which typically account for around 35% of the overall construction costs (Lloret et al., 2015). The use of 3D-AM not only has the potency to substantially lessen the environmental trace linked to conventional building techniques, but it also offers the notable advantage of minimizing post-production waste through a production process that optimizes material consumption and ensures proper management of construction waste (Biernacki et al., 2017; Mohammad, Masad and Al-Ghamdi, 2020). Considering all these benefits, the integration of 3D-AM technology into the construction industry can have a pivotal impact on shaping the changing landscape of our world (Beersaerts, Lucas and Pontikes, 2020).

The primary drawback of 3D-AM lies in the bond strength between layers, attributed to its layered structure. In this context, it is of great importance to determine the physical properties of materials by using different test methods for the impact of various parameters on bond strength. In this regard, it will be innovative for the literature to be able to measure the samples printed in accordance with the standards for each test with diagonal tension and triplet shear tests used specifically for masonry structures, since the layered structure has similar properties to masonry structures.

1.2. Scope and Objectives

This thesis seeks to make a contribution to the widespread use of CDW-based geopolymer materials as a feasible option to PC/concrete production, which requires energy-intensive production, consumes natural resources and harms the environment. In this context;

- Direction dependent compressive strengths of the samples produced as 2 layers with 4 various time intervals (0, 15, 30 and 60-min) were determined and anisotropic behavior was investigated.
- Samples produced in 4 different printing time intervals (0, 15, 30 and 60-min) and 4 different material aging time (0, 30, 60-min and for CDW-based geopolymer also 120-min); bond strengths were calculated by using the direct tensile test, triplet shear test and diagonal tension test.
- The influence of printing direction on bond strength (manufacturing methodology) was determined by subjecting specimens printed in accordance with diagonal tension (11 layers vertically, 6 filaments horizontally) and triplet shear test (3 layers vertically, 3 filaments horizontally) standards to the respective tests.
- The experiments were carried out using both white Portland cement- (WPC) based mixture and CDW-based geopolymer composites. Subsequently, the performance of the two mixtures was assessed.

1.3. Thesis Outline

This study includes five major parts as outlined in the following.

In the "Introduction" part, the thesis outlines the primary issues addressed, elucidates the goals, scope and objectives, and provides a general overview of the activities conducted within the study.

The 2nd chapter, "Literature Review", initially provides information about three-dimensional (3D) printing technology and its application in concrete production. Subsequently, it offers a comprehensive summary that encompasses not only the observation of cemented mixture

usage but also the exploration of waste material geopolymerization and its integration into 3D-AM technology. Both of the summarized studies involving mixtures of cement and CDW-based geopolymer provide an overview of anisotropic behavior, discuss factors influencing bond strength and delve into the methods used for bond strength testing.

In the 3rd chapter named “Experimental Program”, the mixture contents, preparation process of the mixtures, sample production stages regarding the WPC- and CDW-based geopolymer mixtures, respectively, are explained and information is given about the diverse testing methodologies employed to assess the mechanical characteristics of the mixtures.

In the 4th chapter named “Results and Discussion”, the experimental results of the studies are outlined and potential interpretations for the noted outcomes are discussed. In this part, firstly, the directional strength values of the samples produced with different time intervals were compared; then, the effects of printing time interval, material aging time and manufacturing methodology on bond strength were investigated. In addition to evaluating the same parameters and conducting identical experiments for both mixtures, specific additional investigations were undertaken for each individual mixture. The findings were discussed in detail and the results obtained using mixtures were compared.

In the 5th chapter called "Conclusion", a concise summary of the thesis study and outcomes from the experiments carried out in the studies is provided. The crucial findings of thesis study were highlighted.

2. LITERATURE REVIEW

2.1. 3D Technology

Today, many industrial sectors benefit from 3D printing technology to produce customized and complex products because of its broad manufacturing capabilities and the multitude of advantages it offers (Beyer, 2014). The method was initially used for rapid production of prototype products aimed at design and functional validation. The fundamental principles of additive manufacturing find an ideal application in personalized construction practices. Given the diverse local conditions, each building follows a prototype manufacturing approach. Consequently, additive manufacturing in construction brings numerous advantages, including enhanced efficiency, reduced geometric design constraints, personalized design and production, improved quality control in the process and the integration of diverse functionalities in design. It also contributes to resource efficiency in construction, ensuring higher quality and increased safety throughout the construction process (Labonnote et al., 2016; Agusti-Juan et al., 2017). Nevertheless, the seamless integration of additive manufacturing into the building sector encounters difficulties related to the large scale of structures and the transformation of predominantly manual production techniques into fully automated digital processes (Kloft et al., 2020).

2.1.1. 3D Concrete Printing

In the era of the fourth technological revolution, frequently alluded as Industry 4.0, digital construction techniques such as 3D printing were introduced. Since concrete is one of the most used materials, researchers working in this field have also turned to research on concrete production suitable for printing. The construction industry is rapidly turning towards automation in order to reduce costs and increase security measures (Panda, Unluer and Tan, 2019). The 3D Concrete Printing (3D-CP) technology, characterized by its digital and automated construction approach, has garnered increasing attentiveness within the building sector recently (Gosselin et al., 2016; Rahul et al., 2019a). In 3D-CP, also called 3D-AM and defined as "the process of combining materials, usually layer upon layer, to make objects from 3D model data" consistent with the American Society for Testing and Materials (ASTM) standards; 4 methods are applied: extrusion-based, powder-based, d-shape and powder-based new object production (Plessis et al., 2021).

Concrete printing encompasses two prominent techniques: the extrusion-based nozzle printing approach and the powder-based 3D printing method (Arunothayan et al., 2020). In the extrusion-based nozzle printing approach involves the squeezing out of printable cementitious substance using a printing nozzle. The nozzle's movement is guided by a specialized program that translates the 3D model into two-dimensional (2D) slices, creating the 3D object layer by layer (Buswell et al., 2018; Yu, Du and Sanjayan, 2020). Mechanisms developed for extrusion vary as screw type or positive discharge pump (Panda, Paul and Tan, 2017; Papachristoforou, Mitsopoulos and Stefanidou, 2018). On the other hand, the powder-based approach, a stratum of grains is initially distributed over the powder base and a binder is squeezed out from a nozzle onto these particles. Successive layers of particles are added and the bonding occurs through the extruded binder. The 3D structure takes shape by controlling the movement path of the nozzle and reiterating the operation. This technique's advantage lies in the temporary formation of a scaffold with loose particles, facilitating the printing of support structures. Nevertheless, the scalability is constrained due to significant requirements for both unbonded and bonded components.

The most common and straightforward type of 3D-AM is extrusion-based concrete printing. This method relies on additive manufacturing, enabling the production of medium to large-scale buildings. These structures include houses, offices, footbridge and similar constructions (Figure 2.1). The increasing rate at which structures are being produced each day highlights the advancements technology has achieved. Furthermore, some researchers are exploring the design of diverse building components by drawing inspiration from nature, incorporating elements like nacre, bamboo and honeycomb to mimic structures such as beams, columns and slabs (Ye et al., 2021).



Castles Printed in 3D



Castilla La Mancha Bridge Printed in 3D (Madrid, Spain)



3D Printed TECLA Habitat Project (Massa Lombarda, Italy)



3D printed IAAC Pavillion (Barcelona, Spain)



3D-Printed Residence Holds Title for World's Largest (Dubai, United Arab Emirates)



GAIA 3D Printed Housing Project (Shambhala, Italy)



Milestone Project, Urbanization of Houses in 3D (Netherlands)



MARSH Project, NASA's House on Mars Prototype

Figure 2.1. Latest instances of sizable 3D-AM constructions (Robayo-Salazar et al., 2023).

In 1997, Joseph Pegna first proposed an additive manufacturing method based on digital and automated technology to create the 3D architectural structure (Buswell et al., 2007; Vergara et al., 2017). The configurations and contours of 3D-AM structures usually exhibit an organic aesthetic characterized by curves and rounded shapes, deviating from conventional design paradigms. This distinct appearance arises from the layer-by-layer production, which not only adheres to traditional straight lines but also endows 3D printing with a distinctive edge in numerous applications (Plessis et al., 2021). In 2003, Behrokh Khoshnevis developed the concept of Contour Crafting using cementitious materials to create large-scale 3D objects in the field. With this method, also called extrusion-based production, desired objects can be created by using a robot that can move freely in three directions (Kazemian et al., 2017). Subsequent endeavors by researchers have aimed at enhancing this technique across multiple dimensions, encompassing advancements in printing apparatus and substances. In this regard, diverse printing approaches have been the subject of recent scrutiny, such as the cable-suspended robotic contour crafting system (Bosscher et al., 2007), the fixed portal printing system (WASP, 2021) and the robotic arm printing system (Gosselin et al., 2016; Panda, Paul and Tan, 2017). All objects are created as a series of 2D digital images via Computer Aided Design (CAD) software without molds (She et al., 2018). Equipments are tailored for a particular printer, considering precise print configurations like pumping characteristics, flow rate and nozzle type and size, etc. They are not interchangeable elsewhere due to alterations in equipment components or print configuration. Consequently, cementitious materials specific to applications are methodically formulated for extrusion-based 3D-AM.

The advantages of 3D-AM technology compared to traditional construction techniques expressed as; higher efficiency, lower cost, increasing architectural flexibility, enabling more complex designs in terms of structure and aesthetics, reduced reliance on formwork, reduced labor requirement (it is becoming increasingly important for the reduction in workforce due to the aging of the population), lower safety risk, faster construction, advanced technology implementation, reduced potential for errors, improved quality control and increased sustainability with reduced waste by-products (Buswell et al., 2008; Lim et al., 2012; Grampeix, Roussel and Dupoirier, 2013; Labonnote et al., 2016; Agustí-Juan et al., 2017; Sanjayan et al., 2018).

The 3D construction process is estimated to be four times faster than conventional construction methods (Ma, Wang and Ju, 2018; Batikha et al., 2022). This advantage becomes especially significant in situations such as natural disasters (e.g., hurricanes, earthquakes) or armed conflicts. In these scenarios, 3D printing technology can play an important act in rapidly restoring infrastructure and housing that has been impacted (Robayo-Salazar et al., 2023). Weng et al. (2020) conducted a comparative analysis of the productivity, environmental effects and economic costs between a component prefabricated using the traditional ways and the same element produced using 3D printing technology. Their analysis considered factors such as material usage, electricity consumption, labor force and productivity. The findings revealed significant benefits associated with 3D printing technology. There was a notable 25.4% decrease in total costs, an impressive 85% reduction in CO₂ release and a 87.1% decrease in energy consumption when compared to the conventional prefabrication method. Moreover, the use of additive manufacturing technology led to a substantial 48% improvement in overall productivity. Considering these, 3D-AM technology has gained significant attention in the building sector recently (Gosselin et al., 2016; Rahul et al., 2019a). However, for successful implementation of 3D-AM, the mixture utilized must exhibit distinct characteristics. These encompass extrudability, signifying the capacity to be smoothly extruded from the printing nozzle; buildability, indicating the capability to uphold the weight of overlying layers without giving way; open-time, ensuring satisfactory quality throughout the printing process; and interlayer adherence between consecutive layers. Additionally, the printer's size, capacity, robustness and precision must be suitable for the intended structures (Xiao et al., 2020). The flow chart created by Robayo-Salazar et al. (2023) to embody the 3D printing process is presented below (Figure 2.2).

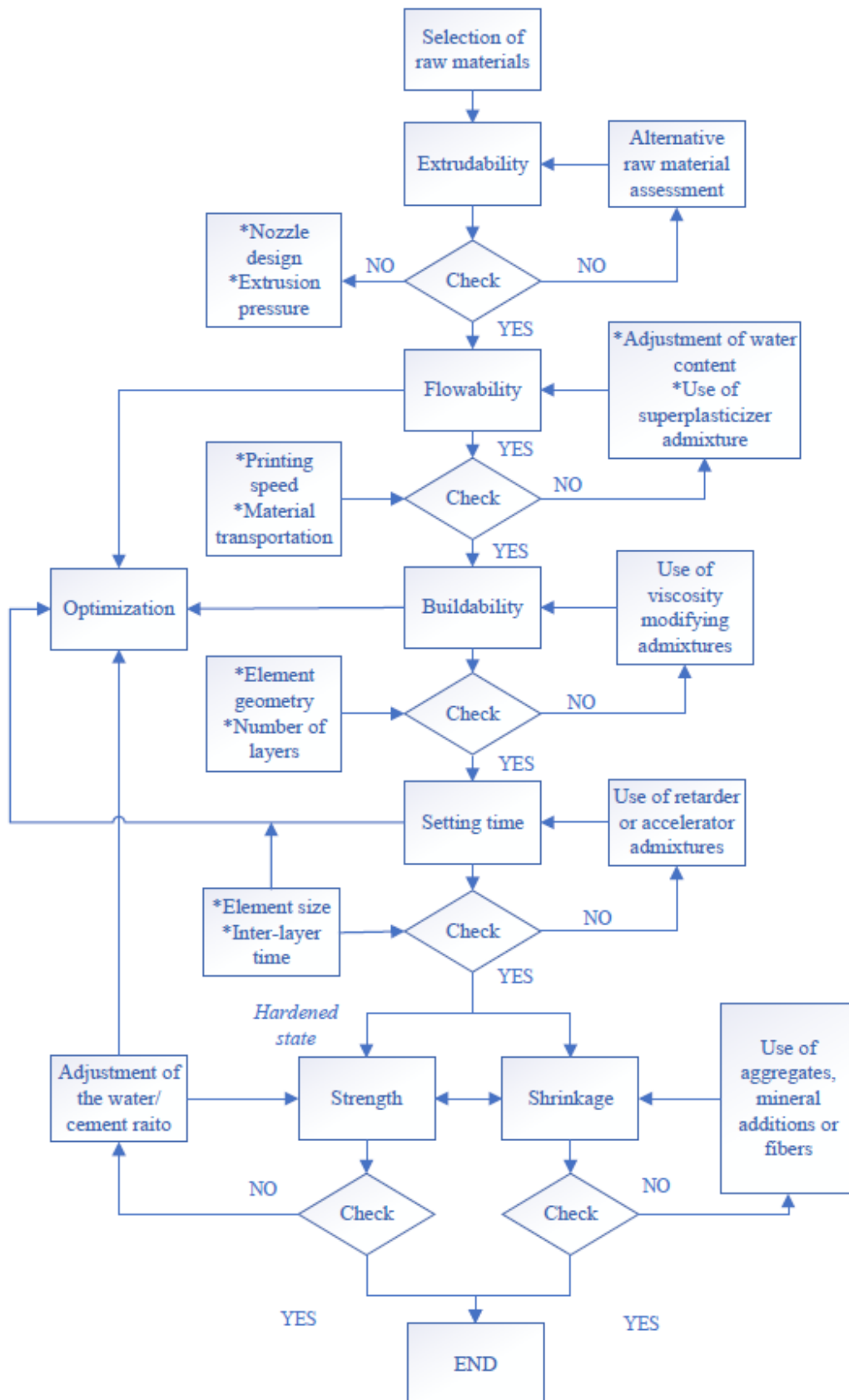


Figure 2.2. Approach for developing and enhancing cementitious material for 3D printing (redrawn after Robayo-Salazar et al., 2023).

2.1.2. Effect of 3D-Printing on Strength

To provide the durability and satisfying strength for the 3D-printed concrete, it is crucial for the layers to have strong connections, avoiding weak "cold joints" at the filament interfaces. The significant challenge in 3D-AM is the distinct anisotropic behavior, wherein the material displays diverse characteristics in distinct aspects. This is a result of the layer-to-layer production, particularly the interlayer bonding, which is less robust than in alternative orientations. This stands in contrast to conventional cast concrete, which usually showcases isotropic behavior. The quality of bonds relies on several factors, including surface roughness, moisture content, the use of interface-modifying materials, fiber type and amount and settings for the 3D printing process like printing speed, printing time interval, layer thickness and nozzle height. These factors can be categorized as indirect and direct. Indirect factors are secondary and can be intentionally adjusted to influence the direct factors, including material composition, surface treatments, printing processes and environmental circumstances. Direct factors directly impact the interfacial bond properties, such as pore structure, bonding area, hydration products and material rheology. Together, these factors form a hierarchical structure that ultimately affects the strength of the interface bonds (Ding, Xiao and Mechtcherine, 2023). Since examining all these factors would greatly expand the size of the thesis, this section presents studies in which researchers focused on determining anisotropic behavior using different types of tests and a review of studies on 3 different factors affecting bond strength (printing time interval, material aging and manufacturing methodology).

This anisotropy and interlayer bonding play a crucial role in determining properties like tensile, flexural and compressive strength, contingent on the orientation of applied loads concerning the print destination (Plessis et al., 2021). Numerous investigations have assessed the compressive strength of 3D-printed cube samples, presenting diverse outcomes compared to traditionally cast samples. The inconsistent strength observed in 3D-printed samples is mainly ascribed to the interfacial bond strength between the stratum. Reports indicate that when subjected to compressive loads, cracks are prone to develop in these weaker interfaces, leading to a diminished strength of the 3D-printed specimens (Nerella, Hempel and Mechtcherine, 2019).

Understanding the behavior under lateral forces of 3D-printed specimen is crucial, especially in pure shear conditions and interface shear characteristics (Wang et al., 2022). The shear strength of interfaces in 3D-printed samples is influenced by cohesion forces at the interface and aggregate clamping on both sides. Various shear test methods, such as single-surface, two-surface, z-shaped, inclined and torsional shear tests, have been implemented to determine interface shear strength (Ding, Xiao and Mechtcherine, 2023). However, there is limited research on determining the interface shear strength of printed materials.

Tensile strength values can vary significantly depending on the manufacturing process. Therefore, when utilizing 3D-AM technology in real constructions, interface matters should be carefully noted and manufacturing operations should be improved to ensure that the mechanical characteristics meet structural demands. Different tension test methods are used for the measurement of interlayer bond strength. The initial approach involves applying a tensile force perpendicular to the layer, the second method employs two opposing longitudinal loads to assess shear capacity between layers and the third technique gauges splitting tensile strength by subjecting a compressive load parallel to the bonding region (Le et al., 2012; Zareiyan and Khoshnevis, 2017b; Panda et al., 2018a; Tay et al., 2019; Wolfs, Bos and Salet, 2019; Ma et al., 2019; Weng et al., 2021).

Currently, there is no standardized method widely agreed upon for evaluating the strength of interfaces in 3D-printed specimens and existing methods often differ in sample shape, size, printing and extraction processes and fixation methods, leading to varying results. Therefore, interface bond strength is typically assessed through relative values and further research is needed to establish a widely accepted testing method (Ding, Xiao and Mechtcherine, 2023).

Upon reviewing the existing literature, it became evident that there was a lack of standardized representation, particularly concerning directions, leading to confusion. In this context, Figure 2.3 outlines the aspects considered in the studies analyzed to establish a standardized approach.

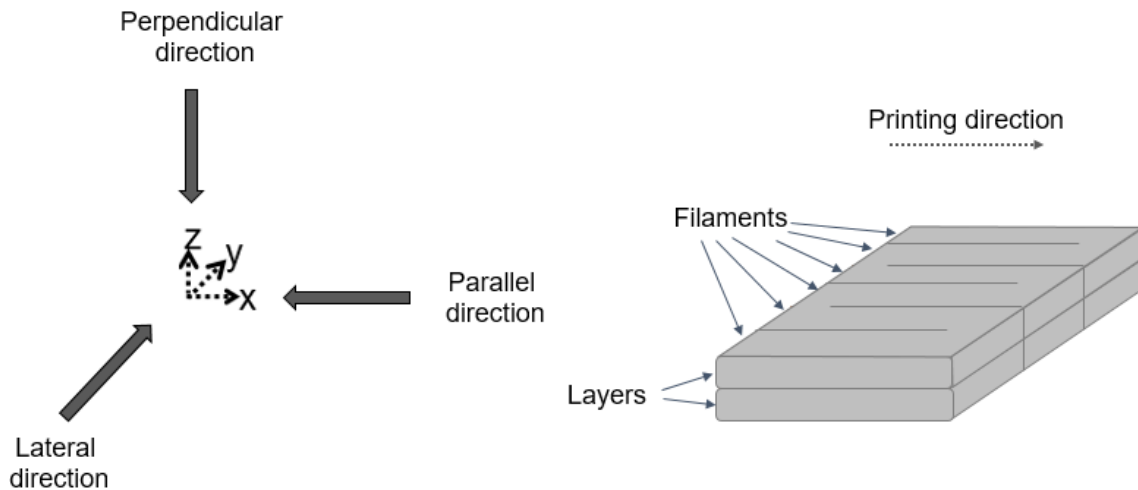


Figure 2.3. Loading directions for a 3D-printed layers and filaments.

In their study, Jianchao et al. (2017) explored the application of cementitious-based materials in construction using 3D printing technology. They found a significant variation in strength relying on the loading direction, mainly due to the stronger bonding within each printed layer compared to the bonding between different layers. The investigation unveiled that the strength values in both flexural and compressive strength tests were significantly elevated when subjected to loads perpendicularly, in stark contrast to loading parallelly. However, even in the parallel direction, the vertical compressive strength reached a respectable 44.6 megapascal (MPa), which is considered sufficient for ensuring structural safety. This highlights the importance of considering directional strength variations in design when using 3D-printed cementitious materials in construction.

Zhang et al. (2019b) investigated the rheological and hardening characteristics of 3D printing concrete with high thixotropy. They found that flexural and compressive strength were remarkably higher (11.3-25.5%) when loaded perpendicular in comparison to parallel and lateral directions. However, excessive stiffness causing voids between layers reduced flexural strength while maintaining high compressive strength. This decrease in flexural strength was attributed to weak bond strength between layers, a potential source of flaws and stress concentrations. To mitigate this, maintaining material openness, similar to sprayed concretes, was suggested. Furthermore, the material's mechanical characteristics were influenced by its layered structure. In axial compressive samples, lateral loading resulted in

the lowest strength due to direction dependent features. However, when bearing forces laterally, Poisson's ratio, Young's modulus and axial compressive strength resembled those of conventional concrete.

Feng et al. (2015) examined the performance of 3D-printed cementitious structures. These structures showcased a stratified orthotropic composition, with each layer formed from parallel strips. Rigorous flexural and compression tests validated the distinct orthotropic characteristics of the 3D-printed materials. Using the collected experimental data, they developed a relationship between stress and strain, as well as a criterion for failure based on the principle of maximum stress, specifically designed for orthotropic materials. Furthermore, their finite element analysis of a 3D-printed shell structure demonstrated the substantial impact of printing direction on the structure's load-bearing capacity.

Ding et al. (2020) conducted a study on 3D-CP using sand that is recycled in place of natural one and examined the characteristics of the resulting printed concrete. They investigated various parameters including the substitution proportion of recycled sand, curing duration, nozzle elevation and directional behavior using tests for splitting tensile, flexural and compressive strength. The research revealed that due to the presence of unhydrated cement paste on the recycled sand and interior curing processes, the compressive and flexural strengths of 3D-printed mixture with recycled sand were slightly reduced by comparison to samples without recycled sand. Anisotropic characteristics were observed in the splitting tensile, flexural and compressive strengths of 3D-printed mixture incorporating recycled sand. Regarding the direction of loading, for compressive strength, the highest values were observed in casted specimens, followed by the perpendicular, lateral and parallel directions, both for natural and recycled sand mixtures. In the case of splitting tensile strength for natural sand mixtures, the arrangement from highest to lowest was cast, lateral, parallel and perpendicular. For recycled sand mixtures, the arrangement was perpendicular, lateral, cast and parallel. Finally, for flexural strength, the arrangement from highest to lowest was perpendicular, parallel, cast and lateral. Digital image correlation results show that the declining in compressive strength in printed specimens can be ascribed to the presence of voids between strata and weak bond strength between filaments.

Le et al. (2012) examined the characteristics of high-strength fiber-reinforced 3D-printed concrete compared to traditional molded concrete. The molded concrete demonstrated impressive strength, including a 107 MPa compressive strength, 11 MPa flexural strength and 3 MPa direct tensile strength. On the flip side, the 3D-printed sample showed subpar results, registering compressive strength in the range of 75 to 102 MPa, flexural strength ranging from 6 to 17 MPa, and a tensile bond strength varied from 2.3 to 0.7 MPa, diminishing with prolonged time intervals between printed layers. Notably, the 3D-printed concrete had little gaps larger than 0.2 mm, constituting only 1.0% of the material. In contrast, molded control concrete had a higher void content of 3.8%. Poorly printed material had even more voids at 4.8%, mainly between layers. Despite variations, the additive extrusion process maintained the material's high performance.

Xiao, Liu and Ding (2021) explored the influence of connections among layers on the direction-dependent performance of 3D-printed specimens. They developed a design that incorporated interfacial bond properties and validated it using experimental data. The study investigated how concrete properties, interfacial bond strength and nozzle dimensions affected flexural and compressive strengths. Findings revealed that horizontal shear deterioration between layers decreased compressive strength, while tensile strength at the midpoint determined flexural strength. Although compressive strength was comparatively lesser, flexural strength was significantly greater in specimens loaded laterally and perpendicularly. The modeling illustrated that the number of interfaces and the shear and tensile characteristics of these interfaces between stratum influenced anisotropy variations in both compression and flexure.

Pham, Tran and Sanjayan (2020) studied high-strength 3D-printed concrete reinforced with steel fibers of varied lengths (3 and 6 mm) and volumes (0.25%, 0.5%, 0.75% and 1%). They found that a crucial combination of fiber length and volume, particularly 0.75% and 1% of 6 mm steel fibers, along with fiber alignment, significantly improved flexural performance by enabling fiber bridging mechanisms. This led to increased deflection hardening behavior, load-carrying capability and reduced fragile failure in particular loading aspects. The flexural and compressive strengths of printed concrete ranged from 70-111 MPa and 6-15 MPa, respectively, in comparison to the control cast concrete with strengths of 90-113 MPa and 11-14 MPa. Micro-CT scanning of cured specimens without fibers revealed that high-

quality layered specimens had reduced void content (8.8%) compared to 9.8% in the cast samples and 11.4% in inferior printed samples. Additionally, over 90% of extracted fibers aligned within 0° - 30° from the layer guidance.

The strengths of 3D-printed samples may also vary according to the manufacturing methodology regarding to the printing direction. This aspect holds significant importance even in real-scale applications, particularly for horizontal-printed specimens, as the transmission of forces from upper layers may not occur in the same manner, potentially impacting the bond strength. When the studies carried out in this context in the literature are examined, it has been seen that the shear and tensile strengths of the samples prepared in the horizontal and vertical printing directions showed differences in performance.

Rahul et al. (2019b) conducted tests to evaluate the performance of 3D-printed wall components. They first examined the impact of interlayer within printed components by assessing porosity and conducting bond shear tests. Porous nature was measured in bulk concrete and at the connection among horizontal and vertical layers. It was observed that bulk concrete had 6-8% lower porosity compared to mold-cast concrete. However, the interfaces had significantly higher porosity, around 11-16% higher. This indicated that while the mass of 3D-printed elements is more compact than mold-cast concrete, the interfaces are weaker with increased porosity. To assess the interfaces more thoroughly, direct bond shear tests were conducted. The shear resistance at the junction of horizontal and vertical layers was 24-30% inferior to that of conventionally cast concrete. Although the compressive strength of 3D-printed concrete was consistent across various loading aspects, it was 12-22% lower than that of traditionally cast concrete. The decrease in strength is linked to an increase in pore volume at the connection parts of layers. The flexural strength varied grounded on the locale exposed to the highest bending stress. When tested in orientations where the highest bending stress occurred at the relatively less robust connection sections, the flexural strength decreased by 32-40%. Conversely, in directions where the peak bending stress was applied to the denser bulk concrete, the flexural strength increased by 13-20%, compared to conventionally cast concrete.

Wang et al. (2022) employed a dual shear test to evaluate the shear bond behavior and deformation-load curve of junctions among vertical layers and horizontal filaments in 3D-

PC. Advanced X-ray computed tomography (XCT) scanning was utilized to identify defects and void content in the connection sections and matrix. Utilizing the principles of elastic brittle damage theory, they proposed designs for shear constitutives at the interfaces between strata and matrices. Notably, the shear strengths identified in connecting regions were established at 5.16 MPa and 4.84 MPa, representing 85.7% and 80.3% of the matrix shear strength, respectively. Void percentages within the matrix, the interlayer interfaces, and the filament interfaces were measured at 2.22%, 3.82% and 4.09%, respectively, showcasing a linear correlation with shear strength. Furthermore, the shear constitutive model of the junction effectively represented the 3D-PC behavior under shear stress, aligning closely with the experimental outcomes. This investigation establishes a robust groundwork for theoretical and numerical examinations of 3D-PC, providing valuable insights into its mechanical characteristics. This investigation establishes a robust groundwork for theoretical and numerical analyses of 3D-PC, providing crucial insights into its mechanical characteristics.

Murcia, Genedy and Taha (2020) investigated the impact of diverse infill patterning on the anisotropic features of 3D-printed concrete. The study encompassed an evaluation of rheological properties, compressive strength and the bonding strength between filaments and layers. The outcomes uncovered directional dependencies associated with infill patterns. In the perpendicular direction, specimens demonstrated reduced modulus of elasticity and compressive strength compared to the parallel and lateral directions. Nevertheless, no substantial differences were discerned in the strength and modulus between the parallel and lateral directions. Interestingly, there was an absence of directional dependency for the strain at failure. Crucially, no notable variations in the characteristics of 3D-printed concrete were attributed to infill printing models. Furthermore, the outcomes suggested that, for two out of the three testing directions (parallel and lateral), 3D-printed concrete displayed superior compressive strength when juxtaposed with conventionally cast concrete. This heightened strength was linked to the compactness achieved through the printing process, strongly influenced by various printing factors.

In addition to evaluating strength in various loading directions, researchers broadly concur that the printing time interval plays a crucial act in diminishing strength. While these studies

primarily emphasize assessing its impact on bond strength, they also examine the effects of printing time interval for 3D-printed samples using a variety of testing methods.

Chen et al. (2020) conducted both experimental and numerical investigations to understand how printing factors influence the strength between layers of 3D-printed cementitious substances made from limestone and calcined clay. They used uniaxial tensile testing to determine the adhesion between successive layers. Moreover, XCT was utilized to capture greyscale images of the microstructure and analyze the air void composition and arrangement in the printed samples. The practical observations indicated that extending the time interval among consecutive layers resulted in a reduction in adhesive strength, while making the nozzle slightly more distant from the surface had minimal influence. The weakened adhesive strength was attributed to the presence of microscopic voids at the junction of the specimens.

Van der Putten et al. (2019) presented the outcomes of their experimental study, investigating the interplay between 3D-CP manufacturing settings and the resulting internal structure. They explored how two specific manufacturing settings -printing speed and printing time interval- affected the internal structure in both initial and cured conditions and checked these findings with mechanical properties. Elevated printing speed resulted in a smoother surface because of the increased kinetic energy of sand grains and greater force that is applied. Internal structural analysis revealed that a lower printing time interval (e.g., 10-min) led to a higher presence of unhydrated cement particles, possibly linked to increased water demand within the printed layer for reconstructing early Calcium-Silicate-Hydrate (C-S-H) bridges, leaving less water present for hydrating afterwards. Additionally, a higher voids quantity and a more pronounced void arrangement were observed with shorter time intervals. Intriguingly, both increasing the printing time interval and raising the printing speed had a detrimental impact on the performance of the 3D-printed samples.

Wolfs, Bos and Salet (2019) conducted an experimental study to understand how 3D-CP process parameters relate to the interlayer strength of 3D-printed concrete. They investigated the impact of three operation factors (printing time interval, surface dehydration and nozzle height) on two mechanical specifications (compressive and tensile strength) in various loading aspects. Their findings indicated that layer orientation had little impact on the

performance when the printing time interval was sufficiently short. However, they noted a decline in the bond strength between layers with the increase in the printing time interval. This decrease in strength was more significant for specimens left uncovered through the time interval, leading to drying. No distinct correlation was identified between the nozzle height and the strength between layers in their findings.

Sanjayan et al. (2018) researched the impact of printing time intervals on the compressive, interlayer and flexural strength of extrusion-based 3D-printed concrete, exploring various aspects. They created specimens with delay times of 10, 20 and 30-min and assessed compressive, flexural, and interlayer bond strengths. The interlayer strengths of samples with a 10-min and 30-min interval were comparable and higher than those with a 20-min delay. A correlation was established between the interlayer strength findings and the moisture content at the layer interface, affected by factors like the rate of bleeding and the speed of surface moisture evaporation. Additionally, the study unveiled variations in the flexural and compressive strengths of 3D-printed concrete based on the testing aspect. Compressive strength exhibited a more pronounced orthotropic behavior compared to flexural strength. The last results that they reached is extruded layer can widen freely in lateral direction and acts on the lowest compression since there is no mold.

In their 2022 study, Huang et al. delved into the impact of printing parameters -specifically printing velocity, time intervals and layer height- on the bond strength of 3D-printed concrete. Employing both orthogonal and single-factor tests, they identified optimal parameters, revealing that an 8 mm layer height, a 10-15 min printing time interval and a speed of 1.6 m/min resulted in the most favorable outcomes. The underlying mechanisms influencing these parameters were thoroughly discussed. The researchers introduced the concept of the layer-diameter proportion (D), which signifies the ratio of layer height to nozzle diameter. As D increases, the pattern of the printed material transitions from overlapping to a wavy swing pattern. Additionally, higher printing speeds were found to decrease both the width and height of the printed concrete. The impact of the time interval on concrete bond strength displayed an initial decrease followed by an increase. This is attributed to water bleeding, which elevates surface water ingredients within 10-15 min, subsequently enhancing splitting and shear strength.

Tay et al. (2019) studied the impact of printing time intervals in 3D concrete extrusion-based printing on printed layers. They employed rheological analysis and macroscopic observations to comprehend the material's behavior in the fresh phase, focusing on the initial and subsequent printed layers. In this layer-wise printing method, printing time interval significantly affects bond performance. The study found that the material rheology of the initial layer play a critical act in bonding with subsequent layers. The modulus of the subsequent layer remains unaffected by the time gap, but the modulus of the first layer increases as the time interval grows. This higher initial layer modulus restricts proper contact and mixing at the interface, resulting in the creation of voids that weaken the bond strength exponentially. However, the high initial layer modulus is essential for supporting subsequent layers and maintaining structural stability.

Van der Putten, De Shutter and Van Tittelboom (2019) conducted an investigation involving layered specimens with different time interval (0, 10 and 60-min) among the printing of consecutive layers. They used two distinct speeds for printing (1.7 cm/s and 3 cm/s) and assessed various structural features, such as interlayer and compressive strength. To further understand the impact, they conducted Mercury Intrusion Porosimetry (MIP) tests to analyze pore dimension and pore dispersion. The initial findings revealed that specimens printed at higher speeds exhibited lower mechanical performance across all time gaps. This was linked to diminished surface irregularities and the creation of more extensive voids within the substance. Additionally, as the printing time interval increased, there was a noticeable rise in porosity. Furthermore, higher printing speeds led to the formation of bigger pores and voids within the printed substance.

Keita et al. (2019) showcased that in a fluid mixture with a low water-to-cement mass proportion (w/c), the decrease in interlayer strength is not a result of structural obstacles within the base layer impeding the blending of successive layers. Instead, their results suggested that the reduction in bond strength stems from localized drying on the surface. They suggested that this specific drying phenomenon takes place when, in low-porosity fresh materials, the liquid does not have adequate time to flow and occupy the space left by the evaporated liquid. Consequently, a region of dryness is expected to form at the drying interface and extend throughout the material. In this region, there is an inadequate supply of

water to support the hydration of the cement powder, leading to a decrease in the strength of the interface.

Nerella, Hempel and Mechtcherine (2019) investigated layer interfaces in 3D-printed elements created through extrusion-based deposition at both macro and micro levels. They conducted flexural and compression tests on two types of 3D-printable cement-based combinations with different binders, PC alone and a mixture with pozzolanic additives. The experiments were conducted at intervals of 1 day and 28 days, investigating the influence of binder combination and time intervals among layer printing on the strength of layer interfaces. The consequences demonstrated that the mixture incorporating pozzolanic additives displayed lower direction-dependent behavior, reduced variability and enhanced mechanical performance in comparison to the mixture using only PC. Particularly, the pozzolanic additive mixture experienced a less significant (below 25%) decline in interlayer strength in flexural tests across all studied time intervals. On the other hand, the flexural resilience of the PC specimens witnessed a reduction exceeding 90%, credited to a rise in porous nature at the interlayer of the printed concrete. Microscopical inspections aligned with the broader indications and images captured by the scanning electron microscope (SEM) provided additional perspectives on interfacial imperfections and the concept of "self-healing".

"Thixotropy open time" means the time session in which a substance maintains its extrudability characteristics. It should be emphasized that this is distinct from the material's aging time, which marks when the material starts to harden and solidify. In extrusion-based concrete printing, the thixotropy open time is typically shorter than the material's regular aging time, meaning that the material becomes less extrudable before it begins to set (Panda and Tan, 2018). The material aging in fresh state is another factor that influences the strength of the printed structure. Given that the 3D printing operation involves a certain period for application and the concurrent occurrence of hydration reactions, the age of the materials becomes a crucial consideration. Furthermore, in order to mitigate material wastage, efforts were made to extend the extrudability performance during the formulation of the mixture. This was aimed at enabling the recovery of materials in the event of incorrect application or operational mishaps during the printing process. Therefore, it was considered crucial to gain

a thorough understanding of how the aging process of the mixture influenced its performance.

2.2. Geopolymers

Concrete stands as the most utilized material globally by mass, second only to water. In the year 2020, approximately 14 billion m³ of concrete was consumed and the worldwide output of cement reached approximately 4.2 billion metric tonnes (Global Cement and Concrete Association, 2020). According to Van Damme's extensive and overarching analysis of the future of concrete in the digital realm, the demand for concrete is projected to remain robust. This is driven by ongoing infrastructure expansions in developing nations like China and India, alongside infrastructure renovations in developed countries (Van Damme, 2018). This requisition puts future pressure on climate change due to the production of PC is a significant contributor, liable for up to 10% of CO₂ releases worldwide (Scrivener, John and Gartner, 2018). Projections of a 50% increase in annual PC production by 2050 further exacerbate the environmental impact (Monteiro, Miller and Horvath, 2017). Moreover, PC and concrete production involves the consumption of natural sources like aggregates, limestone and water, causing additional environmental harm (Cachim, Velosa and Ferraz, 2013).

While low cost, good mechanical features and properties such as fire performance and durability are sufficient for the widespread use of concrete, the environmental burden of concrete must also be considered. When it comes to environmental impact, PC comes to mind. As PC demonstrates impressive thixotropic characteristics when combined with water, it emerges as the most frequently utilized substance for formulating concrete that is printable (Lu et al., 2019). Nevertheless, the manufacturing of PC is highly energy-intensive and releases significant amounts of CO₂ into the atmosphere (Khosnevis, 2004). For this reason, employing sustainable binders that involve partial or complete substitution of PC becomes crucial to manufacture environmentally friendly building materials. In this respect, researches are focused on eliminating the concerns caused by the global problem and developing environmentally friendly binders. Geopolymers are considered a major advance towards the development of greener binders (Provis and Deventer, 2014). Geopolymers have surfaced as a highly promising alternative to binders and materials based on PC, demonstrating a capacity to lower energy consumption, use waste materials, improve

Geopolymers formed through the interaction of primary aluminosilicate precursors like fly ash (FA), rice husk ash (RHA), silica fume (SF), ground granulated blast furnace slag (GGBFS), calcined clays and natural pozzolans; and alkali activators such as potassium silicate (K_2SiO_3), potassium hydroxide (KOH), sodium silicate (Na_2SiO_3), sodium hydroxide (NaOH) and calcium hydroxide ($Ca(OH)_2$) have attracted great interest from the construction industry in recent years. In this context, summaries of studies conducted using major aluminosilicate precursors that investigate anisotropy, bond strength and the factors that influence bond strength (loading directions, printing time interval and material aging effect) presented below.

Nuaklong et al. (2019) examined the resistance to fire and mechanical performance of geopolymer binders using high calcium FA as the primary material, with NaOH and Na_2SiO_3 as alkali activators. The study found that the supplement of RHA effectively enhance the strength performance of recycled aggregate geopolymer concrete, especially when the silicon dioxide/aluminum oxide ratio (SiO_2/Al_2O_3) was increased to 4.17. As a result, the 28-day compressive strengths of recycled aggregate geopolymer concrete containing RHA varied from 36.0 to 38.1 MPa, attributable to the enhanced microarchitecture and a more compact matrix. These strengths were comparable to those observed in recycled aggregate geopolymer concrete made with SiO_2 -rich natural aggregates. However, it should be emphasized that the inclusion of SiO_2 -rich substances had a disadvantageous impact on the post-fire residual strength of geopolymer concretes prepared from recycled aggregates. This adverse effect was primarily due to the decrease in porosity attributed to the inclusion SiO_2 -rich components.

Bong et al. (2018) investigated simply cured mixtures with varying quantities of GGBFS and FA as aluminosilicate precursors and $Na_2SiO_3/NaOH$ or K_2SiO_3/KOH as activators. The study evaluated extrudability, buildability, open-time and compressive strength of the printed samples. Results indicated that lower silicon dioxide/sodium oxide (SiO_2/Na_2O) ratios in Na_2SiO_3 prolonged setting and open times, while higher silicate-to-hydroxide ratios slowed reactions, extending open times. The rate of geopolymerization also influenced shape retention. Regarding mechanical properties, Na-based initiators produced more compressive strength amount than K-based ones. Increasing the silicate-to-hydroxide ratio boosted strength due to added soluble silicate. However, using silicate solutions with higher

$\text{SiO}_2/\text{Na}_2\text{O}$ ratios reduced strength in Na-activated specimens because of the excess silicon content.

Bong et al. (2021) investigated how the composition of geopolymer mixtures affects the properties of 3D-printable geopolymers. The focus of their research was on developing 3D-printable geopolymers that can be cured at ambient temperatures while exhibiting enhanced printability and mechanical performance. They created seven different geopolymer mixtures to investigate how different factors, such as the type and quantity of solid activators and the presence of a retarder (R), influence the properties of these geopolymers when freshly prepared and after hardening. These mixtures were formulated using different combinations of geopolymer precursors, including FA and GGBFS, along with varying amounts of Na_2SiO_3 powder and/or anhydrous Na_2SiO_3 as activators. In the experimental process, components such as silica sand, water and sucrose powder were incorporated, with sucrose acting as a R in specific mixtures. Following experimentation, the optimal mixture was selected for 3D printing, exhibiting favorable direction-dependent compressive strengths of 44.7 to 55 MPa and flexural strengths of 3.5 to 8.4 MPa at the 28th day.

In their study, Panda, Unluer and Tan (2018) aimed to explore the impact of SF, GGGBS and FA, on the properties of geopolymer blends intended for use in 3D concrete printing under ambient curing conditions. They conducted experiments using 3 different precursors as replacements, up to a ratio of 10%. The findings revealed that GGBFS had limited influence on improving the fresh properties of geopolymer pastes but notably enhanced early-age compressive strength. This enhancement may be attributed to a more uniform microstructure and the creation of a robust 3D network due to GGBFS's amorphous phases. However, GGBFS reduced the workability, requiring careful control of its content to balance between strength and workability. In contrast, SF proved effectual in controlling yield stress and viscosity during the fresh state. SF's high surface area and spherical particle shape facilitated smooth extrusion and maintained the shape of deposited layers. It is important to note that the compatibility of additives in geopolymer blends depends on various agents and can't be universally applied because of the odd polycondensation reactivity within geopolymer.

Panda et al. (2018b) delved into the strength between layers of geopolymer mortars printed under ambient conditions. Using SF, GGBFS and FA as aluminosilicate precursors, along with NaOH and Na₂SiO₃ as alkaline initiators, the mixture incorporated sand with a maximum particle size of 2 mm ($D_{\max}=2$ mm) and nano-clay as a flow regulator. Results indicated that increasing the density of the alkaline initiator correlated with reduction in interlayer bond strength, likely due to accelerated polycondensation reactions. The study emphasized the significant impact of geopolymers' hardening duration and the printing time interval on interfacial strength, affecting the humidity levels in the interface zone.

Kashani and Ngo (2018) researched the impact of various substances and operational factors on the 3D printability of geopolymers incorporating SF, GGBFS and FA with Na₂SiO₃ as an initiator. Results showed a reduction in the yield stress of geopolymer mixtures as activator content decreased. However, no consistent trend was observed for the impact of an enhancement in the water-to-solid ratio (w/s) on yield stress. Higher initiator proportion or inferior w/s resulted in faster initial setting. According to mechanical characteristics, lower compressive strength was noted with increased w/s or decreased activator content. The study emphasized the importance of balancing factors influencing open-time, initial yield stress, and rheological variability over time for developing geopolymers suitable for 3D-AM applications.

Alghamdi, Nair and Neithalath (2019) carried out a research emphasized on the improving of geopolymer materials appropriate for extrusion-based 3D printing. These binder materials were formulated using different combinations and quantities of materials, including FA, GGBFS, limestone and alumina powder. Different activation agents were also employed, including sole NaOH, NaOH in combination with Na₂SiO₃ solution, or sodium sulfate (Na₂SO₄). The research outcomes revealed numerous key points. First at all, it was demonstrated that as the amount of FA in the mixture decreased, the compressive strength of the materials increased. Furthermore, formulations activated utilizing Na₂SiO₃ solution demonstrated superior compressive strength in contrast to those initiated by NaOH. This improvement was linked to the heightened presence of highly reactive silica in the sodium silicate-activated formulations. Additionally, mixtures incorporating GGBFS and cured at room temperature conditions exhibited the most noteworthy flexural strength among the evaluated materials.

Netamollahi et al. (2018b) explored the characteristics of cured 3D-printable geopolymer mixtures in an oven setting. Comprising FA, GGBFS, Na_2SiO_3 , silica sand and tap water, the mixtures underwent a two-layer printing process with varying time intervals. The study assessed compressive strength in distinct testing aspects (lateral, parallel and perpendicular) for cubic and prismatic 3D-printed samples. Flexural strength was measured for specimens loaded perpendicularly and laterally to the printing path. The research also examined interlayer bond strength. Results showed anisotropic mechanical behavior, with parallel loading exhibiting the highest compressive strength and lateral loading the lowest. Additionally, longer printing time intervals correlated with reduced bond strength between consecutive layers.

With the aim of developing an environmentally friendly, printable one-part geopolymer mixture, Panda et al. (2019b) conducted a study on geopolymer mortars. These mortars consisted of FA, GGBFS, KOH or K_2SiO_3 as activators and river sand ($D_{\text{max}}=2$ mm). The study focused on evaluating the fresh properties of these mixtures, including aspects like viscosity, yield stress and thixotropy. To assess their printability, optical and dimensional examinations were carried out after the printing process. Moreover, direction-specific experiments were exerted on the 3D-printed samples. The results of the study indicated that elevating the GGBFS content in the geopolymer mixtures led to enhanced thixotropy, greater mechanical performance and increased yield stress. Additionally, the printed geopolymer samples demonstrated direction-dependent characteristics because of additive manufacturing operation.

Panda et al. (2017) formulated a geopolymer mortar suitable for 3D printing. They employed SF, FA and GGBFS and as aluminosilicate precursors, incorporating agents enhancing thixotropy and sand ($D_{\text{max}}=2.15$ mm) as fine aggregates. Alkaline activation was achieved using KOH and K_2SiO_3 . Following initial assessments of 3D printability, they produced cubic and prismatic specimens using both 3D printing and traditional casting methods. These specimens underwent testing for flexural, compressive and tensile strength. Notably, the direction of loading notably affected the mechanical specifications of the printed samples, likely because of their anisotropic characteristics. Considering the test outcomes, the highest compressive strength was achieved in the parallel aspect, while the highest flexural strength was attained in the perpendicular one. Conversely, the lowest compressive strength was

recorded in the lateral aspect and the lowest flexural strength was observed in the parallel one. Additionally, a noticeable decreasing trend in tensile strength was noted as the time gap increased, with the most significant decrease occurring between 5 and 10 min.

Panda, Mohamed and Tan (2018) researched the impact of the orientation of 3D-printed FA-based geopolymers cured at room temperature on their mechanical specifications. These geopolymers utilized SF, GGBFS and FA as precursor substances, K_2SiO_3 as an alkaline initiator, in addition to sand ($D_{max}=2$ mm), tap water and specific agents enhancing thixotropy. Prior to the printing operation, they evaluated the flow characteristics of the improved geopolymer blends, encompassing buildability and thixotropy, utilizing a rheometer. The experimental results uncovered a noticeable direction-dependent behavior in compressive strength, attributable to the layered deposition of geopolymer mortar. Notably, the maximum strength was determined in the parallel aspect, while the lowest strength was recorded in the perpendicular one.

Chougan et al. (2020) investigated the impact of nano supplements on the features of 3D-printed geopolymer mixtures. Their primary basis was to assess the effects of six distinct geopolymers proper for 3D printing, both in their fresh and hardened states. These mixtures were composed of FA, SF, GGBFS, NaOH, Na_2SiO_3 , fine sand and, in some cases, nano-scale platelets made of graphite. The study yielded several important findings. Initially, it was observed that with an increase in the GGBFS amount in the geopolymer mixtures, the open time, setting time and flowability of the materials decreased. Moreover, the introduction of nano-graphite led to improvements in preserving the form of the geopolymer blends. The improvement was credited to the existence of Van der Waals forces amid the nano-graphite fragments and the exceptional sorption capabilities of nano-graphite, thereby augmenting the mixture's ability to maintain its intended form. And finally, it was found that most of the mixtures exhibited anisotropic behavior in terms of Young's Modulus, meaning that the mechanical behavior was connected on the printing direction.

Panda et al. (2018a) investigated the influence of operational parameters, including printing time intervals, nozzle standoff distance, and print speed, on the tensile strength of 3D-printed geopolymer mixtures cured under ambient conditions. These mortars utilized SF, FA, and GGBFS as aluminosilicate precursors, liquid K_2SiO_3 as an alkaline initiator, and sand

($D_{\max}=1.15$ mm). The study involved varied printing speeds, time gaps (ranging from 1 to 360 min), and nozzle standoff distances (0, 2 and 4 cm). Bingham parameters, including viscosity and yield stress, were measured utilizing a rheometer at 5-min gaps, with an open time for the mixture set at 20 min. The results indicated that a rise in the time gap between successive stratum correlated with a reduction in bond strength, whereas slower printing speeds and shorter distances of the nozzle from the surface resulted in enhanced bond strength.

Nematollahi et al. (2018a) conducted an investigation to explore the characteristics of fresh and hardened geopolymer mortars. These mortars were composed of FA, NaOH and Na_2SiO_3 as alkaline activators, silica sand and a viscosity modifier (VM) (sodium carboxymethyl cellulose). Various amounts of polypropylene fibers were incorporated to the mixtures. In the evaluation of the hardened characteristics, the investigation examined the orientation-specific compressive strength of prismatic 3D-printed geopolymer samples under loading conditions in lateral, perpendicular and parallel orientations to the printing route. Moreover, the study assessed the orientation-specific flexural strength of prismatic 3D-printed samples under loading conditions both perpendicularly and laterally to the printing path. Additionally, the study quantified the strength between successive stratum using prismatic 3D-printed samples. The findings unveiled significant directional differences in the solidified characteristics of the printed samples. The introduction of fibers into the blends improved qualities such as resistance to deformation, fracture energy, shape preservation and compressive strength in perpendicular alignments. However, beyond a certain threshold, the adding of fibers led to a reduction in interlayer strength.

Nematollahi et al. (2018c) conducted a research to explore how the type of fiber used in the production of oven-cured 3D-printed geopolymer materials influenced their behavior in respect of flexural strength and interlayer bond strength. These geopolymer materials were formulated using FA, a sodium-based activator ($\text{NaOH}+\text{Na}_2\text{SiO}_3$), a VM (sodium carboxymethyl cellulose) and silica sand. The findings revealed that the inclusion of fibers led to a reduction in both interlayer bond and flexural strength of the printed samples.

Al-Qutaifi, Nazari and Bagheri (2018) conducted a study to explore the impact additive manufacturing on the constructional buildability and hardened characteristics of geopolymer

blends. These compositions included FA, NaOH, Na_2SiO_3 and sand ($D_{\text{max}}=0.3$ mm). To assess their effects, two reinforcing materials -hooked-end steel fibers and polypropylene- were separately integrated into the mixtures. The research focused on evaluating the flexural strength of geopolymer samples, with varied printing intervals between layers and conventionally casted geopolymer samples. The outcomes showed that the introduction of fibers enhanced the flexural strength in standard samples, with the highest strength observed in specimens containing hooked-end steel fibers. However, it was noted that fiber incorporation could negatively impact the bond strength between layers by impeding adhesion at the interface. Furthermore, samples with layered structures displayed diminished flexural strength in comparison to those casted, primarily attributable to the direction-dependent characteristics inherent in the layered configurations. The specific layering model also influenced the flexural strength performance. Additionally, a rise in the printing time interval led to a decline in the flexural strength of the layered specimens.

Lim, Panda and Pham (2018) conducted a research related with the flexural properties of geopolymer specimens produced using 3D-AM technology. These geopolymers were formulated with FA, GGBFS, SF as precursors, K_2SiO_3 as the alkaline activator, river sand ($D_{\text{max}}=1.18$ mm) and magnesium aluminum-silicate nano clay. In addition to these materials, the geopolymers were reinforced with a hybrid combination of polyvinyl alcohol (PVA) fibers and steel wire. The study's findings revealed that when compared to control specimens (geopolymers without hybrid fiber reinforcement), the use of this hybrid fiber reinforcement approach significantly improved the flexural performance of the geopolymers, with an enhancement of up to 290%.

Chougan et al. (2021) investigated how the inclusion of additives affects the material rheology, microscopic structure and mechanical characteristics of geopolymer suitable for 3D printing. The predominant binding element in these mixtures comprised 25% GGBFS, 15% SF and 65% FA, by weight. Activation of these mixtures involved a combination of Na_2SiO_3 and NaOH, constituting 40% of the total binder weight. Graded sand ($D_{\text{max}}=1$ mm) was also integrated into the mixtures. The research incorporated various additives in different combinations and proportions, including PVA fibers for support and attapulgite nano-clay as a thixotropic regulator. Both casted and 3D-printed specimens underwent mechanical tests, such as compressive and flexural strength assessments. Microscopic

structural characterization studies were also conducted. Results indicated that including PVA fibers or attapulgite nano-clay at specific usage rates improved both flexural and compressive strengths. Additionally, the microscopic structure of the alkali-activated additives was enhanced, attributed to void filling and crack bridging mechanisms facilitated by these additives.

Chen et al. (2020) conducted both experimental and numerical investigations to understand how various printing factors effect the interlayer bond strength of 3D printed cementitious substances made from limestone and calcined clay. The results from the experiments indicated that enlarging the temporal interval between the printing of consecutive layers led to a decrease in interlayer strength, whereas rising the distances of the nozzle from the surface had minimal impact. The weaker bond strength was linked to higher microscopic voids in the interlayer region of the sample. Furthermore, numeral works using a 2D lattice breakage pattern were conducted to predict bond strength for various pore contents in the interface layer during uniaxial tensile tests.

Muthukrishnan, Ramakrishnan and Sanjayan (2020) explored the impact of microwave irradiation on the buildability and interlayer strength of 3D-printed geopolymer specimens. Printed layers underwent microwave heating and were then stacked. The study assessed interlayer bond strength, surface and bulk moisture loss to understand microwave heating's impact. Results indicated increased bond strength with microwave heating, accompanied by surface moisture loss due to accelerated polycondensation reactions between layers. Furthermore, improvements in thixotropy (viscosity recovery rate) and buildability were observed.

The main precursors used to manufacture geopolymers are requested by the PC and concrete sector at higher and/or higher costs than PC, given their approved behavior and accomplished use as complementary cementitious substances (Ulugol et al., 2021). In addition, these precursors can have disadvantages such as high transport prices, may require pre-treating and are not available in the first place. Therefore, identifying alternative source materials is crucial for facilitating and expanding the production and application of geopolymers. CDW production is available all over the world and CDW are mainly used as filling material; materials such as concrete, tiles, brick, glass and ceramics can also be

utilized in the production of geopolymers for innovative, high-grade and effective waste recycling. Despite available studies on developing geopolymers from CDW-based materials like concrete, brick, tile, ceramic and glass, these are fewer compared to studies using primary aluminosilicates. Using CDW as a feedstock for aluminosilicates in the formulation of geopolymer binders is specially crucial, given the abundance of fine silt particles containing crystalline aluminosilicates resulting from structural destruction (Dadsetan et al., 2019). Many studies have focused on creating geopolymers through 3D-AM technic utilizing conventional precursors, likely because of the predictable properties of these widely-used materials. However, there is limited exploration in the literature concerning CDW-based geopolymer mixture with 3D-AM technology. For that reason, below, firstly, the studies on obtaining geopolymer mixtures using CDW-based materials are mentioned, and then, although limited, a summary of the studies focusing on the integration of geopolymer mixtures into 3D-AM technology is presented. Furthermore, the last section also discusses some of the studies conducted in recent years to assess the environmental footprint of geopolymer material production in the context of sustainability. These studies involve comparisons with PC production across various parameters.

Khater (2012) investigated the impact of introducing calcium, in the form of hydrated $\text{Ca}(\text{OH})_2$, on the features of geopolymer materials generated through the alkali initiation of aluminosilicate adhering substance, such as those derived from concrete, demolished walls and metakaolin. Initiation agents Na_2SiO_3 and NaOH were utilized. The study discovered that mixtures with $\text{SiO}_2/\text{Al}_2\text{O}_3$ ratios ranging from 3 to 3.8 showed superior mechanical behavior. Moreover, the supplement of hydrated $\text{Ca}(\text{OH})_2$, keeping the specimens for 24 hours at 80°C and water curing at room condition resulted in stronger mechanical performance and substructure.

In their study, Allahverdi and Kani (2009) explored the geopolymerization process using mixtures of Na_2SiO_3 and NaOH as alkali activators for brick and concrete waste. Their findings revealed that brick waste, owing to its higher content of calcinated aluminosilicate, exhibited superior performance in geopolymerization in comparison to concrete waste. They also noted that pastes made from brick waste achieved a 28-day compressive strength of 40 MPa.

Gonçalves Rapazote, Laginhas and Teixeira-Pinto (2010) conducted research aimed at creating geopolymer building materials using CDW. They formulated mixtures utilizing various ceramic products such as bricks, roof and floor tiles, sanitary ware, as well as FA, recycled aggregates, NaOH solution, and Na₂SiO₃. The results indicated that geopolymer mixtures based on CDW demonstrated superior mechanical properties when compared to conventional PC-based mixtures.

Reig et al. (2013a) utilized recycled ceramic bricks as an aluminosilicate precursor along with siliceous sand ($D_{\max}=2$ mm) and alkaline activator solutions containing NaOH and Na₂SiO₃ to create geopolymer paste and mortar mixtures. The study showed that, depending upon the water-to-binder (w/b), SiO₂/Na₂O and binder-to-sand ratio (b/s), it is probable to achieve compressive strengths of up till 50 MPa for mortars when healing at 65°C for 7 days. This research illustrated the potential to convert such waste materials into high-value products.

In another study by Reig et al. (2013b), geopolymer mortars were produced using two distinct ceramic waste materials derived from CDW: recycled ceramic bricks and ceramic tiles. Alkaline activators, Na₂SiO₃ and NaOH were used in the mixtures, along with siliceous sand as an aggregate ($D_{\max}=2$ mm). The integration of Ca(OH)₂ into the materials based on ceramic tiles led to a quicker hardening response, resulting in reduced setting times. It was observed that recycled ceramic bricks required more water compared to ceramic tiles and a declining in the w/b led to improved mechanic characteristics in the blends. Different sodium density of the alkaline initiator and w/b resulted in compressive strengths varying among 22 and 41 MPa for mixtures that underwent healing for 7 days at 65°C.

Sun et al. (2013) explored the combination and heat-related behavior of geopolymer mixtures derived from ceramics. They tested varied compounds of KOH solution (Na₂SiO₃+NaOH, Na₂SiO₃+KOH, and NaOH+KOH), NaOH solution and liquid Na₂SiO₃ as alkaline activators. The study emphasized that the first reaction system and the selection of alkaline solutions remarkably influenced the geopolymerization operation. Their findings indicated that even without calcination, the geopolymer mixtures achieved impressive compressive strength results ranging from 26 to 71 MPa. Furthermore, after subjecting the

geopolymers to calcination at 1000°C, their compressive strength performance improved further.

Komnitsas et al. (2015) made geopolymers using waste materials from tiles, concrete and bricks as aluminosilicate precursors. They utilized Na_2SiO_3 and NaOH solutions as alkaline initiators. In their experiments, concrete-based geopolymers achieved a 7-day compressive strength of 13.0 MPa, brick-based geopolymers reached 49.5 MPa and tile-based geopolymers exhibited the highest strength as 57.8 MPa. The optimal conditions for production included using NaOH with a molarity of 8-10 M, curing at temperatures between 80-90°C and aging the geopolymers for 7 days. The research highlighted that the fragment proportions of the precursor materials contributed significantly to the geopolymerization process. Interestingly, waste tiles and bricks demonstrated better geopolymerization potential compared to concrete precursors.

Vasquez et al. (2016) conducted research on the creation of geopolymers by employing alkaline activation of CDW. They utilized NaOH and Na_2SiO_3 as alkaline activators. In their study, they introduced both hybrid and binary geopolymers by adding PC and metakaolin in quantities of up to 30% relative to the CDW. Their results indicated that the systems activated with Na_2SiO_3 demonstrated the highest compressive strength, facilitating geopolymer formation at ambient temperature. The geopolymer exclusively made up of CDW attained a peak compressive strength of 25 MPa. In contrast, the blended geopolymer, incorporating 30% PC with CDW, accomplished a strength of 33 MPa after 28 days of curing under room conditions. Remarkably, the binary geopolymer composed of CDW with 10% metakaolin displayed a substantial rising in compressive strength, achieving 46.4 MPa, curing at 28 days without the need for heat curing. These outcomes demonstrate the viability of using CDW as a precursor for producing geopolymer cements.

Zaharaki, Galetakis and Komnitsas (2016) conducted a study to explore the potential for utilizing construction and industrial waste materials. Their objective was to create geopolymeric pastes by integrating diverse waste materials, such as red mud, electric arc furnace slag and concrete, tiles and bricks waste as aluminosilicate precursors. The alkaline activators used were NaOH solution and liquid Na_2SiO_3 . Their findings emphasized several critical factors for achieving satisfactory properties in the final product. Maintaining

acceptable $\text{SiO}_2/\text{Al}_2\text{O}_3$ and silicon dioxide/calcium oxide (SiO_2/CaO) proportions and ensuring an adequate density of NaOH were highlighted as essential. Additionally, it was highlighted that maintaining the appropriate water content in the reaction medium is essential for the first times in initiation process. The study achieved highest compressive strength of 76 MPa in mixtures containing CDW, highlighting the potential for effectively utilizing these waste materials in geopolymeric applications.

Khater, El Nagar and Ezzat (2016) investigated the development of geopolymers using diverse waste materials, such as fine sand, ceramic and brick wastes and NaOH compound. They examined different combinations of precursor materials, including individual and binary mixtures of ceramic and clay brick waste with varying weight ratios. The blends were also produced with distinct w/b ratios. The findings indicated that the formulations containing a 20%-80% blend of clay brick and ceramic waste demonstrated the highest compressive strength. This blend was particularly effective in enhancing mechanical properties, attributed to the enhanced form and improved attaching to the matrix displayed by ceramic waste compared to clay brick waste.

Vafaei and Allahverdi (2017b) researched the synthesis of geopolymer mixtures utilizing waste glass as a precursor material. They utilized mix of Na_2SiO_3 and NaOH as alkali initiators, incorporated sand and introduced varied calcium alumina cements aspect additives. The study revealed several key findings. Initially, an increase in the quantity of calcium alumina cement hastened the hardening duration of the mixtures. Secondly, the inclusion of calcium alumina cement improved geopolymerization, characterized by an increased formation rate of Sodium-Alumino-Silicate-Hydrate (N-A-S-H) gel with a more joined molecular form. This enhancement in geopolymerization was associated with the elevated amount of reactive alumina in the blends. Additionally, the mixtures containing calcium alumina cement exhibited higher compressive strength compared to those without it.

Rovnaník et al. (2018) explored the microscopic structure and material rheology of geopolymers prepared using metakaolin, red brick waste and an activator composed of Na_2SiO_3 ($\text{SiO}_2/\text{Na}_2\text{O}=1.4$) and NaOH. In their experiments, samples were created with distinct blends of metakaolin and red brick powder. The study revealed significant findings.

Firstly, the mixtures containing 75% metakaolin and 25% red brick powder exhibited the maximum flexural and compressive strength outcomes. This was credited to the combined impact of these two sources of aluminosilicate on the mechanical properties of the geopolymers. Furthermore, higher amount of brick waste resulted in a decrease in the plastic viscosity of the materials, although it did not importantly influence the yield stress of the mixtures.

Sedira, Castro-Gomes and Magrinho (2018) conducted a research to investigate the combination of geopolymer using mix of recycled concrete blocks and tungsten mining waste as precursors, with NaOH and Na₂SiO₃ serving as an alkali activators. The study's findings indicated that an increase in the recycled concrete content within the mixtures led to higher compressive strength consequences. This improvement in mechanical characteristics was attributed to the addition of recycled concrete, which facilitated the dissolution of certain phases within the precursors, including recycled concrete blocks and tungsten mining waste.

Hwang et al. (2019) undertook a study with the objective of creating high-strength alkali-activated paste mixtures by integrating GGBFS, FA and waste from red clay brick and ceramic powder. These mixtures were activated using a solution containing NaOH and Na₂SiO₃. Various combinations of FA, GGBFS and one of the waste materials were used to prepare the mixtures. The study's results revealed that mixtures containing red clay brick waste exhibited lower workability compared to those containing ceramic waste. This discrepancy in workability was ascribed to the greater specific surface area and increased porosity of red clay brick. Moreover, a rise in GGBFS content was observed to improve compressive strength outcomes. Intriguingly, red clay brick, with its finer particle size and elevated CaO ingredient, delivered superior mechanical characteristic in comparison to ceramic waste. The maximum compressive strength result, achieved at 56 days, was 70 MPa and was derived from the mixture comprising 60% red clay brick waste, 30% GGBFS and 10% FA.

Ouda and Gharieb (2020) conducted a study using two types of materials, calcined-dolomite and raw-dolomite concrete powder, in conjunction with waste of brick to formulate geopolymer mixtures. NaOH was employed as the alkaline initiator in their mixtures, with

varying proportions of the powder materials. The study revealed that an optimal NaOH employment rate of 12% by mass, relative to the produced geopolymer, resulted in the maximum compressive strength. Furthermore, the inclusion of both calcined- and raw-dolomite concrete crushes in the mixtures positively influenced the results of compressive strength.

In their study, Kim and Choi (2012) explored the utilization of waste concrete powder, a by-product generated during the production of high-quality recycled aggregate. As they increased the substitution rates of waste concrete powder, they observed a significant decrease in the flow value, up to 30%, when compared to mortar that used only PC. Additionally, the compressive strength of the mortar experienced a substantial reduction of up to 73% as the level of waste concrete powder rising. Furthermore, the moisture absorption rate enhanced by 70%. Based on the test consequences, it is advisable to limit the substitution of PC with waste concrete powder to below 15% to maintain desirable properties in the mortar.

According to a study conducted by Alhawat et al. (2022) CDW can be utilized in geopolymer systems to enhance mechanical and durability performance. The results show that because of the different kinds of factors included in the preparing of geopolymers mixture, a trial and error approach is required. Also superior performance can be achieved when the ratios of activators and thermal curing are appropriate and heat treatment in the range of 60-90 °C can remarkably increase the speed of polymerization. Furthermore, using additives as slag and metakaolin can improve mechanical performance and durability, the mechanical properties improve with high NaOH concentration. Finally, the most effective activators that can be used are Na_2SiO_3 and NaOH to be used at 1.0 and 2.0 ratios and polycarboxylate-based superplasticizers (SP) show the best performance as a SP.

Silva et al. (2019) conducted optimization analyses to discover the optimal preparing circumstances for natural pozzolana- and fired clay brick-based geopolymers. The outcomes showed that when the appropriate production conditions were applied, these materials could achieve 37 MPa compressive strengths for fired clay brick-based geopolymers (Silica modules=0.60, Na_2O content of 8% and a w/b=0.27) and 26 MPa for natural pozzolana-

based geopolymers (Silica modules=1.08, 8% Na₂O content and a w/b=0.52). These geopolymers were also cured in an oven for a duration of 7 days.

Robayo-Salazar, Rivera and Gutiérrez (2017) aimed to assess the feasibility of utilizing concrete, glass and red clay brick waste to create geopolymer binder suitable for manufacturing pavers, regular tiles, roof tiles and blocks. The activation process involved using either NaOH or a combination of NaOH and waterglass solutions. The highest strength at room temperature was achieved with red clay brick waste mixed with 20% PC and activated using NaOH and waterglass as 102 MPa. The second-highest strength result was achieved by mixing concrete waste with 30% PC and the same activators as 33 MPa. For 100% glass waste, the maximum compressive strength of 57 MPa was acquired using NaOH at a 4.6% Na₂O proportion and 24 hours heat curing at 70°C.

Vafaei and Allahverdi (2017a) managed a research to evaluate the resilience of geopolymer mixtures against acid effect. They produced samples employing waste glass powder, sand, calcium alumina cement and combinations of Na₂SiO₃ and NaOH. Samples were also produced utilizing either calcium alumina cement or glass waste alone for comparison. The results suggested that the geopolymer samples prepared by combining glass waste and calcium alumina cement exhibited greater resistance to acid attacks. These specimens exhibited lower mass and compressive strength losses when subjected to acid attack compared to the control specimens.

As per Sata and Chindaprasirt (2020), CDW has the potential to serve as aggregates in geopolymer concretes, potentially enhancing properties like heat insulation and low density. Nonetheless, akin to traditional concrete, there is a marginal reduction in both durability and mechanical behaviors.

Since CDW-based materials are obtained in bulk in construction and demolition events, binders were developed as a result of using CDW as aluminosilicate precursors in combination at different rates and NaOH solution as alkali activator with different curing temperatures/times and molarities in the study examined by Yıldırım et al. (2021). Characterization through SEM analysis was complemented by X-ray diffraction (XRD) and energy-dispersive X-ray spectroscopy (SEM/EDX). Following curing for 48 hours at 115

°C, an impressive compressive strength of 80 MPa was achieved with the application of a 15M NaOH solution. It was observed that, among the various precursors utilized, this specific mixture contributed significantly to the compressive strength of the hollow brick. The primary reaction products of the geopolymer binders were identified as N-A-S-H gels, encompassing distinct zeolitic polytypes ranging from amorphous to polycrystalline.

Ulugol et al. (2021) conducted a study in which they formulated geopolymer mixtures using various CDW-based substances like hollow brick, glass, red tile and red clay brick. They employed NaOH as the alkaline activator for these mixtures and prepared them with different concentrations of NaOH solution along with one of the CDW-based precursors. Their findings revealed that the maximum compressive strength outcomes, reaching up till 45 MPa, were achieved from the mixtures containing hollow brick as the precursor and NaOH solution with a concentration of 12%. This enhanced performance was credited to the increased overall content of Al₂O₃ and SiO₂ found in hollow brick. Moreover, the mixtures based on red tile and red clay brick exhibited similar compressive strength results, which were lower than those obtained from hollow brick-based mixtures. On the other hand, glass-based mixtures displayed the minimum compressive strength performance, likely because of the absence of Al₂O₃ in glass fragments and their huge proportions.

Özçelikçi et al. (2023) conducted a research to develop and characterize specimens curing in room conditions that utilize mixture of fine recycled concrete aggregates and CDW-based geopolymer. In this research, a combination of CDW-based substances as roof tile, red clay brick, glass, hollow brick and concrete were used in the role of the precursor. Additionally, GGBFS was incorporated into some mixtures to partially displace CDW precursors. The results of this study demonstrated that it is probable to have 28-day compressive strength outcomes surpassing 30 and 50 MPa with both slag-substituted and entirely CDW-based mixtures. These mixtures were found to have the potential for use in structural concretes composed entirely of CDW-based materials. While the drying shrinkage of these mixtures was moderately high compared to cementitious systems, it could be notably reduced through mixture improvement. The water absorption values were determined to be similar to those documented in the literature. One notable advantage of CDW-based geopolymer mortars is their superior behavior in respect of CO₂ emissions and energy requirements compared to PC mortars. This study underscores the possibility of creating construction substances that

are more environmentally friendly, possessing allowable strength and long-term performance. This is accomplished by using CDW-based components as precursors and integrating recycled aggregates.

Figliela et al. (2022) conducted a study in which they partially replaced metakaolin and FA with clay bricks and concrete debris. For samples containing metakaolin, clay brick and rubble, the compressive strength reached 20.1 MPa, while the flexural strength was 5.3 MPa. On the other hand, geopolymers containing FA, clay brick and rubble displayed a compressive strength of 19.7 MPa and a flexural strength of 3.0 MPa. These findings indicate that it is possible to create construction materials with satisfactory mechanical characteristics by incorporating CDW-based materials and industrial byproducts into the geopolymer matrix.

Tan et al. (2022) investigated the impact of duration for milling on CDW-based precursors and resulting geopolymers. They found that prolonged milling enhances reactivity, leading to a silicon-rich gel formation and higher strength in CDW-based geopolymers, reducing CO₂ emissions per unit strength. However, reactivity improvements diminish with longer milling, likely due to particle aggregation and surface activation. They also recommend extending milling up to 2 hours for improved reactivity and strength without diminishing returns from excessive milling.

The research made by Sahin et al. (2021) aimed to assess the viability of a 100% CDW-based geopolymer for 3D-AM without additional curing. The CDW included roof tile, glass, red clay brick and hollow brick for geopolymer production, with NaOH, Ca(OH)₂ and Na₂SiO₃ used in various combinations as activator. The study found that the geopolymer mixture initiated with 10% Ca(OH)₂ and 6.25M NaOH exhibited optimal behavior in the context of compressive strength and rheology. Na₂SiO₃ was noticed to accelerate geopolymerization but led to shortened hardening/open time, making it less suitable for 3D-AM. The conclusion drawn was that fully CDW-based geopolymers, when printed with a lab-scale printer, can be utilized for 3D-AM implementations without inclusion of any chemical additives.

In contrast to the approach taken by Sahin et al. (2021), CDW-based geopolymers were combined with recycled aggregates in the research made by Ilcan et al. (2022). The obtained results showed that geopolymer mortars designed entirely based on CDW and having sufficient compressive strength can be extruded with 3D-AM without any defects/discontinuities, retain their original form under the load of upper strata and seamlessly align with the intended printed framework.

In their study, Annapareddy et al. (2018) explored the initial and cured characteristics of cement-based formulations, encompassing PC and geopolymer (SF, GGBFS and FA + K_2SiO_3 + glass). The rheologic characteristics of these formulations were evaluated through viscosity recovery tests using a rheometer, slump evaluations and observed scrutiny of the printed samples. The results revealed that the binder based on PC exhibited better recovery of thixotropy compared to the geopolymer. This difference is likely associated with the lack of colloidal interconnection in the geopolymer and the sticky nature of the alkaline initiator. The study also effectively demonstrated the viability of incorporating recycled glass aggregates in 3D printing with two distinct binder mixtures.

Demiral et al. (2022) assessed the direction-dependent characteristics of 3D-printed geopolymer mortars made entirely from CDW materials. Their study employed a combination of CDW substances such as roof tile, glass, red clay brick, hollow brick and concrete waste sourced from distinct deconstructions areas. Geopolymerization was achieved using disparate mixture of alkaline initiators, including $Ca(OH)_2$ and NaOH and concrete waste was incorporated as a fine aggregate. The investigation revealed that the concentration of alkaline activators had a considerable impact on the performance of the geopolymer mixtures. Flexural and compressive strength tests revealed anisotropic behavior in 3D-printed geopolymer mortar specimens, with bonding between consecutive layers identified as a key factor affecting this anisotropy. Interestingly, specimens loaded in a perpendicular manner demonstrated comparable or slightly superior performance in comparison to conventionally cast specimens, showing that the bond section had limited effect on perpendicular loading. The research emphasized the possibility of diminishing the anisotropic characteristics of 3D-printed forms by improving the adhesion bond between successive layers. This improvement could be achieved through optimization of the flow characteristics and matrix performance of the geopolymer mixtures.

Munir, Afshariantorghabeh and Karki (2022) introduced a pre-treatment method for recycling CDW along with various industrial by-products such as flotation sand, fiber waste, green liquor sludge and FA. The objective of this recycling process was to generate geopolymer materials proper for 3D printing in construction. The study revealed that the economic effect and environmental implications of these recycling ways, peculiarly in terms of energy depletion, were contingent on factors like the chosen separation method, treatment line and the volume of waste refined. Ultimately, the research demonstrated that these recycled wastes could serve as sustainable substances in geopolymer concrete production, making a positive contribution to the sustainability of the building sector.

Iıcan et al. (2023) investigated the fresh properties of 100% CDW-based geopolymer mixtures, offering innovative waste upcycling solutions for sustainable construction. These mortars used roof tile, red clay brick, glass, hollow brick and concrete waste as precursors and concrete fragments as aggregates. Various mixing of $\text{Ca}(\text{OH})_2$ and NaOH were employed for activation. The study found that adjusting alkaline activator content can influence the mortars' rheological properties. Viscosity recovery performance ranged from 65% to 82% in the three interval thixotropy test (3ITT). The mixtures were extruded successfully, with some experiencing different types of failures after resting for more than 60 min. Nevertheless, apart from 15M-activated mixtures, all provide extrudability characteristics even after 120 min.

Nematollahi et al. (2019a) explored the influence of time intervals between printing on the interlayer strength, as well as the compressive and flexural strengths of the improved 3D-printed 'one-part' geopolymer with various orientations. Two distinct printing time intervals, 2 and 15 min, were employed in the printing process. The results demonstrated a significant impact of the printing time interval on the interlayer strength of the 3D-printed 'one-part' geopolymer, while its impact on the compressive and flexural strengths of the geopolymer was observed to be minimal.

Panda and Tan (2018) focused on designing and characterizing the fresh properties of geopolymer mortar tailored for 3D-CP applications. These findings are valuable for scenarios where the target printing time falls within the range of 15-20 min, as they suggest that using a higher proportion of slag can enhance buildability. The key to successful

concrete printing lies in employing a thixotropic material with an open time of 10-15 min. This allows for the deposition of a few initial layers that can start to harden, providing support for subsequent layers. To execute this process effectively, a continuous mixer is essential, enabling immediate mixing and pumping without resting periods, unlike traditional batch mixing. In summary, by taking into account the thixotropic open time effect, materials can be pre-designed to align with the total printing time and the complexity of the intended printed structure.

Researchers aim to enhance sustainability in 3D printing by integrating waste and locally sourced materials into the system. In terms of environmental sustainability, the usage of geopolymers in 3D printing offers significant benefits. Amran et al. (2022) reported that in contrast to traditional cementitious substances based on PC, geopolymers in 3D printing can reduce the carbon footprint by approximately 61% (3D geopolymer: 0.114 kg•CO₂/l vs. 3D PC: 0.296 kg•CO₂/l). Similarly, Zhong and Zhang (2022) observed a 59% reduction in CO₂ releases from a geopolymer for 3D printing, which was depended on a mixing of 50% FA and 50% GGBFS, compared to traditional cementitious substances using PC and supplementary cementing materials. It is important to note that the ingredient and sort of alkaline initiator used play a vital act in quantifying the extent of carbon footprint decline in geopolymers. Specifically, Na₂SO₄ and Sodium Carbonate (Na₂CO₃) are among the most environmentally attractive options in this regard (Valencia-Saavedra, Robayo-Salazar and Mejía de Gutiérrez, 2021).

Khan et al. (2023a) aimed to measure the environmental pros and cons of new geopolymer materials derived from CDW for 3D printing in construction. The outcomes demonstrated that geopolymer-based 3D printing had the least global warming effect, emitting 488 [kg CO₂ eq], in comparison to 595.6 [kg CO₂ eq] for PC-based structures and 533.7 [kg CO₂ eq] for equivalent traditional fabrication. The primary environmental concern, or "hot spot," recognized for geopolymer-based 3D printing was the substantial energy consumption during the mechanic procedures of waste substances, accounting for over 61% of the total global warming potential impact.

Mir et al. (2022a) conducted an environmental sustainability assessment for the production of geopolymer binders intended for 3D-AM. In this innovative approach, CDW materials,

including red tile, glass, hollow brick and red clay brick were utilized in the role of a sustainable replacement for PC in geopolymer synthesis. The aim of the study was to recognize critical hotspots within the production process or concerning raw materials. This early insight helps enhance the overall environmental performance of the process and assesses the ecological effect concerning energy consumption, water usage and waste releases. The process to create geopolymer binders from CDW involved crushing, milling/grinding and mixing, all of which consumed electrical power. The results of a life cycle impact assessment comparative study suggest that this geopolymer binder has the potency to be a more eco-friendly substitute to PC within the building industry. Table 2.1, where the data regarding the materials within the scope of the study is compared, is given below for detailed comparison.

Table 2.1. The evaluations of the environmental footprint for manufacturing 1 m³ PC 32.5 and the innovative CDW-based geopolymer binder (Mir et al., 2022a).

Material	Global warming potential (kg CO ₂ eq.)	Acidification potential (kg SO ₂ eq.)	Eutrophication potential glass (kg N eq.)	Ozone layer depletion potential (kg CFC 11eq.)	Ecotox air (CTUe.)
PC 32.5	807	1.4	0.0693	2.39E-10	17.9
CDW-based geopolymer	635	5.06	0.104	3.14E-10	12.2

In another study conducted by Mir et al. (2022b), a sensibility settlement was performed with varied compositions of CDW and alkaline initiators, including, NaOH, Na₂SiO₃ and Ca(OH)₂. The consequences showed that increasing the amount of Na₂SiO₃ and Ca(OH)₂ reduced the environmental impacts related to acid attack and reduction in the ozone layer, as measured by acidification and ozone layer depletion potential. This suggests that utilizing NaOH alone as the alkali initiator is a more environmentally preferable option for addressing concerns related to acid attack and ozone layer depletion. Nevertheless, for other environmental impacts like global warming potential, eutrophication potential and ecotox air, the effects increased when Na₂SiO₃ and Ca(OH)₂ were added as binary and ternary

mixtures. The combination of NaOH and Ca(OH)₂ as alkali initiators was deemed less sustainable compared to using NaOH alone. However, it is essential to consider both environmental impact and product performance and quality, as the single NaOH activator may not provide the desired mechanical characteristics.

In the study by Mir et al. (2023), a life cycle assessment, spanning from cradle to gate, was conducted to assess the environmental footprint of fresh formulated self-healing geopolymers exclusively sourced from CDW. The objective was to optimize the environmental sustainability of both the production process and the final product. These geopolymers are developed to replace PC in traditional concrete, primarily due to the significant global warming impact associated with PC production, which generates substantial CO₂ emissions. The precursors used for these geopolymers are waste materials like glass, red clay brick, concrete, hollow brick and roof tile waste. Additionally, concrete aggregate which is recycled used as the aggregate material. The study investigated six different scenarios based on various mixture compositions. The results of the life cycle assessment indicate that scenarios involving CDW/NaOH-Ca(OH)₂ and CDW-Slag/NaOH-Ca(OH)₂ perform the best in terms of reducing environmental impacts. These scenarios are promising for developing more sustainable construction materials with lower environmental footprints.

Khan et al. (2023b) assessed the suitability of newly developed geopolymer materials sourced from CDW for 3D printing in construction. They also assessed the efficiency of a computational model developed for 3D printing of structures in the built environment. The results demonstrated that the geopolymer materials they developed were indeed proper for 3D printing. They found close agreement in outcomes and high reproducibility, indicating the reliability of the geopolymer materials in the printing process. Additionally, their numerical model proved to be an effective tool for predicting structural failures in various designs. Consequently, this way can be employed to assess whether structure is buildable or not before actual 3D printing, offering substantial time and cost savings in construction projects.

2.3. Interlayer Bond Strength

Ensuring that these materials meet the strength standards necessary for replacing ordinary PC is crucial in the realm of 3D-CP. The interlayer bond strength stands out as one of the most crucial benchmarks in 3D-CP. Similar to material designs in other 3D printing processes, it is well established that process parameters and printing conditions can exert a considerable influence on the bond strength of 3D-printed concrete (Babafemi et al., 2021). In the examinations conducted in this context, it has been observed that a variety of test ways are used to evaluate the bond strength of samples produced through the additive manufacturing method.

2.3.1. Macroscale Characterization

The existing literature indicates that various tests utilized in 3D-CP are adapted from different interlayer test ways originally advanced to measure the interlayer strength between old and new concrete. Each of these test methods comes with its own set of advantages and disadvantages. For instance, direct tensile tests are easily implementable both in the field and in the laboratory. However, results might be adversely affected by eccentricity. On the other hand, shear test methods can unintentionally impede the interlayer bending moment (Babafemi et al., 2021).

Zareiyan and Khoshnevis (2017a) proposed that the selection of a test way should consider loading conditions similar to the stress conditions experienced by the 3D-printed structure. Consequently, interlayer strength tests for the printed structure are often configured in the printing aspect, namely perpendicular, parallel and lateral. The measurement methods for interlayer bond strength provide insights into the mechanical aspects at the macrostructure level (Babafemi et al., 2021).

If it is necessary to categorize the tests performed to determine the interface bond strength, the first category can be expressed as tensile, direct tensile and splitting tensile, which are also mostly the preferred method. The second one stands out as direct shear methods such as L-shaped shear, single-sided shear and bi-faceted shear. The third one evaluates bond strength under a stress condition combining shear and compression (Momayez et al., 2005). In this context, it has been observed that, tension (Momayez et al., 2005), uniaxial tension (Ye et al., 2021; Sanjayan et al., 2018), splitting tensile (Zareiyan and Khoshnevis, 2017a;

Wolfs, Bos and Salet, 2019), uniaxial compression (Kloft, et al., 2020; Nerella, Hempel and Mechtcherine, 2019), compression test with iron blades at the interlayer region of the consecutive layers (Keita et al., 2019), compression test with iron angles (Keita et al., 2019), bending (Chu, Li and Kwan, 2021), three-point bending (Kloft et al., 2020; Nerella, Hempel and Mechtcherine, 2019), interface shear bonding (Wang et al., 2020; Liu et al., 2019), shear (Wang et al., 2020; Ma et al., 2020), bifacial direct shear (Momayez et al., 2005), splitting by wedge-load equipment at the interface (Tschegg and Stanzl, 1991) and torsion shear (Silfwerbrand, 2003) bond strength tests have been done in the literature.

Investigations on the determination of interfacial bond strength have also been observed using non-destructive techniques such as the multi-element array ultrasonic pulse method (Helsel et al., 2021). It is remarkable that the consequences from these distinct tests vary considerably and that similar variations in results are noticed for cast samples. Beushausen and Alexander noted that the tensile test result was different from the shear test result (2008), while Momayaz et al. (2005) noted that the slant shear test method produced eight times higher results than the tensile and splitting tensile tests. It was found by Abu-Tair, Rigden and Burley (1996) that the flexural test offers low efficiency as the connected surface area under load is small in comparison to the sample volume and only a very small portion of the bonded plane is exposed to maximum stresses. It was concluded that shear tests were more efficient in this regard.

Apart from the interface bond strength test methods categorized above, it has been determined that the diagonal tension test method is preferred by some researchers to determine the bond strength in masonry structures (Corinaldesi, 2009; Dizhur and Ingham, 2013; Bolhassani et al., 2015). It has also been observed that the triplet shear test is preferred by some researchers for determining the shear strength in masonry structures (Corinaldesi, 2009; Alecci et al., 2013; Lan et al., 2020).

2.3.2. Microscale Characterization

In contrast to the macro-scale tests, micro-scale examinations aim to evaluate the mechanical performance as well as to comprehend the variables influencing the mechanical behavior at the contact interface. Therefore, interface properties are investigated at micro scale using

XCT, SEM, MIP, Energy Dispersive Spectroscopy (EDS), XRD, optical microscope, flatbed scanner and nano-indentation (Babafemi et al., 2021).

The literature review suggests that researchers often have the flexibility to choose mechanical test methods (including flexural, tensile, compression and shear) based on their preferences, and many studies lack explicit justifications for the chosen test method. Determining bond strength lacks a standardized procedure, and establishing a direct tensile test without eccentricity, ensuring that each tested sample breaks at the interface, is considered challenging. Moreover, it's noted that some researchers utilize multilayer specimens for observing bond strength measurement, whilst some prefer bilayer specimens. In general, studies on 3D-AM and the characteristics of 3D-printed structures indicate that the bond strength of specimens can be influenced by the manufacturing methodologies, anisotropic behavior, printing time intervals and open-time performance. However, based on the authors' best knowledge, there is a lack of information about the behaviors and characteristics of CDW-based geopolymer prepared via 3D-AM in terms of time-dependent printing, material aging (time the mixture waits in the pump) -dependent printing, and printing/testing directions.

The unique aspect of this research lies in its extensive experimental investigation, thoroughly evaluating the bond performance of mixtures based on both WPC and CDW. Various testing methods are employed to provide a detailed examinations. In that context, this thesis study focused on producing both WPC-based and CDW-based geopolymers using components through 3D-AM technology while emphasizing the significance of directions-dependent properties (anisotropy performance), printing time interval and material aging time performance of specimens and manufacturing methodologies. Since there is no such comprehensive study in the literature, 3D-printed WPC-based and CDW-based geopolymer mortars were investigated through a sequence of examinations, encompassing compressive strength, triplet shear and direct tensile testing at various printing time interval (0, 15, 30 and 60-min); diagonal tension and triplet shear testing at different material aging time (0, 30, 60-min and for CDW-based geopolymer mixture also 120-min), with different manufacturing methodologies (e.g., mold-cast, vertical- and horizontal-printed). The printable WPC-based mixture was obtained using CEM I 52.5R type cement along with three distinct admixtures (SP, VM and R). The CDW-based geopolymer mixture comprised not only clay-derived

masonry components such as red clay bricks (RCB), hollow bricks (HB), roof tiles (RT), along with concrete (C) and glass (G) waste, but also industrial waste-based blast furnace slag (BFS). The mixture was triggered using a mixture of Ca(OH)_2 and NaOH in certain proportions. With this thesis study, the combined evaluation of the impact of manufacturing methodology, printing time interval and material age on interlayer bond strength will be addressed. The applicability of test methods commonly used in the context of masonry structures will be observed on samples produced by 3D-AM, contributing valuable insights to the literature.

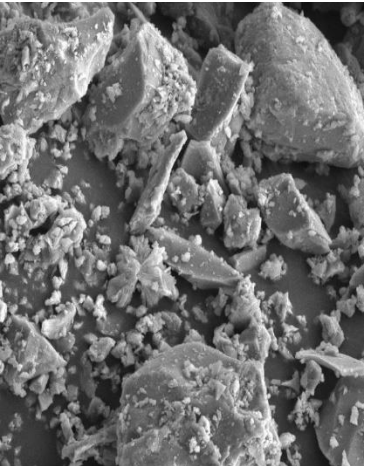
3. EXPERIMENTAL PROGRAM

3.1. WPC-Based Mixture

3.1.1. Materials

In the mixture design, the main binder material employed was WPC of CEM I 52.5R type, which fully complied with the EN 197-1 cement standard. Table 3.1 presented the chemical structure, physical characteristics and SEM image of WPC. To develop the mortar phase, quartz sand (QS) was incorporated into the mixture as a fine aggregate. D_{max} of the sand was set at 2 mm, considering the risk of clogging during printing.

Table 3.1. Details regarding to the binder phase.

CEMI 52.5R		SEM Image
Chemical Composition	(%)	
SiO₂	22.45	
Al₂O₃	3.81	
Fe₂O₃	0.30	
CaO	65.71	
Na₂O	0.31	
MgO	0.68	
SO₃	2.73	
K₂O	0.29	
TiO₂	0.07	
P₂O₅	0.04	
Cr₂O₃	0.01	
Mn₂O₃	0.01	
Loss on Ignition	3.59	
Specific Gravity	3.15	

To adjust the fresh properties in favor of 3D-printability, three different admixtures were used. Polymer-based SP with commercial code EBA 1447, obtained from “BASF Construction Chemicals”, was used in the mixture to contribute to better workability, increased slump and improved performance of the final hardened concrete, while

maintaining or improving its mechanical properties. Methyl cellulose-based Culminal brand VM was added to the mixture to strengthen buildability and workability performance and prevent sagging. Peramin brand citric acid based R supplied by “ATA Kimya” company was used to increase open time performance and reduce rapid loss of workability. The details about these admixtures are presented in Table 3.2.

Table 3.2. Admixtures used in this study and their details.

Name of additive	Detailed informations
SP	<ul style="list-style-type: none"> • polymer- based • maximum drying loss 2% • unit weight 300-600 kg/m³ • density 1.184-1.244 kg/l • powder form • yellowish colour
VM	<ul style="list-style-type: none"> • methyl cellulose-based • <100µm • purity of 92% • powder form • whitish colour
R	<ul style="list-style-type: none"> • citric acid- (C₆H₈O₇) based • purity of 99.96% • powder form • whitish colour

3.1.2. Mixture Proportion and Preparation

For providing the necessities of the 3D-AM operations, mixture designs were carried out, aiming to achieve a balance between high buildability and extrudability. In this context, as a result of the preliminary studies, a mixture with a flow diameter of 150 mm was selected to achieve a printable blend resembling the geopolymer composition. The mixture contents are presented in Table 3.3. During the mixture design process, 0.35 w/b and 1.25 aggregate-to-binder (a/b) were determined. The mixture demonstrated printability for up to 60-min, after which it began to exhibit clogging issues and defects on the printed surface.

Table 3.3. Mixture proportion of WPC-based 3D-printed object.

Mixture proportion (for 1000g Binder)					
WPC	QS	Water	SP	VM	R
1000	1250	350	1.6	2.0	1.1

The mixture for 3D printing was formulated and mixed employing a pan-type mixer (Figure 3.1-a). The mixing process involved three phases: (i) blending all dry ingredients for 2 min, (ii) adding water to the mixing container within a min, and (iii) further mixing the mixture for an additional 2 min. Subsequently, the prepared mixtures were transferred to the pump (Figure 3.1-b) for the extrusion process. After producing specimens in different configurations, each specimen was initially cured in a water tank for a period of 3 days, after which they were transferred to ambient circumstances (relative humidity of $50 \pm 5\%$ and temperature of 23 ± 2 °C) and left to cure for 28 days.



a)



b)

Figure 3.1. Pan-type mixer (a) and pump (b) used in the study.

3.2. CDW-Based Geopolymer Mixture

3.2.1. Materials

Waste materials including CDW-based RT, RCB, HB, C and G were utilized as precursors in the synthesis of geopolymer mortar. CDW was sourced from various demolition sites in Türkiye, initially crushed and then milled into powder forms using a jaw crusher and a ball mill, respectively (Figure 3.2). Additionally, BFS was included in the blend formulation to enhance mechanical properties. BFS was brought from the Hatay-Iskenderun iron-steel plant. The morphological properties were examined through SEM at 12 kV under suction conditions with a working distance of 10 mm after the collection and preparation of the precursors. Digital and SEM visuals of CDW- and industrial waste-based precursors shown in Figure 3.3. Chemical composition determination was performed using X-ray fluorescence (XRF) tests on the previously dried precursors (Table 3.4). Particle size distribution (PSD) analysis of the precursors was conducted utilizing the laser diffraction method, which had a size range sensibility of 0.02–2000 μm (Figure 3.4).



a)



b)

Figure 3.2. Jaw crusher (a) and ball mills machines (b) used in the study.

Table 3.4. Composition and density characteristics of CDW-derived source materials.

Oxides, %	HB	RCB	RT	G	C	BFS
SiO₂	39.7	41.7	42.6	66.5	31.6	32.1
Al₂O₃	13.8	17.3	15.0	0.9	4.8	11.2
Fe₂O₃	11.8	11.3	11.6	0.3	3.5	0.6
CaO	11.6	7.7	10.7	10.0	31.3	36.1
Na₂O	1.5	1.2	1.6	13.6	0.45	0.3
MgO	6.5	6.5	6.3	3.9	5.1	5.6
SO₃	3.4	1.4	0.7	0.2	0.9	1.2
K₂O	1.6	2.7	1.6	0.2	0.7	0.8
TiO₂	1.7	1.6	1.8	0.1	0.2	1.1
P₂O₅	0.3	0.3	0.3	0.0	0.1	0.0
Cr₂O₃	0.1	0.1	0.1	0.0	0.1	0.0
Mn₂O₃	0.2	0.2	0.2	0.0	0.1	1.5
Loss on ignition	7.8	8.0	7.5	4.3	21.1	9.5
Specific gravity	2.89	2.81	2.88	2.51	2.68	2.74




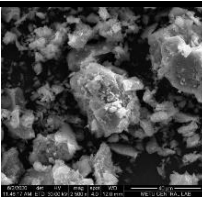



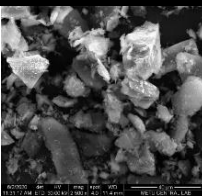



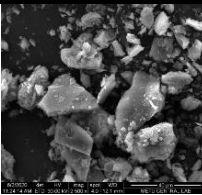



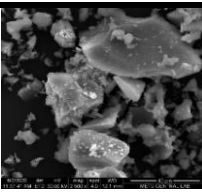



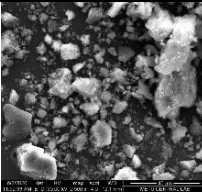

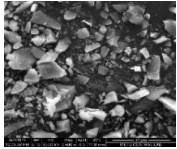
CDW-based precursor	Initial collection	Crushed	Ball milled	SEM images
HB				
RCB				
RT				
G				
C				
Industrial waste-based precursor	Powder phase			SEM images
BFS				

Figure 3.3. Digital and SEM images of the precursors.

Observations from the SEM images (Figure 3.3) indicate that CDW-based precursors and BFS possess an angular shape, a result of the manufacturing processes applied. The chemical composition in Table 3.4 reveals that clay-originated CDW, such as RCB, RT and HB, share similar contents rich in SiO₂, Al₂O₃, Fe₂O₃ and CaO. G exhibits high amounts of SiO₂, Na₂O, and CaO, while C is primarily consisted of CaO and SiO₂. Notably, C has a higher loss on ignition value compared to other precursors due to the deterioration of hydroxyl and calcium carbonate (CaCO₃) compounds. The PSD results (Figure 3.4) show that, although clay-originated precursors and BFS exhibit similar and finer PSD, C and G have a coarser grain size. These variations in the PSD of CDW materials may be attributed to distinction in density, pore structure, grindability index and hardness.

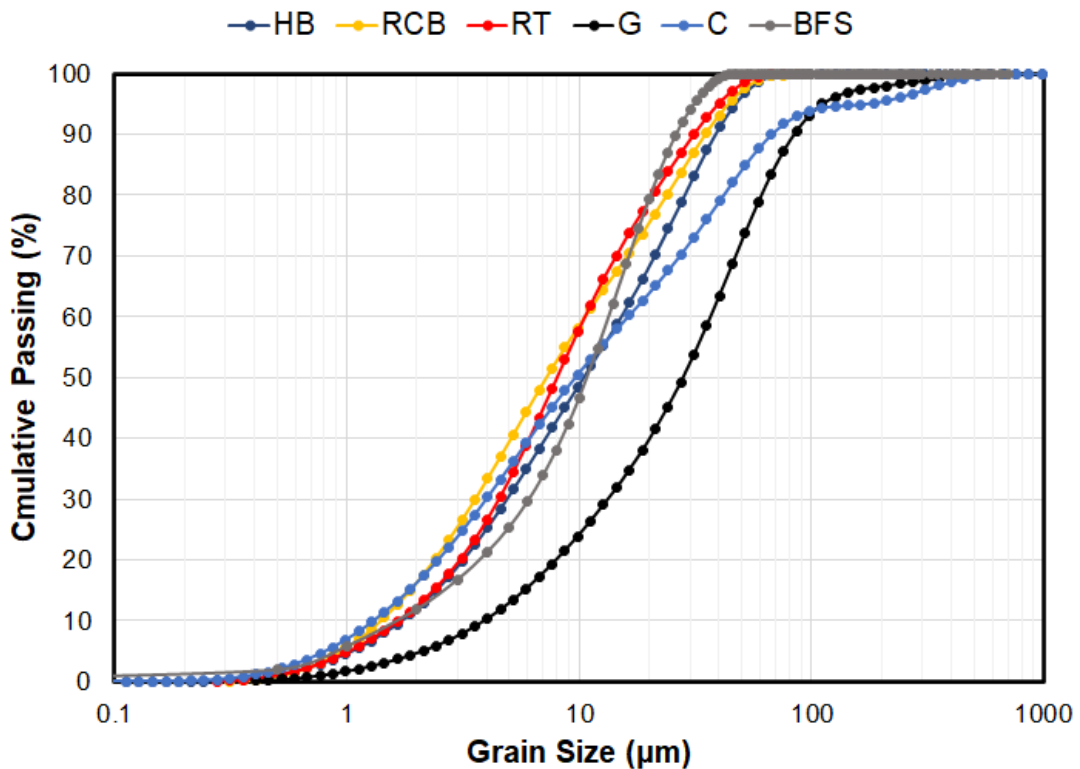


Figure 3.4. Particle size distribution of the precursors.

In the mixture, recycled concrete aggregate (RCA) with a D_{max} of 2 mm was used in geopolymer mixtures to produce geopolymer mortars instead of natural aggregate. The aggregate size used in the mixture was limited to 2 mm in order not to endanger the pumping function of the laboratory-scale 3D-printer. RCAs were produced by crushing concrete rubbles with the jaw crusher having an open side setting of approximately 2.5 mm and

sieving through the sieve having a 2.0 mm opening. Obtained RCAs were incorporated directly into the mixtures without the treatment process, considering generating a general solution for feasibly utilizing those wastes (Figure 3.5-a).

Moreover, for the activation of BFS-included CDW-based geopolymer mixture, Ca(OH)_2 and NaOH were employed. Ca(OH)_2 , widely used in various industries, results from the careful mixture of CaO with water. In geopolymerization systems, it plays a crucial role by increasing the alkalinity of the reaction medium, potentially speeding up reactions and encouraging the formation of additional hydration products, such as C-S-H or Calcium-Aluminate-Silicate-Hydrate (C-A-S-H), due to its calcium substance (Temuujin, Van Riessen and Williams, 2009). Ca(OH)_2 can strategically act as an supplementary calcium source to enhance the engineering characteristics of materials by promoting the formation of hydration products, contributing to a denser structure. Its application can be in the form of a suspension or powder, facilitating the activation of geopolymer response mechanism. The Ca(OH)_2 used in this study (Figure 3.5-b) was supplied by “Tekkim Kimya San. ve Tic. Ltd. Şti.”, and detailed information is presented in Table 3.5.

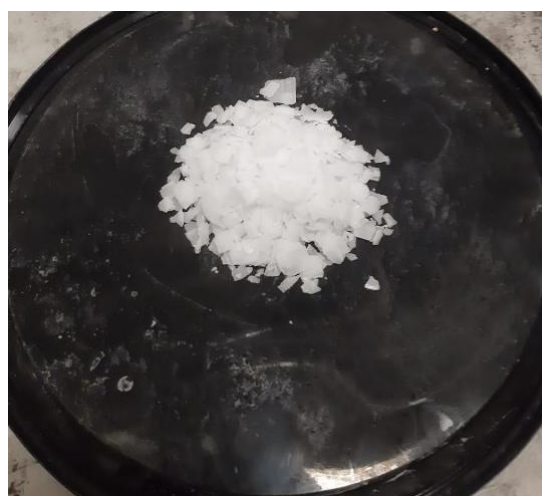
NaOH is a fundamental component in the chemical industry. It possesses moisture-absorbing properties and appears as a white substance. Known for its easy solubility in water, it exhibits a smooth, slick and soap-like structure and is available in both solid and liquid forms. The electrolysis of a sodium chloride (NaCl) solution is the process through which NaOH is produced, accompanied by the release of chlorine gas and the vaporization of the water content in the solution. Upon interaction with water, it undergoes a rapid and exothermic reaction. During the geopolymerization stage, this reaction releases Na^+ and $(\text{OH})^-$ ions. The $(\text{OH})^-$ ions contribute to a reduction in the pH of the medium and an augmentation in alkalinity. As highlighted earlier, high alkalinity plays a significant role in initiating geopolymerization and facilitating the dissolution of aluminosilicate precursors. The NaOH employed in this study (Figure 3.5-c) supplied by “Koruma Klor Alkali San. Tic. A.Ş.” and details about it is outlined in Table 3.5.



a)



b)



c)

Figure 3.5. Images of RCA (a), powder Ca(OH)_2 (b) and flaked NaOH (c).

Table 3.5. Detailed informations about Ca(OH)_2 and NaOH that used in this study.

Name of activator	Detailed informations
Ca(OH)_2	<ul style="list-style-type: none"> • solid phase • molecular weight 74.09 g/mol • purity of 87% • whitish colour
NaOH	<ul style="list-style-type: none"> • white flake form • density 2.12 g/m³ • minimum 98% NaOH, maximum 0.4% Na_2CO_3, 0.1% NaCl and maximum 15 mg/kg iron

3.2.2. Mixture Proportion and Preparation

The 3D-printable CDW-based geopolymer material used in this study was decided giving consideration to the previous studies conducted by the same laboratory. The dry foundational blend included 60% of clay-based wastes such as RCB, RT, and HB, along with 20% of BFS, 10% of C and 10% of G. Considering the similarity of chemical composition and PSD of the clay-originated wastes, their usage rates in the dry blend were decided to be equal at a level of 20% for each. As in the prior researches (Demiral et al., 2022; Ilcan et al., 2022; Ilcan et al., 2023), G and W content was specified as 10% in favor of Si/Al balance of the medium during geopolymerization. To improve the mechanical characteristics of the geopolymer blend based on CDW, BFS was incorporated at a ratio of 20% by considering the ion balance in the reaction medium. For the mixture, the w/b was 0.33 (by weight), while the a/b was chosen as 0.35 considering the ease of extrudability and the higher water demand associated with RCAs. To activate dry-blend mixture, NaOH and Ca(OH)₂ were employed. The concentration of NaOH was chosen as 10 M, and employment of Ca(OH)₂ was decided to be 4% of total precursors by weight. The created BFS incorporated CDW-based geopolymer mortar was a 3D-printable mixture by showing proper printability and buildability performance without any kind of additional chemical admixtures such as VM, SP, etc., apart from the alkaline activator. Table 3.6 includes details regarding the proportions, flow diameter and setting times of the formulated CDW-based geopolymer mixture.

Table 3.6. Details of geopolymer mortar mixture.

Precursors (1000g)						Alkaline Activators				Agg.	W/B	Flow Diameter (cm)	Initial- Final Setting Time (min)
CDW- Based Precursors					Industrial Waste- Based Precursor BFS	NaOH		Ca(OH) ₂		RCA (g)			
HB	RCB	RT	G	C		M	g	%	g				
200	200	200	100	100	200	10	132	4	40	350	0.33	15.0-15.5	165-505

The preparation of the geopolymer mixture started with producing of the NaOH solution by dissolving the solid NaOH flakes in tap water with the help of a stirrer in the predetermined proportions. As the dissolving reaction of NaOH in water is exothermic, the bottle used for the preparation of the solution was chosen steel-made and to prevent the rapid setting of the mixture because of accelerated reaction due to the high temperature generated, the ready solution was kept at the ambient circumstances to cool down to the level of room temperature. All solid components, comprising precursors, aggregates and $\text{Ca}(\text{OH})_2$, were blended for 2 min in a pan-type mixer. Subsequently, the cooled NaOH solution was slowly introduced into the rotating mixer to achieve a uniform mixture, and the blending process persisted for an additional 5 min. The resultant mixture was then moved to the pump. Following the preparation of specimens in various configurations, each specimen underwent curing under ambient conditions (relative humidity of $50 \pm 5\%$ and temperature of 23 ± 2 °C) for a duration of up to 28 days.

3.3. Specimen Preparation

In the scope of this study, cast specimens and horizontal and vertical 3D-printed specimens in different dimensions were produced considering the varied testing methodologies and standards followed to investigate the effects of 3D-printing- and material-related parameters and manufacturing methodologies on the performance of the WPC-based and CDW-based geopolymer mixtures.

Figure 3.6-a illustrates the specifics of the 3D printer employed in this study. The optimal printer speed, determined from preliminary trials and based on the pump's flow rate, was set at 60 mm/sec. A rectangular nozzle was utilized for the printing process. Figure 3.6-b and Figure 3.7 provide a comprehensive visual overview of the study's sample dimensions through both schematic representations and actual depictions.

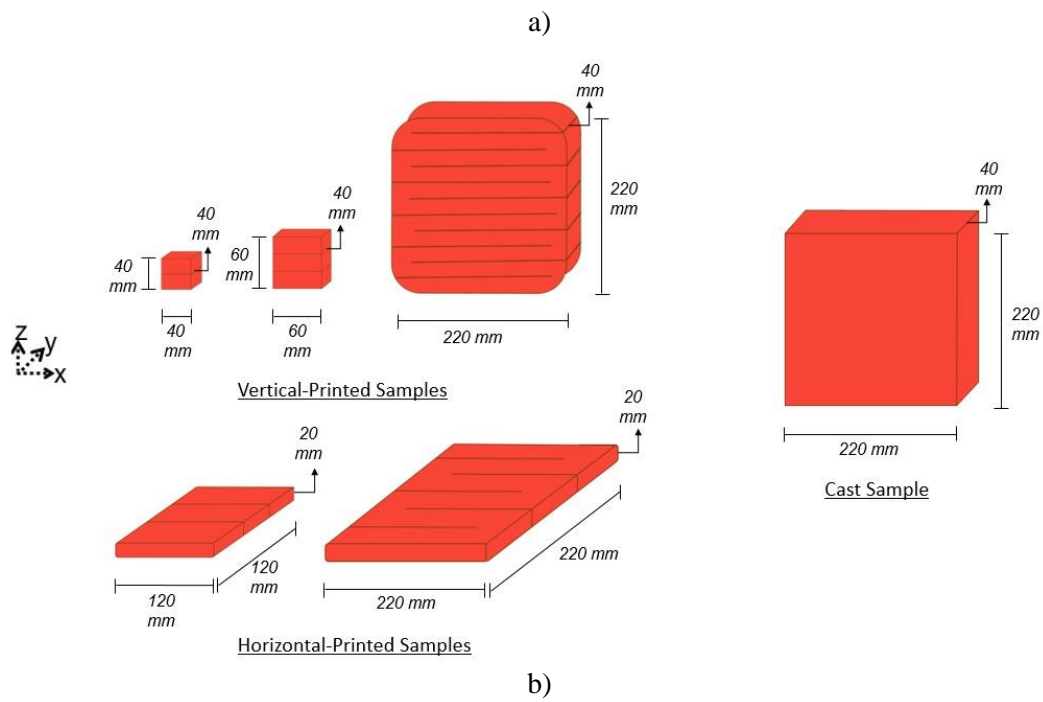
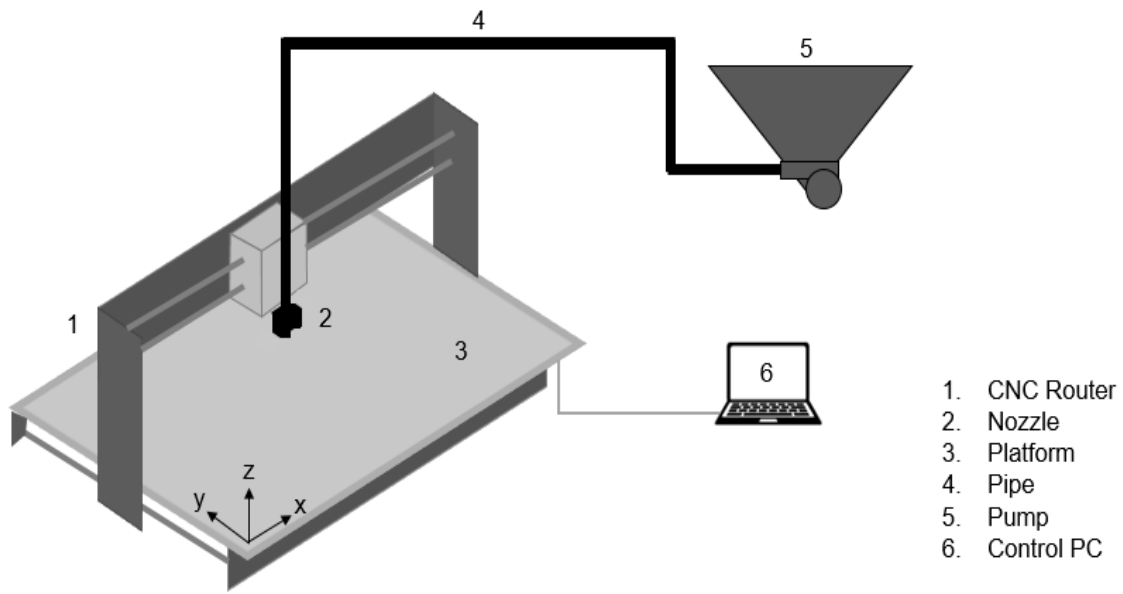


Figure 3.6. Detailed parts of 3D printer (a) and schematic depiction of samples printed in 3D (b).



a)



b)



c)



d)



e)

Figure 3.7. Real time view of printed samples for different tests (a,b,c,d) and mold-cast samples (e).

For the preparation of the cast specimens, 40×220×220 (width×length×height) mm prismatic mold was used and mixtures were placed in pre-oiled molds with the help of a vibration table. For the 3D-printed specimens, the 2-layered, 3-layered and 11-layered samples with the dimensions of 40×40×40 mm cubic, 40×60×60 mm prismatic and 40×220×220 mm prismatic specimens were produced through the vertical printing direction via a lab-scale gantry type 3D printer. While 2-layered cubic and 3-layered prismatic specimens were obtained by extracting them through the cutting process of freshly layered filaments with the thin fishing line according to the desired dimensions (Figure 3.8), 11-layered specimens were directly printed without applying any process. In addition to vertical-printed specimen (XZ plane), 20×220×220 mm and 20×120×120 mm prismatic specimens were printed through the horizontal printing direction (XY plane) without applying any extraction process. The details regarding the 3D printer (100x100x40 cm [width × length × height] effective printing area), mortar conveying pump (a screw pump with a capacity of 20 liters and capable of generating pressure up to 25 bar) and printing parameters are the same as those in the studies by Sahin et al. (2021), Ilcan et al. (2022) and Demiral et al. (2022). This study explored the impact of the printing time interval and material aging on the performance of 3D-printed specimens. The printing time intervals of 0, 15, 30 and 60-min were thoughtfully selected based on a comprehensive review of existing literature studies and careful consideration of the elapsed time required between two consecutive layers during real-scale 3D-printing applications (Sanjayan et al., 2018; Van Der Putten, De Schutter and Van Tittelboom, 2019). The material aging intervals of 0, 30 and 60-min (for CDW-based geopolymer mixture, also 120-min aging) were selected based on the elapsed time required for workability loss and setting time. The aim was to closely observe and analyze the material's behavior at these specific time points, as they are critical stages in its aging process.



Figure 3.8. The freshly printed mixtures and the subsequently extracted specimens.

3.4. Testing Methods

3.4.1. Compression Test

The samples printed with varied printing time intervals, representing the time elapsed between two successive layers, underwent compressive strength testing in three different directions to explore the impacts of printing time intervals on anisotropic performance. In this context, 2-layered samples having a dimension of 40×40×40 mm, which were printed at varied printing time intervals including 0, 15, 30 and 60-min, were tested through perpendicular, parallel and lateral directions as shown in Figure 3.9. To ensure a consistent pressure area for each sample, plates measuring 40×40 mm were positioned on the top and bottom parts of the samples during the testing procedure. Vertical-printed samples were exposed to compressive strength tests with a hydraulic test machine (Figure 3.10), which has a 150-ton capacity, with 0.9 kN/s loading rate. Four replicates of each specimen underwent testing, and the average strength values were recorded. To assess the means and standard deviation, a statistical analysis was conducted based on the sample results. The comparison of the outcomes was accomplished through one-way ANOVA analysis.

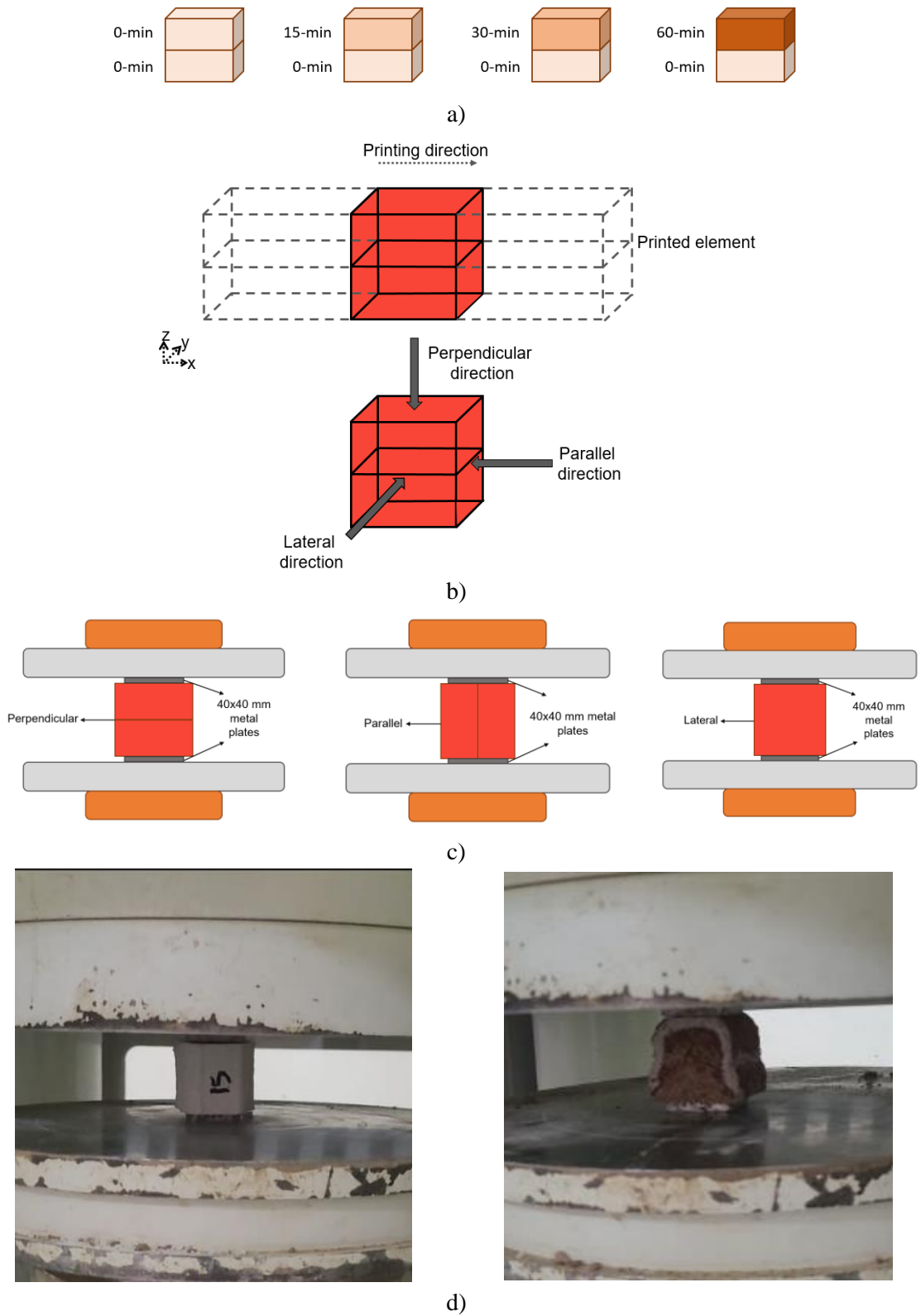


Figure 3.9. Schematic depiction of printing time intervals (a), printing directions (b), compressive strength loading details (c) and representative images from experiments (d).

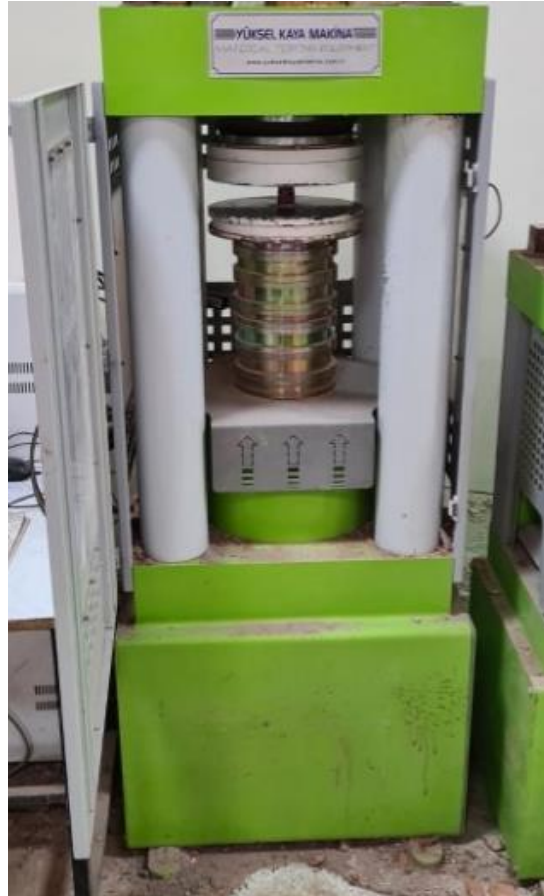


Figure 3.10. Compressive strength test machine.

3.4.2. Direct Tensile Test

Two-layered specimens printed at various printing time intervals underwent a direct tensile strength test following the approach outlined by Nematollahi et al. (2019b) to investigate the strength of the interface between the successive layers and the influence of printing time intervals on the bond strength. In this context, 2-layered samples having a dimension of $40 \times 40 \times 40$ mm, which were printed at printing time intervals of 0, 15, 30 and 60-min (Figure 3.9-a), were tested with a displacement-controlled electromechanical testing device (Figure 3.11). To conduct the test on the specimens, T-shaped metal plates, produced in Hacettepe University Laboratories (Figure 3.12-a), were affixed to the lower and upper parts of the printed cube specimens that has 40 mm dimension, five days prior to the testing day. An epoxy-based adhesive was used to ensure the required adhesion between the plate and the sample. On the test day, the T-plates adhered to the samples were attentively inserted into the single-hole metal plate (Figure 3.12-b) to avoid any eccentricity during the test, so that the specimens were fixed to the test machine and subjected to direct tensile stress as shown

in Figure 3.13. The tensile capacity of the vertically printed samples was assessed by dividing the force at fracture by the cross-sectional area under the tensile load. The mean strength results of the tested four replicates were calculated. An analysis of the results was conducted, comparing the outcomes using one-way ANOVA.



Figure 3.11. Displacement controlled test machine.

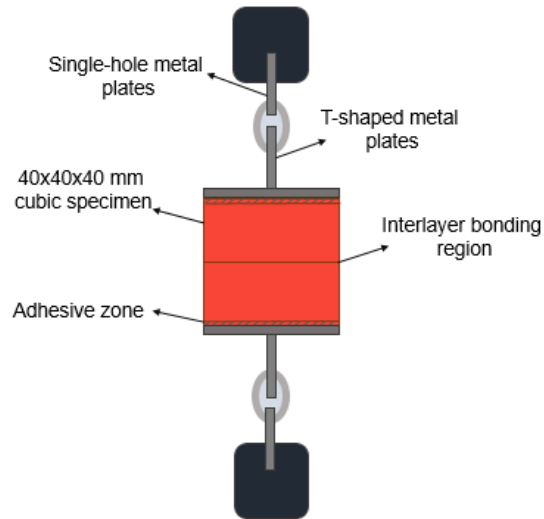


a)



b)

Figure 3.12. Schematic depiction of T-shaped (a) and single-hole metal-plates (b).



a)



b)

Figure 3.13. Schematic depiction of direct tensile test (a) and representative images from experiments (b).

3.4.3. Triplet Shear Test

The triplet shear test provides the determination of the in-plane initial shear strength (i.e., the shear strength excluding the contribution of friction) at the horizontal bearing joints of the sample subjected to a shear load. Samples are subjected to shear effect until the fracture (TSI, 2002). Considering 3D-AM as a masonry structure due to its layered nature, inspiration was taken from the relevant standard to evaluate the applicability of the triplet shear test used in masonry structures. By taking the standard into account, it was decided to produce

specimens having a dimension of 40×60×60 mm (for vertical printing) and 20×120×120 mm (for horizontal printing).

To investigate effects of printing time intervals and material aging time performance of the mixture, specimens were vertically-printed in two approaches. In the first approach (Figure 3.14-a), specimens were printed with printing time intervals of 0-15-30-60 min to exhibit the effects of elapsed time between two successive layers on the mechanical capacity of the mixture. However, specimens were printed with the mixture prepared immediately after the mixing procedure (0-min) and 30-60 min aged aged-(for geopolymer material, also 120-min) mixture without any time interval between the consecutive layers to present material performance over time, in the second approach (Figure 3.14-b,c). In addition to that, horizontal-printed specimens prepared with fresh mixture without any printing time interval were tested to determine the impact of manufacturing methodologies on the performance of the CDW-based geopolymers.

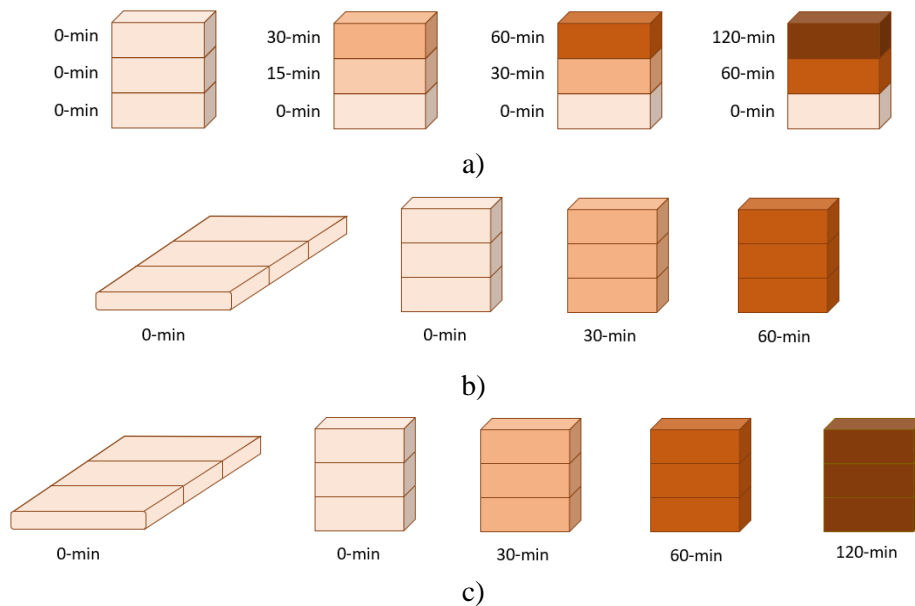
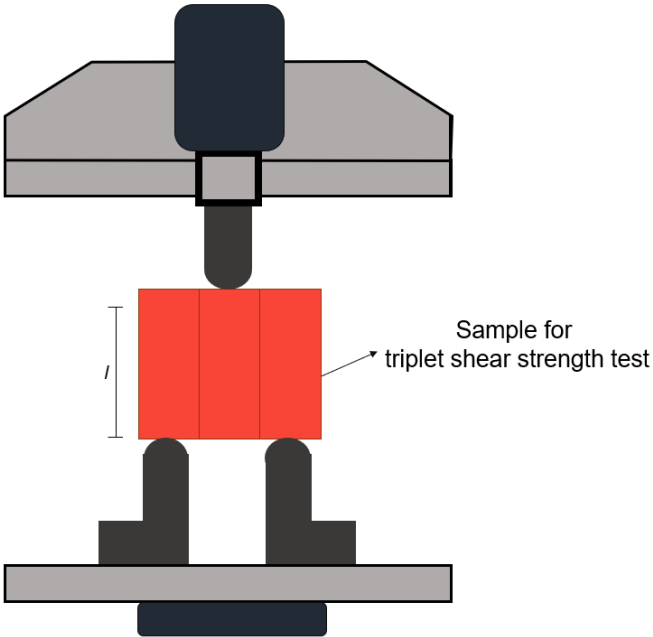


Figure 3.14. Schematic depiction of WPC- and CDW-based specimens printed at different time intervals (a), WPC-based specimens printed at different aging time (b) and CDW-based geopolymer specimens printed at different aging time (c).

The prepared specimens were tested from 3 points by using universal displacement-controlled test machine (Figure 3.11) as shown in Figure 3.15 with an applied rate of 25 N/s.

The four replicates for each approach were tested, and the outcomes were subjected to an averaging process. The acquired results were compared through the application of one-way ANOVA analysis.

Additionally, the study involved the observation of crack propagation and the fragments resulting from these cracks. This was accomplished by visualizing 3D-printed specimens, followed by the processing of 3D image representations of the cracked surfaces using specialized image processing software, specifically ImageJ for surface examination.



a)



b)



c)

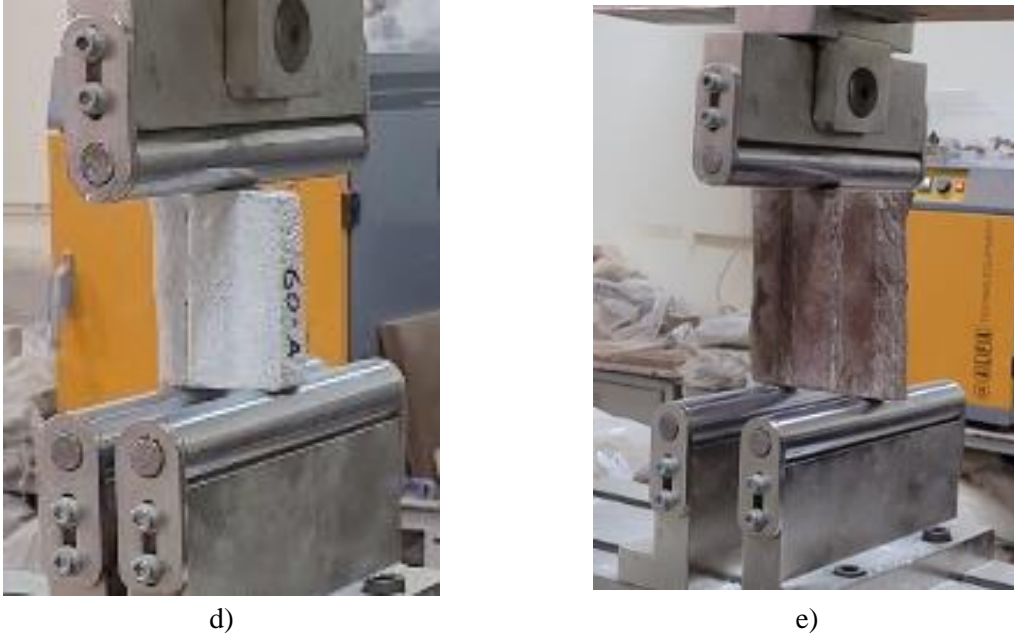


Figure 3.15. Schematic depiction of triplet shear test (a) and representative images from the experiment (b,c,d,e).

The value of F_{voi} (triplet shear strength, N/mm²) is calculated using the following equation,

$$F_{voi} = \frac{F_{i,max}}{2 * A_i} \quad (1)$$

Where $F_{i,max}$ (N) is the maximum shear load, and A_i (mm²) is the cross-sectional area: A_i is the area calculated with the equation below using the dimensions determined as w_1 (width, mm), w_2 (width, mm), and their average, the w_{av} , and l (length, mm) below.

$$A_i = l * w_{av} \quad (2)$$

3.4.4. Diagonal Tension Test

ASTM E519-02 (2002) enables replicating the pure shear stress condition of the wall by exerting diagonal forces on a square wall. This replicates the impact of vertical and horizontal mortar joints in masonry. As in the triplet shear test, the strength values of the specimens produced with 3D-AM were calculated by taking inspiration from the diagonal tension test used in masonry structures. The test was conducted via a displacement-controlled electromechanical testing device (Figure 3.11) with a loading speed of 0.05 mm/s.

The approach adopted by ASTM was preferred in this study, and the relevant calculations were made using the formulas below.

$$A_n = \left(\frac{l + h}{2}\right)w \quad (3)$$

$$f_t = 0,707 \frac{P_{ult}}{A_n} \quad (4)$$

Where, A_n is the area (mm^2), l is the length (mm), h is the height (mm), w is the width (mm); P_{ult} is the ultimate load (N), f_t is the diagonal tension strength of the specimen (N/mm^2).

Schematic representation of cast ($40 \times 220 \times 220$ mm), horizontal-printed ($20 \times 220 \times 220$ mm) specimens produced with freshly prepared mixture (0-min) and, vertical-printed specimens ($40 \times 220 \times 220$ mm) produced with fresh (0-min), 30 and 60-min aged mixture (for geopolymer material, also 120-min) shown in Figure 3.16.

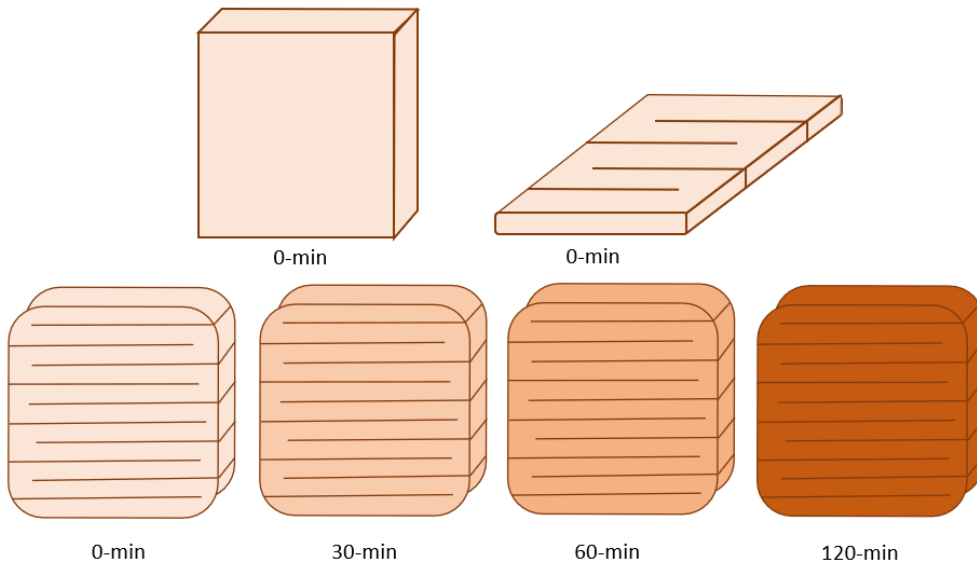
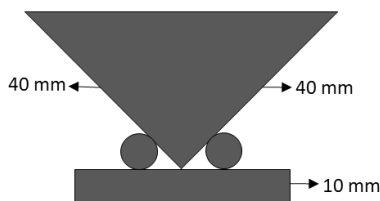
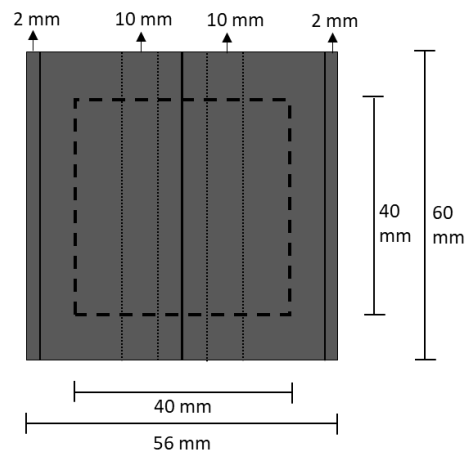


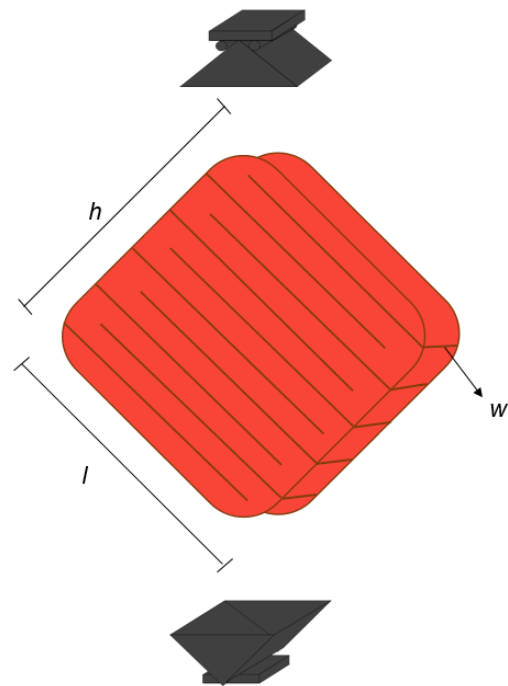
Figure 3.16. Schematic depiction of WPC- and CDW-based geopolymer specimens printed at different aging times.

To transfer the load in the diagonal tension test, a steel head was used to support the upper and lower parts of the samples. The head sizes were decided according to ASTM E519-02

(2002) and produced in Hacettepe University Laboratories (Figure 3.17-a). For the samples to be subjected to diagonal tension test (Figure 3.17-b), fast-setting plaster (approximately 25 MPa) was used to connect the steel head and sample to prevent corner breaks, provide stability and ensure that the load can be transferred directly to the specimen (Figure 3.17-c). After the heads of the samples to be tested were prepared using fast-setting plaster, 2 holes were drilled on 2 surfaces in order to place the Linear Variable Differential Transformer (LVDT), which will be used to measure the lateral and vertical displacements during loading, on the sample. Iron rods, which can be tightened with screws, are placed in the corresponding holes and fixed with epoxy (Figure 3.17-d). Before the test day, the LVDT was placed on the sample to measure the displacements during loading. Prepared specimens were tested to investigate the effects of manufacturing methodologies, printing direction and material ages on the mechanical performance (Figure 3.17-e,f,g,h). Three specimens for each case were tested, average results were computed and compared utilizing one-way ANOVA analysis.



a)



b)



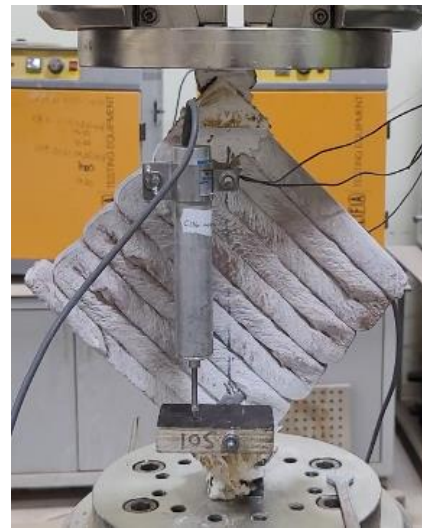
c)



d)



e)



f)



g)



h)

Figure 3.17. Schematic depiction and image of steel head (a), diagonal tension test (b), preparation of samples (c,d), representative images from testing (e,f,g,h).

4. RESULTS AND DISCUSSIONS

4.1. WPC-Based Mixture

4.1.1. Compressive Strength

The structural features of 3D-printed cementitious samples exhibit direction-dependent alteration, giving rise to the phenomenon of anisotropy, where the material's behavior is influenced by the direction of applied force. The anisotropic behavior in 3D-printed cementitious samples, attributed to the weaker mechanical properties in the interlayer bonding zones caused by the addition of material layers, prompted the investigation of mechanical characteristics based on loading direction.

To comprehensively assess anisotropic mechanical properties and study the influence of printing time intervals, compressive strength tests were conducted by applying loads in perpendicular, parallel and lateral orientation to the printing aspect (Figure 4.1-a). The compressive strength values acquired from 28-day cured specimens are depicted in Figure 4.1-b. The specimens that were continuously printed (0-min printing time interval) and loaded perpendicular, parallel and lateral to the printing orientation exhibited compressive strength results of 65.40 MPa, 59.10 MPa, and 55.80 MPa, respectively. The findings reveal that specimens printed with a 0-min printing time interval and subjected to parallel and lateral loading demonstrated a reduction in strength by 9.6% ($p>0.05$) and 14.7% ($p<0.05$), respectively, in comparison to the perpendicular-loaded specimens. This aligns with the expected results, as the perpendicular loading way corresponds to the bond region between successive printed layers, facilitating efficient load transmission through the specimen without negatively impacting the bond region and high pressure implemented to the substance throughout the squeezing out operation in this particular aspects (Panda et al., 2017; Sanjayan et al., 2018; Yu et al., 2021). Moreover, the mass of the extruded layers facilitated effective consolidation of the fresh material vertically, leading to increased compressive strength in these samples (Panda et al., 2017; Sanjayan et al., 2018). The specimens loaded in the lateral direction showed a 5.6% ($p>0.05$) decrease in strength compared to those loaded in parallel. This can be attributed to the lower pressure experienced by the lateral direction from the pump and upper layers during printing, led to reduced compressive strength (Sanjayan et al., 2018).

Additionally, when samples are loaded in parallel or lateral directions, cracks generated by compressive stress can propagate along the bonding region and separate the layers upon reaching the interfacial bond region (Panda et al., 2017; Yu et al., 2021; Demiral et al., 2022). Consequently, the choice of crack propagation path becomes an important factor in discovering the performance of the printed samples. The elevated compressive strength evident in specimens subjected to parallel loading, as opposed to those experiencing lateral loading, can be attributed to an additional factor: the greater concentration of the fresh mixture in the path of the nozzle's motion, a consequence of the substantial hydraulic pressure employed throughout the 3D-printing procedure (Panda et al., 2017; Lim, Panda and Pham, 2018; Panda et al., 2019b; Yu et al., 2021; Demiral et al., 2022).

In the 3D-AM process, the time interval between successive layers is unavoidable due to the long printing path. Thus, it is crucial to identify the optimal printing time interval that ensures adequate adherence between layers, leading to satisfactory bond strength (Sanjayan et al., 2018). The results revealed a consistent decrease in compressive strength values as the printing time interval increased, regardless of the loading direction. Minor variations in compressive strength were observed between intervals of 15-min and 30-min for all loading directions. At a 30-min printing time interval, reductions in strength of 3.9%, 5.9% and 4.0% were observed for perpendicular, parallel and lateral loading directions, respectively, in comparison to the 0-min printing time interval. On the other hand, specimens printed with a 60-min printing time interval exhibited compressive strength reductions of 13.4%, 14.1% and 13.1% under perpendicular, parallel and lateral loadings, respectively, when compared to the samples printed at 0-min (Figure 4.1-b). Additionally, the decrease in strength for the perpendicular, parallel and lateral loading directions at the 60-min interval was 10.3% ($p < 0.05$), 8.7% ($p > 0.05$) and 9.5% ($p > 0.05$), respectively, in comparison to the 30-min interval.

These findings indicate that longer printing time intervals, specifically the 60-min interval in this study, significantly reduce compressive strength. This observation aligns with prior research indicating a decline in interlayer bonding as the printing time interval increases, resulting in reduced compressive strength across various loading directions (Sanjayan et al., 2018; Rehman and Kim, 2021). Insufficient interaction between layers may lead to decreased effective bond areas, attributed to enhanced stiffness of the initial layer caused by

increased production of C-S-H phases with longer time intervals (Wolfs et al., 2018; Tay et al., 2019; Xu et al., 2021). Evaporation and drying during printing intervals contribute to a loss of interlayer moisture content, further diminishing bond strength and compressive strength. Sedimentation of particulate material within the mixture during longer intervals can lead to uneven distribution and density variations in the printed layers, ultimately impacting compressive strength. Prolonged exposure to environmental conditions due to extended printing time intervals can cause material degradation and decrease compressive strength. Further, longer intervals may affect the curing process of cementitious materials, leading to incomplete or delayed curing, weaker interlayer bonds, and decreased compressive strength (Keita et al., 2019; Marchment, Sanjayan and Xia, 2019; Van Der Putten et al., 2019).

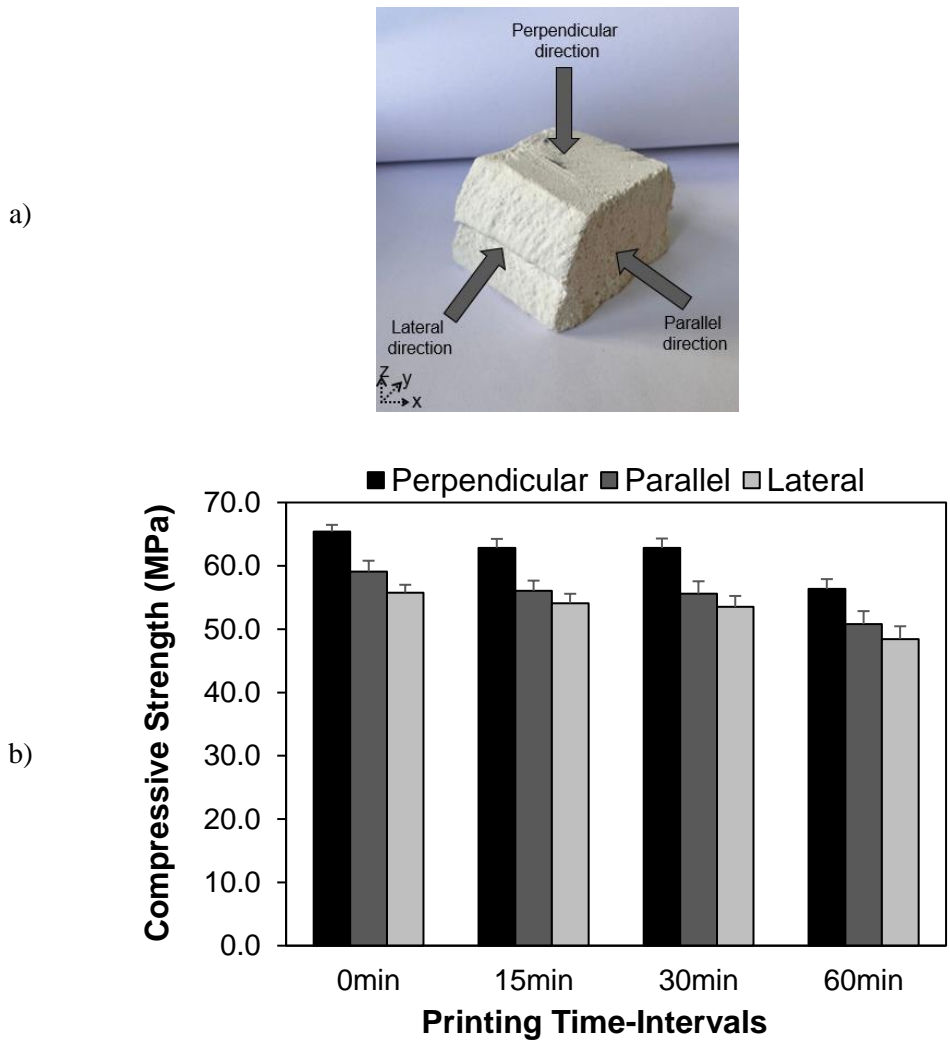


Figure 4.1. Loading directions (a) and the results of the compressive strength tests carried out on the 28-day aged cementitious specimens printed vertically (b).

4.1.2. Bond Strength

4.1.2.1. Printing Time Interval

The bond strength characteristics of vertical-printed specimens, subject to varying printing time intervals, were assessed using triplet shear and direct tensile tests. The bond strength values acquired from 28-day cured specimens are depicted in Figure 4.2. The findings revealed a gradual decline in bond strength as the printing time intervals increased. The specimen printed continuously (with a 0-min time interval) exhibited bond strength values of 3.13 MPa and 4.91 MPa from the triplet shear and direct tensile tests, respectively. In the case of the triplet shear test, reductions of 6.4%, 10.2% and 18.5% ($p < 0.05$) were observed for the 15-min, 30-min and 60-min printing time intervals, respectively, compared with the 0-min interval. Similarly, for the direct tensile test, reduction rates of 4.7%, 12.2% and 27.5% ($p < 0.05$) were recorded as the printing time interval increased up to 60-min.

The observed pattern aligned with expectations and closely resembled the findings reported by Le et al. (2012). Nonetheless, the outcomes from the study conducted by Sanjayan et al. (2018) were not replicated in this investigation. In their research, printing intervals of 10-min and 30-min exhibited comparable performance, surpassing the outcomes of the 20-min interval. This divergence was attributed to the favorable impact of bleeding, which contributed moisture and consequently improved bonding between successive layers. On the contrary, the present study demonstrated a consistent decrease with the extension of the time interval, which can be ascribed to differences in the printing procedure (including factors like extruder type and size, as well as pressure) and the material's state (such as ingredient properties, bleeding rate and evaporation rate, etc.). The attained bonding strength, even with a 60-min printing time interval, exceeded the minimum bond strength recommended by the Concrete Society of 0.8 MPa (Austin, Robins and Goodier, 2000), consistent with conclusions drawn in previous literature investigations (Wolfs, Bos and Salet, 2019; Chen et al., 2020; Lee et al., 2019).

Overall, the reduction observed with the extended printing time interval can be attributed to the improvement in the stiffness of the bottom layer, leading to the formation of macropores along the interface and a reduced effective bonding area (Chen et al., 2020; Tay et al., 2019; Özkılıç et al. 2023). Moreover, heightened stiffness may hinder the intermixing of the bottom and upper layers, resulting in less alignment of the bottom layer's surface (Chen et

al., 2020; Tay et al., 2019; Xu et al., 2021; Panda et al., 2019a). Furthermore, the loss of moisture between layers due to ongoing hydration and evaporation might contribute to the development of inadequately formed hydration elements between the layers (Sanjayan et al., 2018; Wolfs, Bos and Salet, 2019; Pan et al., 2022; Marchment, Sanjayan and Xia, 2019). Additionally, non-uniform shrinkage between layers may also contribute to the weaker bond strength with the increased printing time intervals (Federowicz et al., 2020; Moelich, Kruger and Combrinck, 2020).

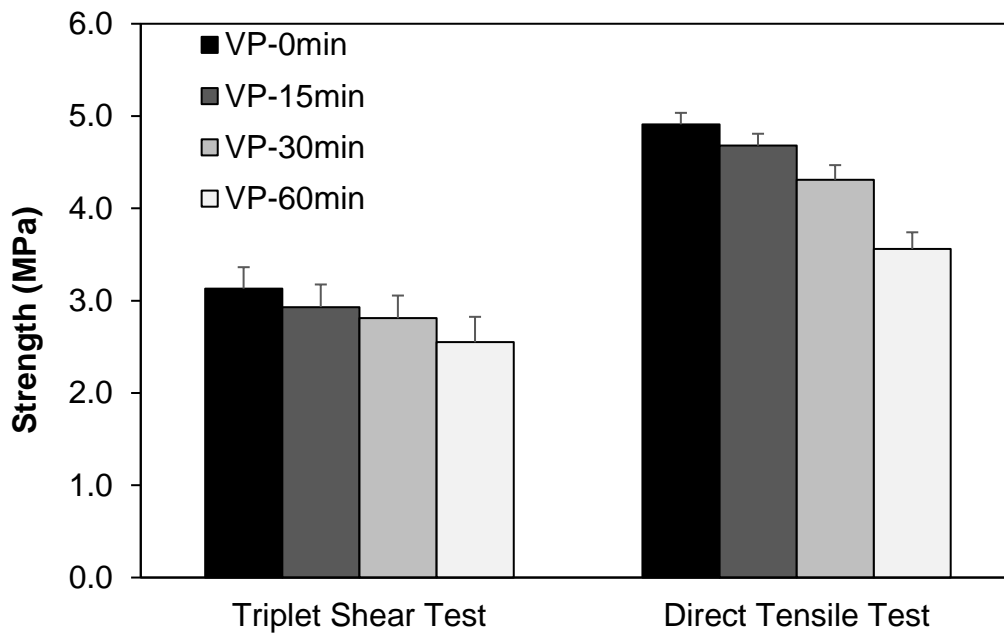


Figure 4.2. Bond strength of vertical-printed WPC-based mixtures with varied printing time intervals (VP: Vertical-printed specimen).

Furthermore, the fracture surfaces of the samples prepared with 2 different printing time intervals (0- and 60-min) were examined with ImageJ software after the triplet shear test. An examination of images obtained from 3D-printed specimen revealed a distinctive difference in rupture interfaces (Figure 4.3-a,b). In the context of freshly printed specimen, a recessed rupture interface was observed, characterized by conspicuous irregularities and variations in depth (Figure 4.3-c). This can be attributed to an interplay of contributing factors to bond strength.

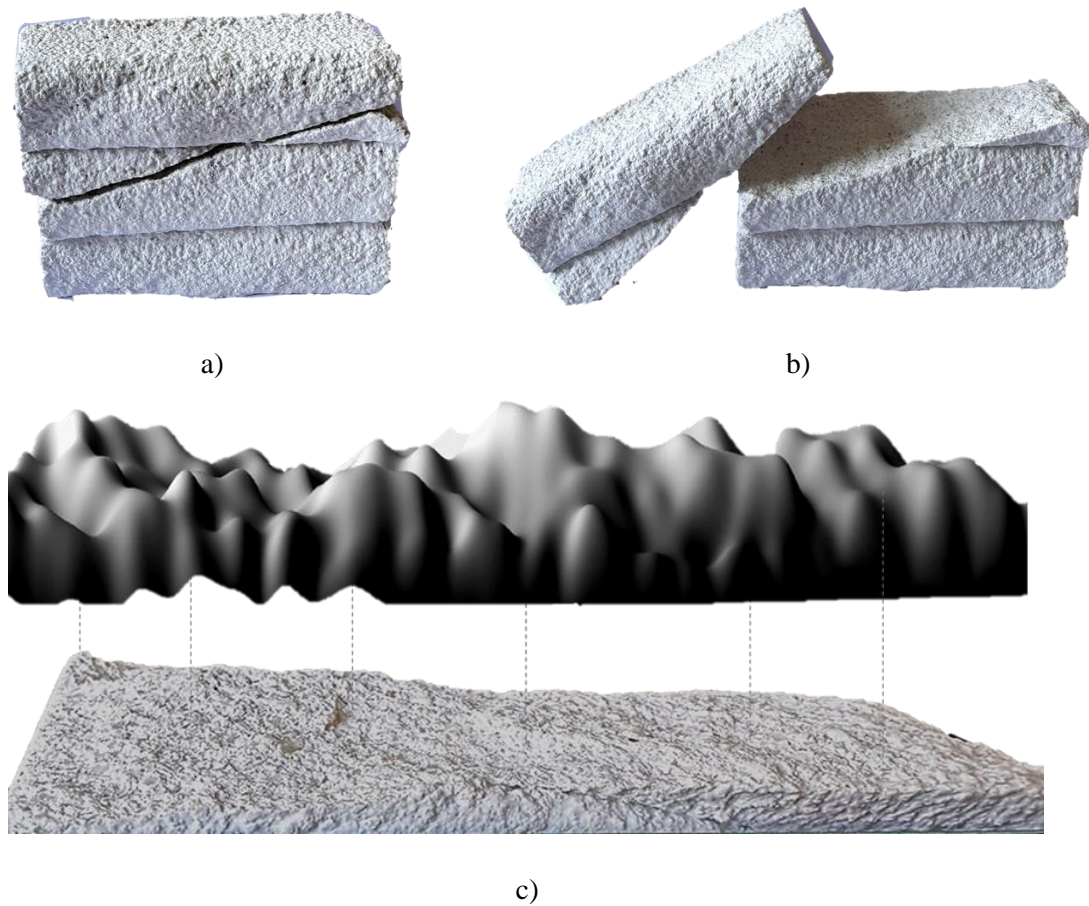


Figure 4.3. The images depict various aspects of a freshly 3D-printed specimen at the 0-min, including: The progression of crack propagation (a), fragments resulting from the cracks (b) and processed representations of the cracked surface (c).

The observed contrast between a 3D-printed specimen at 60-min printing time interval, which displayed a smooth and flat rupture interface (Figure 4.4-a-c), and other specimens suggests a considerable influence of the printing procedure on the structural robustness of the cementitious system. This discrepancy underscores the importance of printing interval as a crucial element affecting the structural characteristics and fracture behavior of the printed components. The smooth and flat rupture interface in the specimen at 60-min printing time interval may indicate a less cohesive and possibly hardened material, which could potentially lead to lower mechanical performance and bond strength. The processed figures serve as a visual medium for representing the evolution of bond strength in 3D-printed concrete during the hardening duration by supporting the strength results obtained from implemented testing methods.

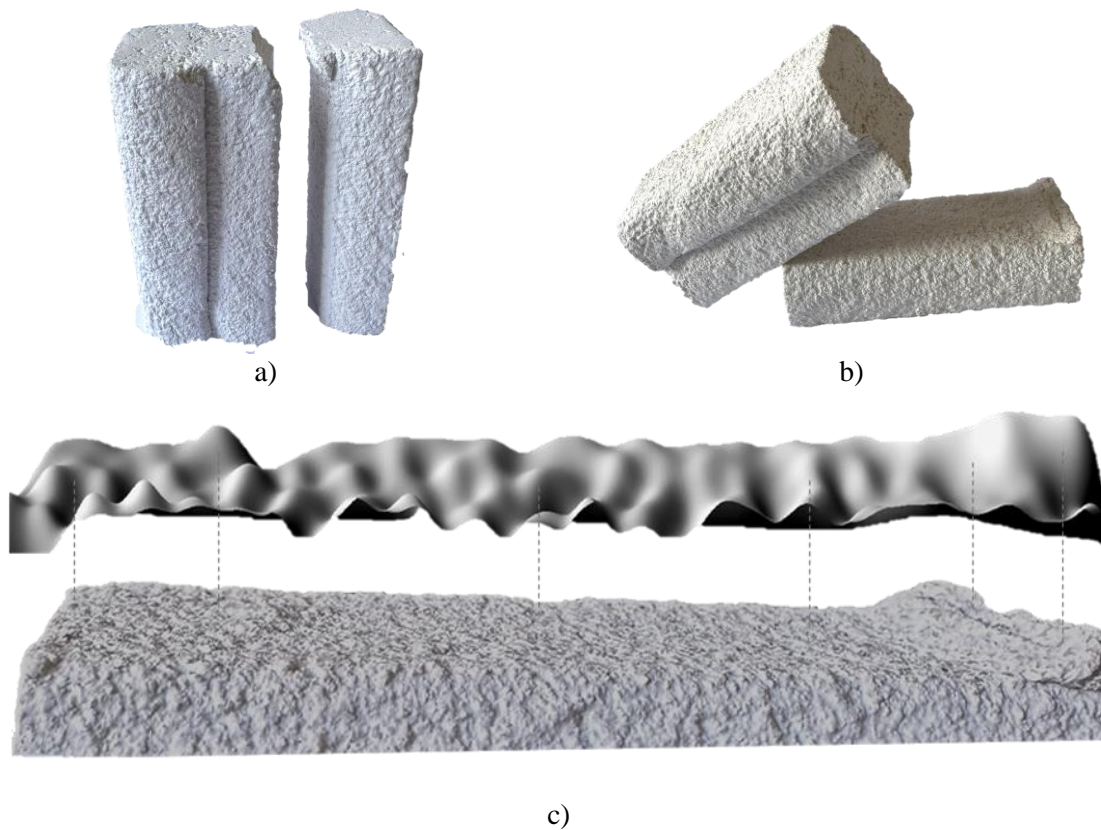


Figure 4.4. The images depict various aspects of a 3D-printed 60-min aged specimen, including: The progression of crack propagation (a), fragments resulting from the cracks (b) and processed representations of the cracked surface (c).

4.1.2.2. Material Aging

In practical 3D-AM, the temporary residence of the mixture in the pump chamber is common, aiding uninterrupted material flow through the pipeline. Therefore, material aging plays a crucial role in maintaining structural integrity. An investigation into the aging behavior of printed specimens with 0-min printing time intervals was undertaken, utilizing the diagonal tension and triplet shear test methods. The outcomes of the diagonal tension and triplet shear tests, conducted on vertical-printed specimens and subjected to ambient curing conditions for a duration of 28 days, are illustrated in the Figure 4.5. As depicted in Figure 4.5, the consequences of both the diagonal tension and triplet shear tests exhibited similar patterns in terms of material aging performance. A substantial reduction in strength was evident in specimens printed with mixtures aged for 60-min. In summary, there were recorded declines in mechanical performance of 18.2% ($p < 0.05$) and 40.6% ($p = 0.01$) from 0-min to 60-min concerning the diagonal tension and triplet shear tests, respectively. The

reduction in mechanical performance observed in vertically printed specimens as material ages for an extended period can be attributed to various factors. These factors include an increase in mixture viscosity and the development of static and dynamic yield stresses, which result from both evaporation and ongoing cement hydration during the material's resting period (Xu et al., 2021). These alterations reduce workability, leading to inadequate integration between consecutive layers, promoting void formation and reducing bonded regions (Tay et al., 2019; Panda et al., 2019a; Chen et al., 2020). Additionally, augmented stiffness can hinder the development of inadequately formed hydration elements between layers due to restricted ion mobility (Sanjayan et al., 2018; Wolfs et al., 2019; Marchment et al., 2019).

The outcomes of the study show that extended material aging durations adversely impact the structural features of the printed samples, aligning with the prior investigations of Pan et al. (2021), who noted a decline in bond strength with prolonged aging periods. While a decrease in mechanical performance with material age was expected, the results at the 30-min material aging were relatively consistent and slightly lower compared to the fresh mixture (0-min). This slight reduction could be attributed to water evaporation from the bulk mixture's surface during the resting period, leading to increased stiffness. Additionally, shear forces from the auger feed screw during pumping disrupted the hydration product structures formed in the early stages, potentially reducing the stiffness of the rested mixture (Ilcan et al., 2022). The mitigating effect of applied shear stress by the auger feed screw was less pronounced in the 60-min aged mixture, as the shear force may not be sufficient to disrupt the hydrated gels that had formed by that point. Consequently, the significant reduction observed in the 60-min aged mixture can be attributed to both ongoing hydration and water evaporation. Extended periods of material aging resulted in noticeable shifts in fracture mechanisms, transitioning from primarily material-driven modes of fracture to those predominantly occurring within the interface zone. This shift is attributed to diminished adhesion between successive layers (Le et al., 2012; Wolfs et al., 2019).

The results of the triplet shear test, taking into account both different printing time intervals and material aging time, indicated that material aging had a more important impact on the interlayer bond strength of the 3D-printed cementitious system. The decrease in bond

strength was more significant in samples printed with 30-min and 60-min material aging, in contrast to those printed with 30-min and 60-min printing time intervals.

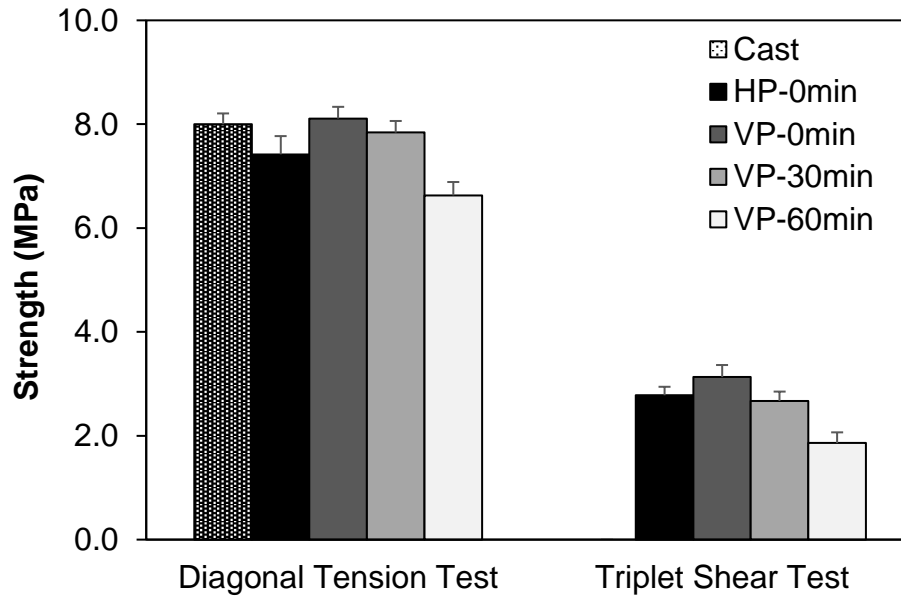


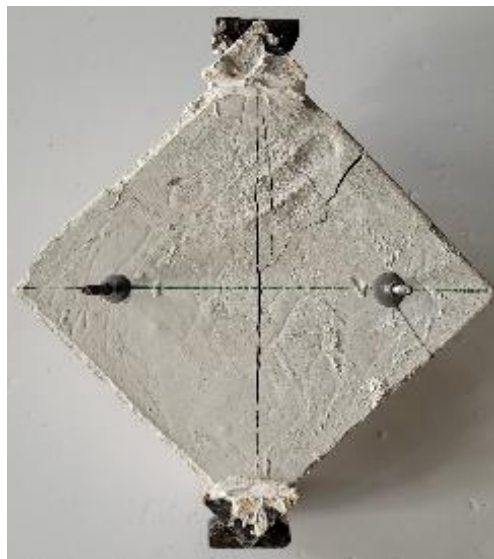
Figure 4.5. Average diagonal tension tension and triplet shear test results of white-cemented mortars (HP: Horizontal-printed specimen, VP: Vertical-printed specimen).

4.1.3. Manufacturing Methodology

It is important to consider the determination of strength differences between the interlayer interfaces (vertical-printed) and interfilamentous interfaces (horizontal-printed) due to the layered production of printed samples in different directions, and to compare these results with the test results of cast samples produced for control purposes. In this study, vertical and horizontal-printed specimens were prepared alongside cast specimens using fresh mixture without any printing time interval. These specimens were subjected to triplet shear and diagonal tension tests after 28-day. The outcomes depicted in Figure 4.5 revealed that in the triplet shear test, the shear strength of the vertical-printed specimen was 3.13 MPa, while it was 2.78 MPa for horizontal-printed specimen, resulting in a decrease of 11.18% in strength ($p < 0.05$). This aligns with the findings in the literature, where the strength values of vertical-printed samples were generally higher than those printed horizontally (Rahul et al, 2019b; Murcia, Genedy and Taha, 2020; Wang et al, 2022). In the diagonal tension test, which is not encountered in the literature on 3D printed samples, the vertical-printed sample (8.11 MPa) exhibited a higher strength value compared to the horizontal-printed sample (7.42

MPa), leading to a reduction of 8.5% in strength. The strength value of the cast sample (8 MPa) remained between the strength values of the vertical and horizontal-printed samples.

These results indicate that the mechanical characteristics of 3D-printed samples may be impacted by the printing operation, and the orientation of the printed layers can exert a remarkable impact on the properties of the end result. Vertical printing aligns the layers with the load direction, and the applied pumping pressure and the mass of the above stratum effectively increase the diagonal tension and triplet shear strength of the samples (Rehman and Kim, 2021; Roussel, 2018). Conversely, when the layers are printed horizontally, it can result in lower mechanical properties (Rahul et al, 2019b). Some studies have also observed micro pores between layers and macro pores between filaments when assessing porosity. Accordingly, in the additive manufacturing process, the void ratio between the layers decreases with the effect of pressure during printing; it has been determined that this situation is not valid between filaments (Le et al, 2012; Zhang et al, 2019a). In other words, the void distribution and pore structure cause anisotropic behavior which leads to weak interlayer bonding (Murcia, Genedy and Taha, 2020; Van Den Heever et al., 2022). When the fracture mechanism of the cast and vertical/horizontal printed samples were examined (Figure 4.6), it was noticed that while crack/fracture of mold-cast and vertical-printed specimens were similar, samples printed horizontally exhibited a brittle appearance, possibly attributed to the presence of micro/macro pores within the bonded sections, resulting in a greater number of scattered cracks.



a)

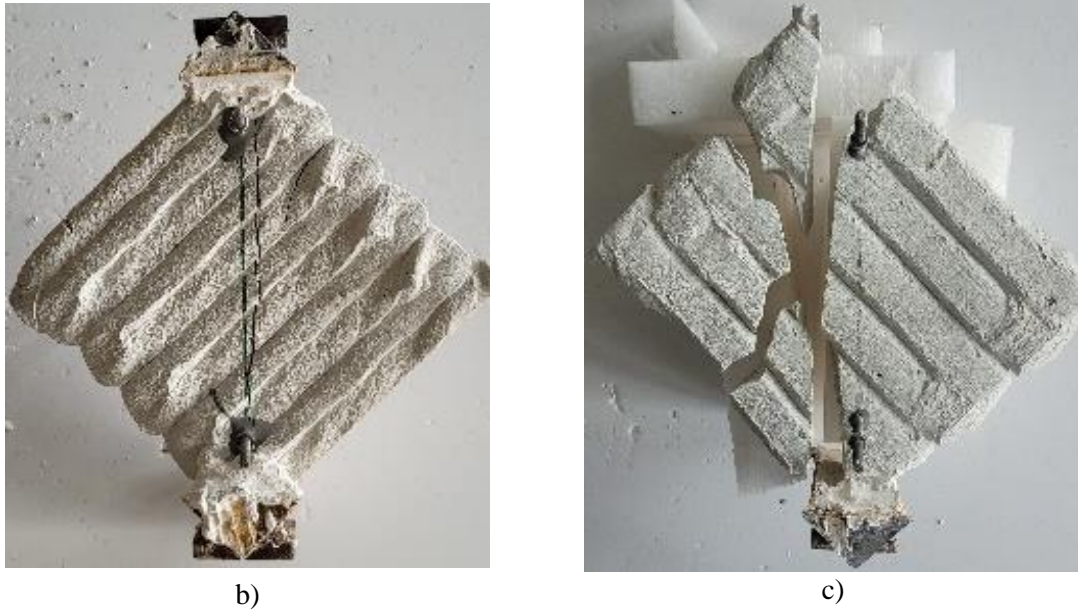


Figure 4.6. The view of cast (a), vertical-(b) and horizontal-printed (c) specimens under diagonal tension test.

4.2. CDW-Based Geopolymer Mixture

4.2.1. Compressive Strength

The performance of 3D-printed samples may change based on the force application aspect. The inferior mechanical attributes of interlayer bonding regions in 3D printing, resulting from the layering of material, lead to diminished strength compared to the central area of successive layers. This induces a performance discrepancy termed anisotropy, influenced by both the printing and loading directions. To assess the anisotropic mechanical features of created 3D-printed samples and examine the impact of printing time intervals on the mechanic attributes of CDW-based geopolymer materials, compressive strength tests were executed on specimens in varied loading orientations: perpendicular, parallel and lateral to the printing way. Continuously printed samples (0-min printing time interval) loaded perpendicular, parallel and lateral to the printing way had compressive strength results of 24.3 MPa, 22.1 MPa, and 20.1 MPa, respectively, as seen in Figure 4.7. The results indicate that the printed specimens with 0-min printing time interval subject to parallel and lateral loading exhibited a reduction in strength of 9.2% ($p>0.05$) and 17.6% ($p=0.02$), respectively, in comparison to perpendicular-loaded. This was in line with the anticipated finding, as the perpendicular loading direction aligns with the bond region, thereby accounting for the superior strength outcomes observed in such specimens (Panda et al., 2017; Muthukrishnan,

Ramakrishnan and Sanjayan, 2021). The effectiveness of geopolymers in a perpendicular load can be ascribed to the requirement for the bond region between successive printed layers to unite under compression in that particular orientation (Panda et al., 2017). This enables the direct transmission of the load through the sample without causing adverse impacts on the interlayer region, thus leading to better overall mechanical performance (Yu et al., 2021). Another potential explanation for the higher compressive strength observed in specimens loaded perpendicularly is the effective compaction of the fresh mixture in that direction, which is facilitated by the weight of the extruded layers (Panda et al., 2017; Sanjayan et al., 2018). Furthermore, the printed specimens under lateral loading exhibited a reduction in strength of 9.3% compared to parallel loading ($p < 0.05$). The behavior under lateral loading can be related to that as the lateral direction experiences the lowest pressure by the pump and upper layers during printing, resulting in a reduction in compressive strength (Sanjayan et al., 2018). Moreover, when samples are loaded in parallel or lateral directions, the cracks resulting from compressive stress may propagate along the bonding region and separate the layers; once they have reached the interfacial bond region (Panda et al., 2017; Moïni, 2020; Yu et al., 2021; Demiral et al., 2022). For that reason, it can be concluded that the choice of propagation path for microcracks can be a critical factor in analyzing the structural response of printed specimens (Demiral et al., 2022). The increased compressive strength in specimens loaded parallel to the laterally loaded ones can be attributed to the more concentrated fresh mixture along the nozzle movement direction, influenced by the substantial pumping pressure applied during the 3D-printing procedure (Panda et al., 2017; Sanjayan et al., 2018; Lim, Panda and Pham, 2018; Panda et al., 2019b; Demiral et al., 2022).

In the 3D-AM process, the time interval between successive layers is inevitable because of the long printing path; therefore, it is necessary to find the optimal printing time interval enough for the ensured adherence between printed layers to develop sufficient bond strength (Sanjayan et al., 2018). Thus, this study also determined the impact of printing time intervals on the compressive strength of specimens under different loading directions. The results revealed a decreasing tendency in the compressive strength values as the printing time interval raised irrespective of loading directions. For all loading directions, slight deviations in compressive strength were observed between 0-min and 15-min intervals. At the 30-min printing time interval, there were strength reductions of 18.6% ($p = 0.006$), 12.4% ($p > 0.05$),

and 9.1% ($p>0.05$) for the perpendicular, parallel and lateral loading directions, respectively, in proportion to the 0-min printing time interval. Furthermore, the samples printed with 60-min printing time intervals exhibited a decrease in compressive strength of 19.8% ($p=0.019$), 18.9% ($p=0.016$) and 12.5% ($p=0.046$) under perpendicular, parallel and lateral loadings, respectively, when compared to the samples printed at 0-min (Figure 4.7). Conversely, the reduction in strength observed for the specimens subjected to perpendicular, parallel and lateral loading directions at the 60-min was 1.4%, 7.4% and 3.9%, respectively, compared to the 30-min ($p>0.05$). Consequently, the outcomes of this study show that the printing time interval in this study demonstrated a significant decrement in compressive strength for 30-min printing time intervals. This is in line with most studies that have reported a decrease in interlayer bonding as the printing time interval increases (Sanjayan et al., 2018; Rehman and Kim, 2021). The reasons for that can be related to the fact that weak interlayer bonding causes lesser compressive strength properties from different loading directions. This phenomenon can be described by the limited bonding interaction areas between two layers that can be ascribed to the increased production of N-A-S-H, C-A-S-H, C-S-H with longer time intervals leading the enhanced stiffness of the initial layer. This decreases the amount of effective bond areas between the layers (Wolfs, Bos and Salet, 2018; Tay et al., 2019; Panda et al., 2019a; Xu et al., 2021). Additionally, the reduction in compressive strength and interlayer strength can be ascribed to the moisture loss from the interlayer surface through evaporation and drying throughout printing time intervals (Keita et al., 2019; Marchment, Sanjayan and Xia, 2019; Van Der Putten et al., 2019). Thus, the findings indicate that the decrease in adhesion was anticipated as the printing time interval increased (Le et al., 2012).

When printing geopolymers specimens with a 60-min time interval considered, the dominant factor influencing compressive strength is the printing time interval, rather than the direction of loading (anisotropy) when compared to 0-min. According to the results, the direction dependence was more effective at the 0-min; as the printing time interval increased, a reduction in the compressive strength was determined in all loading directions, and the loading direction dependence was decreased. This may be due to the fact that specimens began breaking from the bond region in all loading directions after specific printing time intervals.

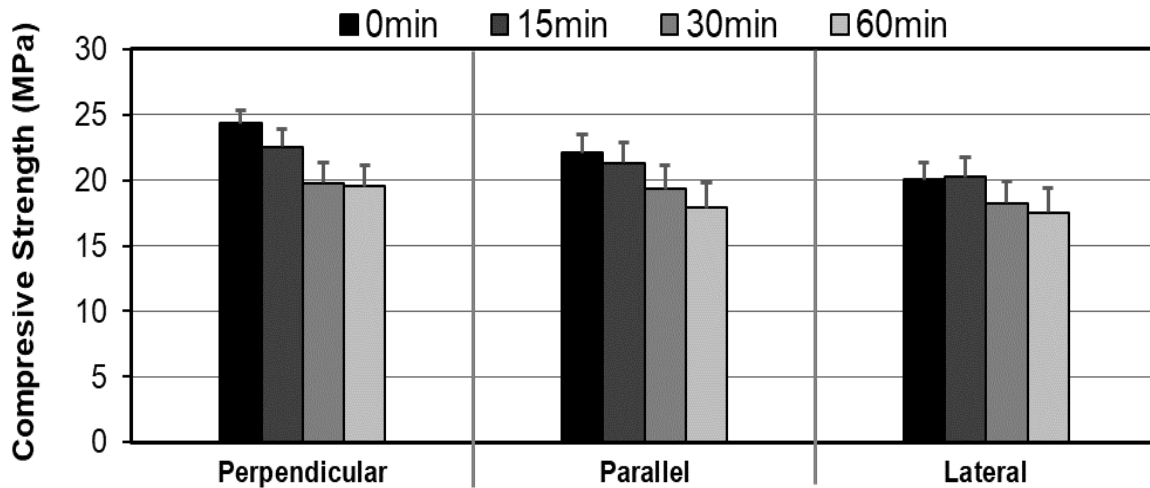


Figure 4.7. Compressive strength outcomes of vertical-printed geopolymer mortars with varied printing time intervals and loading directions.

4.2.2. Bond Strength

4.2.2.1. Printing Time Interval

28-day direct tensile and triplet shear test results of the vertical-printed specimens with varied printing time intervals cured under ambient circumstances are demonstrated in Figure 4.8. As seen from the Figure 4.8, the interlayer strength of the CDW-based geopolymer material was lessened with the increased printing time interval or delay time between two successive layers. The direct tensile test showed that although decrements in bond strength were obvious with increased time intervals up to 30-min, the bond strength values recorded from the printed specimens with 30-min intervals were similar to the ones produced with 60-min intervals. The maximum bond strength value obtained from the direct tensile test was noted as 2.2 MPa and the decrement ratios were calculated as 14.0%, 29.4% and 34.8% for the 15-30-60-min printing time intervals compared to the continuous printing (0-min), respectively ($p < 0.05$). For the triplet shear test, after 30-min printing time interval, decrement was not evident as in the direct tensile test results. However, the decrement in interlayer strength for the samples printed with 15-min printing interval was not prominent compared to direct tensile results, with a ratio of 9.4% ($p > 0.05$). The maximum bond strength value recorded from the triplet shear test was approximately 1.5 MPa and the decrement ratios were calculated as 24.6% ($p = 0.03$) and 28.3% ($p = 0.07$) for the 30- and 60-min printing time intervals compared to the continuous printing (0-min), respectively.

From Figure 4.8, relations between the printing time and the loss of direct tensile strength and the loss of the initial shear strength were also determined by fitting a polynomial to the strength loss ratios for direct tensile strength and initial shear strength, respectively (Eq. 5-8). The R-Squared (coefficient of determination, R^2) for these fitted polynomials to the strength loss ratios for direct tensile strength and initial shear strength were calculated as 0.987 and 0.975, respectively. These equations could be used to adjust the estimated strength values obtained from the 0-min batch of geopolymer. Therefore, these equations could be used a coefficient to identify the direct tensile strength and initial shear strength of 3D printed geopolymer at distinct printing time intervals. In addition, these equations are useful in estimating the possible deviations from the target strengths due to (i) printing operation time limitations and (ii) unpredicted delays occurring at the printing stage.

$$f_{ct,corrected}(t) = C_1 f_{ct,t_0} \quad (5)$$

$$C_1 = 0.0227t^2 - 0.232t + 1.216 \quad (6)$$

$$\tau_{o,corrected}(t) = C_2 \tau_{o,t_0} \quad (7)$$

$$C_2 = 0.0183t^2 - 0.19t + 1.18 \quad (8)$$

Where $f_{ct,corrected}$ is the direct tensile strength at the chosen printing time interval, C_1 is the coefficient for the direct tensile strength loss due to chosen printing time interval, f_{ct,t_0} is the direct tensile strength at 0-min batch of geopolymer, $\tau_{o,corrected}$ is the initial shear strength at the chosen printing time interval, C_2 is the coefficient for the shear strength loss due to chosen printing time interval and τ_{o,t_0} is the direct tensile strength at 0-min batch of geopolymer. These equations are specifically applicable to the CDW-based geopolymer mixtures like studied in this research. However, they can be potentially adapted for use with other materials by conducting respective experiments to obtain relevant data and validate applicability.

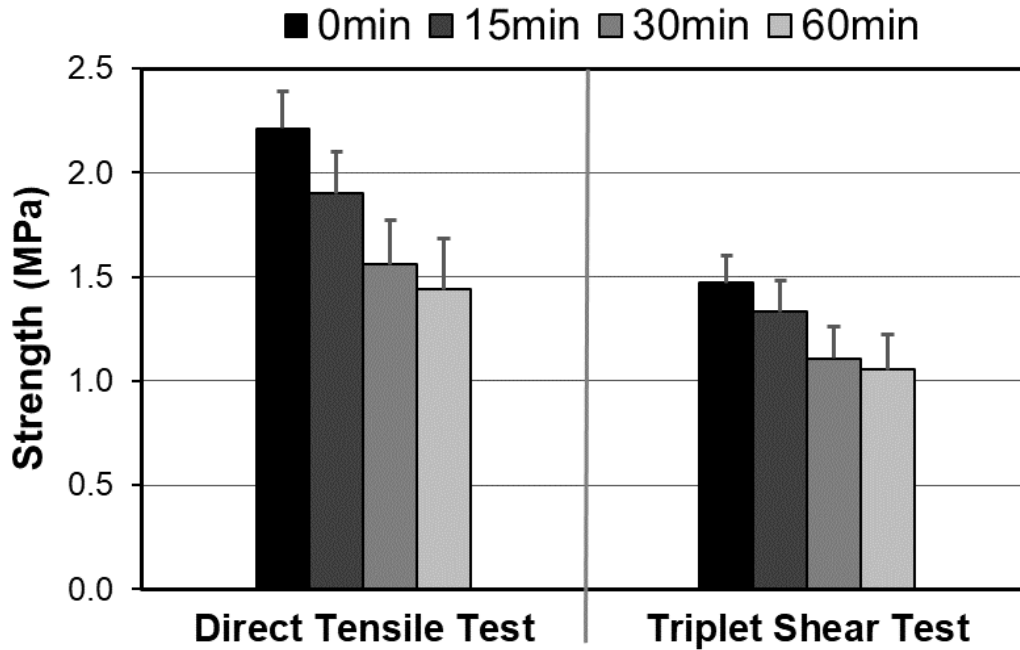


Figure 4.8. Bond strength results of vertical-printed geopolymer mortars with varied printing time intervals.

The decrement in interlayer strength with increased printing time interval can be ascribed to likely following causes: (i) macropores formation and reduced bonding interfaces between consecutive layers because of enhanced stiffness of first layer (Tay et al., 2019; Panda et al., 2019a; Chen et al., 2020; Xu et al., 2021), (ii) less orientation capacity to rearrange the surfaces of the layers because of enhanced stiffness, preventing intermixing with the subsequent layer (Tay et al., 2019; Panda et al., 2019a; Chen et al., 2020; Rehman and Kim, 2021; Xu et al., 2021), (iii) evaporation-induced reduction in moisture on the interlayer face because of ongoing reaction and evaporation, causing less ion mobility and formation of insufficient hydration products between layers in favor of good adhesion (Sanjayan et al., 2018; Tay et al., 2019; Wolfs, Bos and Salet, 2019; Keita et al., 2019; Xu et al., 2021; Marchment, Sanjayan and Xia, 2019; Roussel, 2018).

Because of the ongoing geopolymerization and water loss due to external factors with elapsed time, the viscosity of the CDW-based geopolymer material increased, resulting enhancement in the stiffness of the mixture (Tay et al., 2019; Sahin et al., 2021; Ilcan et al., 2022). Therefore, the load caused by the pressure of the pump and the weight of the upper

layer started to be insufficient to rearrange the surface of the bottom layer and to intermix both layers in favor of increasing the bond area and filling the pores/voids between the two layers, resulting formation of weakness on the bond area and decrement in bond strength. Besides that, because of evaporation with elapsed time, the mobility of dissolved ions was limited, which may yield the formation of less geopolymerization products on the interlayer, resulting weaker bonding capacity. As a result of this weak bonding, the failure modes of the specimen were changed regarding the printing time interval. As seen from Figure 4.9-c,d,e,f, while specimens having a strong bonding between two successive layers failed in the bulk of the layers, specimens with weak bonding failed at the interface zone (Wolfs, Bos and Salet, 2019; Le et al., 2012). Although the material itself may withstand the higher load, because of the weak bonding performance, the specimen failed at lower load.

The results showed that after a 30-min printing time interval, the decrement was not significant (Figure 4.8). The possible reason for obtaining similar performance from the specimen printed with 30-min and 60-min printing time intervals could be explained by evaporation and geopolymerization rate. Because 30-min was enough to dry off the upper face of the bottom layer and beyond that time, the effects of vaporization were limited as most of the humidity available atop the surface of the underlying layer was lost. Besides that, the adhesive properties of the geopolymer mixture containing CDW because of its clayey nature compensated for the decrement in bond adhesion after a certain point (Sahin et al., 2021). Moreover, geopolymerization rate of CDW-based geopolymer initiated with NaOH and $\text{Ca}(\text{OH})_2$ was slow after the initial dissolution and reaction phase because of low-activity precursors and the absence of fast-setting alkaline activators (e.g. Na_2SiO_3), thus geopolymerization prolonged for up to hours (Sahin et al., 2021; Ilcan et al., 2022). Therefore, the development of stiffness after 30 min was not significant which provided similar stiffness for the first layers resulting in similar intermixing and interaction area for bonding.



a)



b)



c)



d)



e)



f)

Figure 4.9. Representative images showing details of failure modes on specimen of a diagonal tension (a,b), triplet shear (c,d) and direct tensile test (e,f).

4.2.2.2. Material Aging

During real-scale 3D-AM application, in some manufacturing setup (especially for the low-tech application) the produced mixture may wait for a while in the pump-chamber until delivered to the pipeline to provide continuous flow. In addition, to eliminate material wastage, while developing the mixture, extrudability performance tried to be prolonged to recover used materials in case of a wrong application or operational accident during printing. Therefore, realization of the material aging time capability of the mixtures was needed for the CDW-based geopolymer material. In this context, the material aging performance of the mixture was investigated through diagonal tension and triplet shear test methods. 28-day diagonal tension and triplet shear test outcomes of the vertical-printed samples cured under ambient circumstances are demonstrated in Figure 4.10.

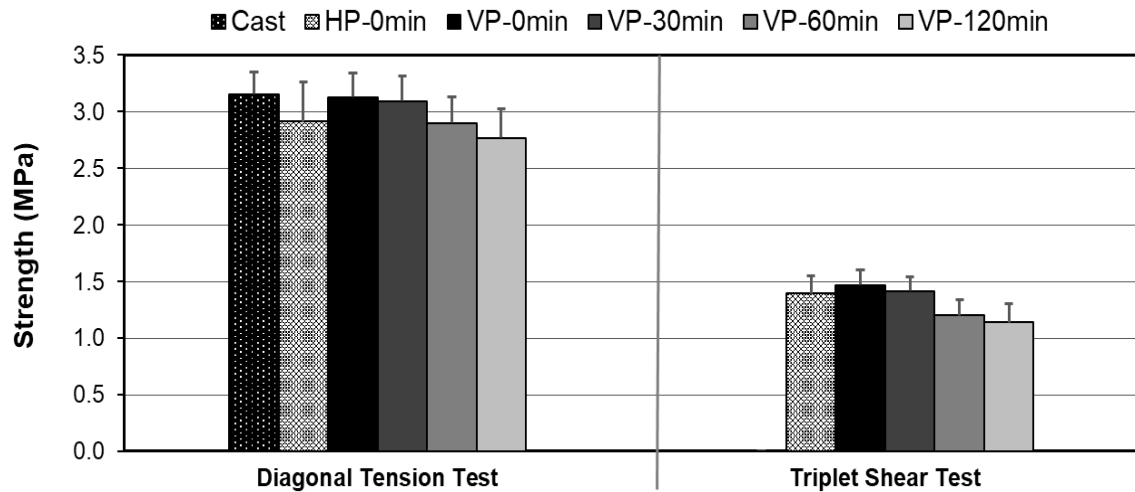


Figure 4.10. Average diagonal tension and triplet shear test results of geopolymer mortars (HP: Horizontal-printed specimen, VP: Vertical-printed specimen).

As seen from Figure 4.10, diagonal tension and triplet shear test results had similar trends regarding the material aging time performance. The vertical-printed specimens with the fresh mixture (0-min) and mixture at the age of 30-min showed similar mechanical performance because of longer initial setting time. However, a considerable decrease was observed from the specimen printed with the mixture having an age of 60-min because of ongoing geopolymerization and evaporation ($p=0.04$). After the 60-min mixture resting time, the reduction in mechanical performance was not significant because of limited amount of evaporation from the surface of the mixture. Overall, the decrease rates in mechanical

performance with the increased material aging time were recorded as 11.5% and 22.5% from 0-min to 120-min for the diagonal tension and triplet shear test, respectively ($p < 0.05$). The possible reasons for the decrease in the performance of the vertical-printed CDW-based geopolymer specimen produced with increased material aging time could be the increment of viscosity and dynamic and static yield stresses of the material because of the evaporation and ongoing geopolymerization during the resting time (Xu et al., 2021). Because a decrement in workability can cause limited intermixing of consecutive layers resulting formation of pores/voids and less amount of interacted bond areas (Chen et al., 2020; Tay et al., 2019; Rehman and Kim, 2021; Panda et al., 2019a). Besides that, enhanced stiffness may cause the formation of insufficient hydration products between layers because of limited ion mobility (Sanjayan et al., 2018; Wolfs, Bos and Salet, 2019; Keita et al., 2019; Marchment, Sanjayan and Xia, 2019; Roussel, 2018).

Although it was expected to decrease in mechanical performance with increasing material age, 30-min results were comparable even if slightly lower regarding the fresh mixture (0-min). The slight decrease observed could be due to the vaporization of the water from the face of the bulk mixture during the resting time, which resulted in an increment of stiffness, rather than ongoing geopolymerization because of longer initial setting time of CDW-based geopolymer mixture. Furthermore, while the pumping procedure, the prepared mixture went through the auger feed screw, which apply a shear force to the mixture, resulting in the breaking of the limited amount of flocculated structure of the hydration products in early ages (Ilcan et al., 2022). Therefore, the stiffness of the waited mixture may lessen, and ongoing geopolymerization up to 30-min may cause fewer negative effects on the bond strength of the mixture. However, the mitigation effect because of applied shear stress by auger feed screw has diminished for 60-min aged mixture since applied shear force may not be enough to break hydrated gels formed until that time as the materials get close to the initial setting time. Thus, a sudden decrease observed for 60 min-aged mixture can be due to both ongoing geopolymerization and evaporation of water. Considering the 120-min aged mixture, the observed decrease in bond strength was not prominent, although material aging is getting close to the initial setting time (165 min). This could be attributed to the effect of evaporation was diminished after the initial 60-min. The decrement in strength with increased aging time resulted in different fracture mechanisms as shown in the Figure 4.10. Since the adhesion between two consecutive layers decreased with increased resting time

because of discussed reasons, fracture modes changed from materials to the interface zone in time (Wolfs, Bos and Salet, 2019; Le et al., 2012).

The triplet shear test results for both varied printing time intervals and material aging showed that printing time intervals had more apparent impacts on the bond strength of the mixture. The decrement observed for samples printed with 30-min and 60-min printing time intervals was higher compared to the specimen printed with the 30-min and 60-min aged mixture. This can be attributed to the following possible reasons: (i) less interlayer humidity for printing time intervals, (ii) enhanced stiffness of first layer for printing time intervals resulting in less orientation capacity causing the formation of weakness on interacted bond areas, (iii) mitigation effect of applied shear by auger feed screw in favor of viscosity reduction enabling more intermixing of consecutive layers.

4.2.3. Manufacturing Methodology

After a period of 28 days, CDW-based cast specimens, and vertical- and horizontal-printed specimens prepared with fresh mixture without any printing time intervals (0-min time interval between two consecutive layers) were subjected to diagonal tension and triplet shear tests, and the test results were recorded and plotted in Figure 4.10. When considering strength properties, Observations indicate comparable behavior between vertically printed geopolymer specimens and cast specimens, while horizontally printed specimens demonstrate slightly diminished performance. The study revealed that the diagonal tensile strength of specimens printed horizontally exhibited a reduction of 7.6%, compared to cast specimens, and a 6.9% decrease compared to vertically printed specimens ($p < 0.05$). Conversely, the diagonal tensile strength of vertical-printed samples showed a slight decrease of 0.7% compared to cast specimens ($p > 0.05$). Similarly, in the triplet shear test results, horizontal-printed specimens showed a 5.3% decrease compared to vertical-printed ones ($p < 0.05$). These observations suggest that the performance of printed samples are susceptible to the printing procedure, and the alignment of printed layers can markedly affect the ultimate mechanical attributes of the end product. Vertical printing aligns layers with the load direction, and the applied pumping pressure and weight of upper layers effectively enhance the specimens' diagonal tension and triplet shear strength (Rehman and Kim, 2021; Roussel, 2018). Conversely, when layers are horizontally printed, they are perpendicular to the load direction, which may result in diminished mechanical characteristics (Rahul et al.,

2019b). Moreover, the performance of 3D-printed geopolymer specimens are influenced from their pore structure, including the presence of micro/macropores between layers. Under the impact of pressure during the printing duration, the void ratio between layers decreases, thereby increasing the strength capacities of vertical-printed and cast specimens (Panda, Paul and Tan, 2017; Zhang et al., 2019a). Additionally, vertical-printed geopolymer specimens may have a more consistent and uniform pore structure, which could result in better strength properties. Conversely, specimens that are horizontally printed may have a less uniform pore structure, leading to weaker mechanical properties (Moini et al., 2021). Moreover, Figure 4.11-a illustrates the load-displacement behavior during diagonal tension testing, providing a representative example of how printing directions impact the load-bearing capacity and displacement behavior of printed geopolymer specimens. Figure 4.11-a showed that while displacement behaviors of the cast and vertical-printed samples were alike and smoother, sudden breakouts were observed through increasing loading for the horizontal-printed specimen due to weaker bonding capacity. Upon analyzing the results, it was concluded that the fracture behavior of the cast and vertical-printed samples was comparable, whereas the horizontal-printed samples showed a more brittle appearance, potentially due to the presence of micro/macro pores in the bonding sections, manifesting themselves with more numerous and scattered cracks. Figure 4.11-b,c exhibits similar trends in crack propagation tendency under different loading directions, highlighting the impact of homogenous and compact structures of cast and vertical-printed samples, like that of the specimen subjected to perpendicular loading (Demiral et al., 2022). Considering the results obtained, the distinction between the vertical-printed specimens and the horizontal-printed specimens lies in the fact that the top layers of the former do not experience compressing forces and pressure in the horizontal-printed ones. Conversely, as the horizontal-printed specimens are positioned closer to each other and interlock, they can function as a single layer and can narrow the gap between the horizontal and vertical-printed samples.

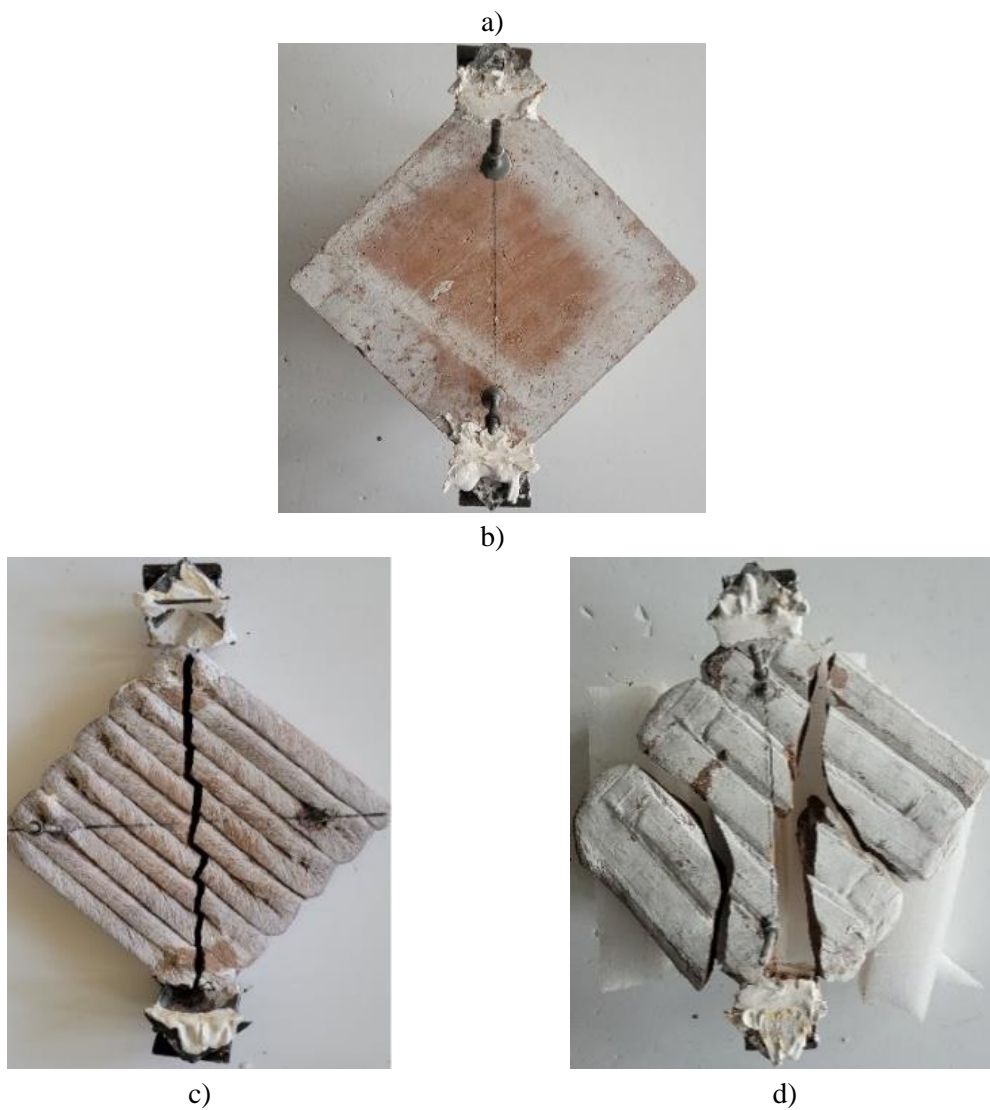
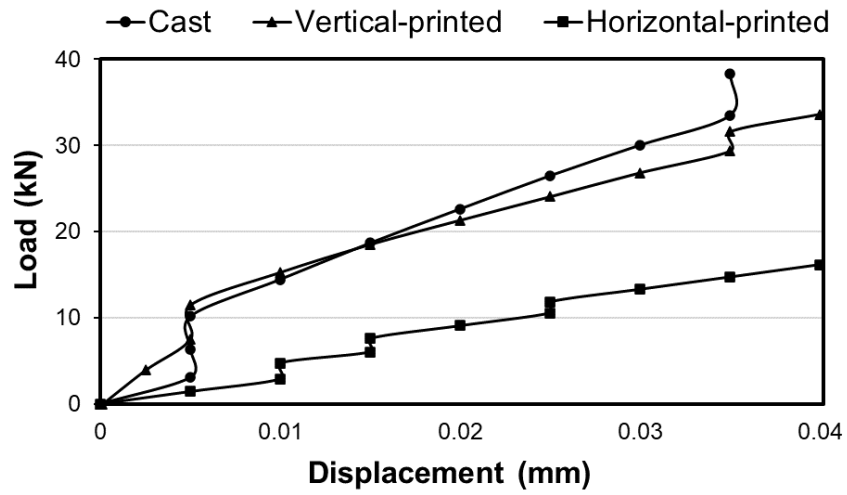


Figure 4.11. Representative load-displacement curves for manufacturing methodologies (a) and the view of cast (b), vertical- (c) and horizontal-printed (d) specimens under diagonal tension test.

4.2.4. Correlation in Test Results

Mechanical characteristics of the 3D-printed CDW-based geopolymer were assessed through varied testing protocols in this study. To analyze the linear correlation between the obtained results, linear regressions were conducted by applying a trendline to the results. R^2 was calculated for each regression to provide the proportion of the variance. In this context, the correlation between compressive strength in different directions and bond strength obtained from both triplet shear and direct tensile tests with varied printing time intervals was plotted and examined as in Figure 4.12. Considering the R^2 , compressive strength outcomes performed in perpendicular and parallel directions were in a linear correlation with bond strength, by showing a linear increment in compressive strength with enhanced bond strength. However, compressive strength results from the laterally tested specimen were not linearly correlated with the bond strength. As the lateral direction regarding the printing path was the weakest point because of fewer constraints and pressure, a lower R^2 value can be anticipated. Figure 4.12-a also showed that bond strength results obtained from both triplet shear and direct tensile highly coincided with each other, as the R^2 recorded from both tests had a similar value regarding the compressive strength results gathered from the varied testing direction. Besides to the compressive strength, diagonal tension test outcomes were examined regarding the correlation between bond strength obtained from the triplet shear test. Linear regression consequences were illustrated in the Figure 4.12-b. The results showed that diagonal tension test outcomes highly coincided with the bond strength results, with the R^2 value of 0.9717, indicating an increment in bond strength results in enhancement of diagonal tension performance. Considering obtained results, it could be stated that compressive strength and diagonal tension of 3D-printed CDW-based geopolymer are significantly dependent on the bond strength, and vice versa. And, the correlation in its simplest form could also be assumed to have linear nature with changing slopes and constants.

Overall, these correlations are preliminary and not universally applicable. However, they hold the potential for adaptation to other materials through respective experiments to gather relevant data. It is crucial to keep in mind that further experimental studies and modeling are necessary to support and validate these correlations. Nevertheless, the results offer promising indications of a potential correlation between compressive strength and bond strength characteristics.

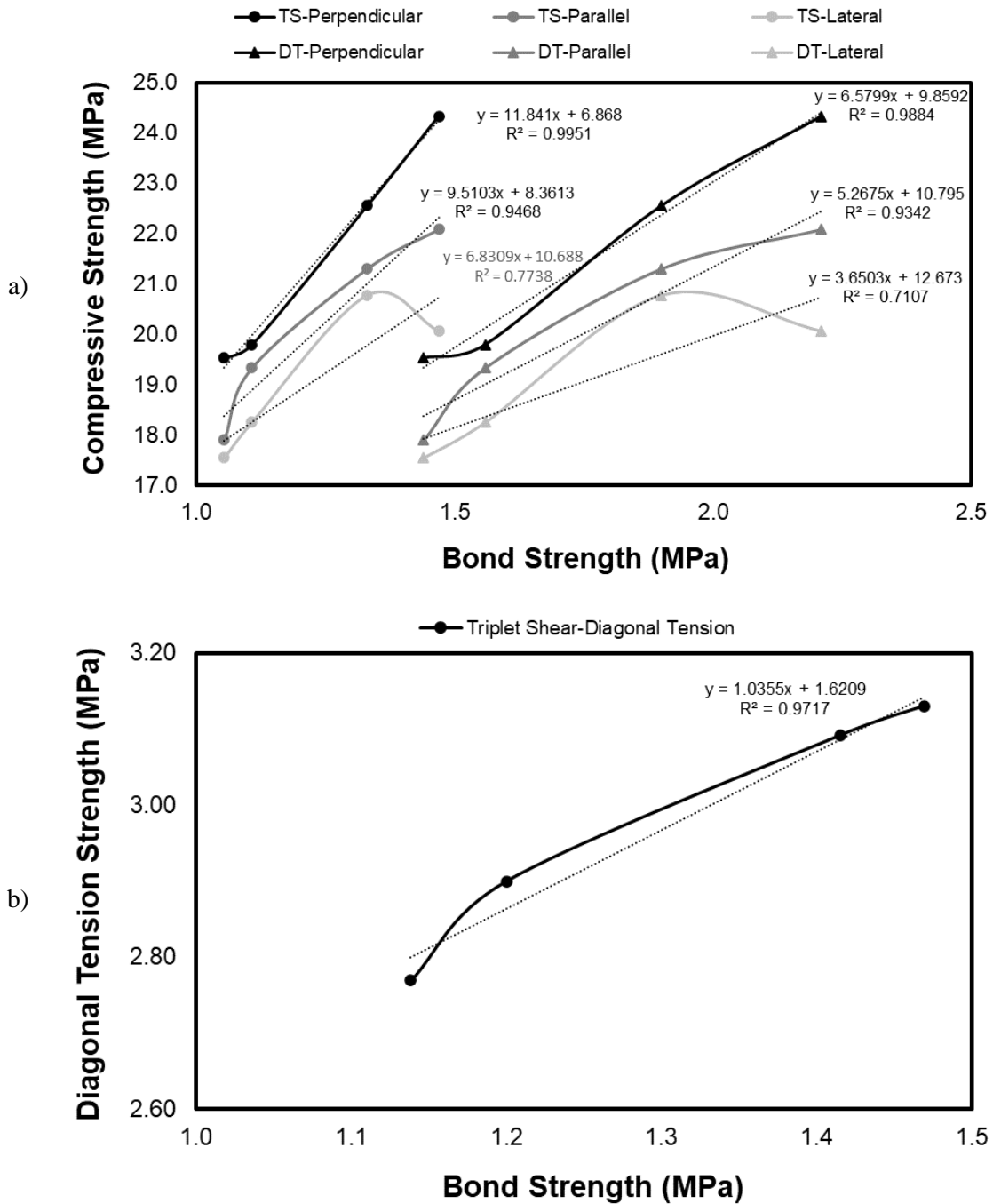


Figure 4.12. Correlation bw. compressive strength in different directions and bond strength obtained from both triplet shear and direct tensile test with varied intervals (a) and linear regression results of bond strength and triplet and diagonal tension tests (b) (TS: Tripler Shear, DT: Diagonal Tension).

4.3. Comparison of Cementitious Composites and CDW-Based Geopolymer

In this study, two distinct mixtures were employed to assess various experimental parameters. The first is based on WPC, while the other is a geopolymer derived from CDW. This section aims to compare the results of experiments conducted with these two mixtures and draw conclusions regarding the performance of CDW-based mixtures in comparison to their WPC-based counterparts.

Initiating the comparison with the results of the compression test within the framework of this study, an assessment of two distinct parameters was conducted. The initial focus was on observing the impact of printing time intervals on compressive strength, achieved by subjecting the 2-layer samples produced at printing time intervals of 0, 15, 30 and 60-min to the compression test. Following this, an exploration of the anisotropic properties of the 2-layer samples at the same printing time intervals was undertaken, examining their response to loading in perpendicular, parallel and lateral directions.

It became evident that lower strength values were obtained as the printing time interval increased for both WPC-based cementitious and CDW-based geopolymer mixtures. In the WPC-based mixture, the strength loss was considerable in samples printed at 15-min intervals, attributed to mainly drying of first layer (evaporation). Similar performance was observed for the 30-min interval, influenced by positive effects of bleeding. However, a notable decline was evident in the strength of the specimens printed at 60-min intervals, attributed to factors such as enhanced stiffness of the initial layer, reduced water content at the interface, distribution disparities and density differences in the printed layers. In the CDW-based geopolymer mixture, samples printed at 0-15 min intervals exhibited similar performance, while those printed at 30-min intervals displayed a considerable decrease compared to other samples, attributed to evaporation and geopolymerization. The 30-60 min interval showed a slight decrease due to slow geopolymerization and decreasing evaporation.

Furthermore, anisotropic behavior was noted in the samples from both mixtures, and the order, ranked from the highest to lowest strength values, was determined as perpendicular (direct transmission of load, effective compaction), parallel and lateral (lowest pressure applied by the pump) directions. While the decrease in the WPC-based mixture from 0 to 60-min exhibited similarity in loading across different directions, the reduction in strength

in the lateral direction in the CDW-based mixture was comparatively lower than in other directions. Additionally for the CDW-based mixture, the direction dependence was more effective at the 0-min; as the printing time interval increased, a reduction in the compressive strength was determined in all loading directions, and the loading direction dependence was decreased. Moreover, it was revealed that the strength results obtained with the WPC-based mixture were approximately 2.8 times higher, on average, than those obtained with the CDW-based geopolymer material. The strength outcomes of mixtures subjected to compressive test in different directions and at different printing time intervals are shown in Table 4.1, and graphical interpretation of compressive strength test outcomes shown in Figure 4.13.

Table 4.1. Comparison of compression test results.

Direction	Printing Time Interval (min)	WPC-Based mixture (MPa)	CDW-Based Geopolymer mixture (MPa)
Perpendicular	0	65.40	24.34
	15	62.85	22.55
	30	62.83	19.80
	60	56.34	19.53
Parallel	0	59.09	22.08
	15	56.06	21.30
	30	55.59	19.34
	60	50.78	17.90
Lateral	0	55.57	20.06
	15	54.08	20.27
	30	53.51	18.26
	60	48.44	17.55

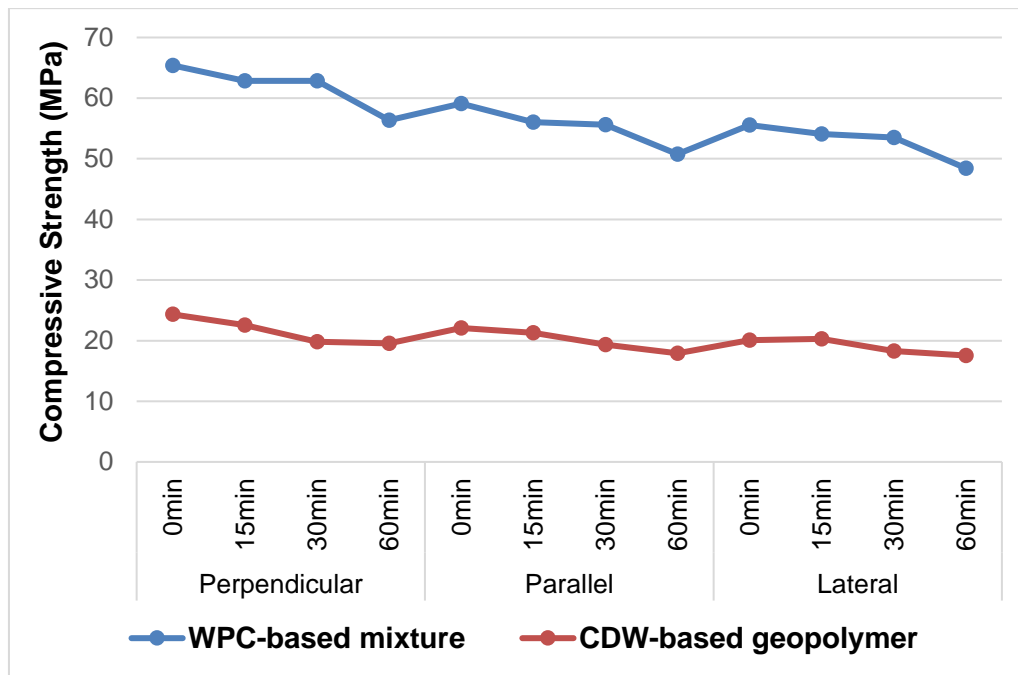


Figure 4.13. Graphical interpretation of compressive strength test results.

To explore the impact of printing time intervals on bond strength, two separate examinations were carried out on specimens created using various mixtures: direct tensile and triplet shear tests. In this context, vertically printed 2-layer samples with intervals of 0, 15, 30 and 60-min were prepared to assess the impact of printing time intervals through direct tensile and triplet shear testing. Upon evaluating the test results, a decreasing trend in bond strength was observed with increasing printing time intervals for both WPC-based cementitious and CDW-based geopolymer mixtures. In the WPC-based mixture, although in both tests there was a greater decrease in strength in samples prepared at 60-min intervals compared to those produced at other intervals due to factors such as improvement in the stiffness of the bottom layer and loss of moisture, the decline was more pronounced in the direct tensile test. In the CDW-based mixture, based on the outcomes of the direct tensile and triplet shear tests, a considerable decrease in strength was observed up to 30-min, attributed to factors such as macropores, evaporation, geopolymerization and less ion mobility (the decline at 15-min in direct tensile was more pronounced than in triplet shear). However, there was no significant decrease observed after the 30-min interval, attributed to the slow geopolymerization and diminishing effect of evaporation over time. Furthermore, according to the direct tensile test results, the strength values of the samples produced with the WPC-based mixture are, on average, approximately 2.48 times higher than those produced with the CDW-based

geopolymer mixture. Similarly, a 2.32-fold difference is noted based on the triplet shear test outcomes. The strength results of specimens subjected to direct tensile and triplet shear test at different printing time intervals are shown in Table 4.2, and graphical interpretation of test outcomes shown in Figure 4.14.

Table 4.2. Comparison of direct tensile and triplet shear test results (VP: Vertical-printed specimen).

Sample	Direct Tensile Test		Triplet Shear Test	
	WPC-Based mixture (MPa)	CDW-Based Geopolymer mixture (MPa)	WPC-Based mixture (MPa)	CDW-Based Geopolymer mixture (MPa)
VP-0min	4.91	2.21	3.13	1.46
VP-15min	4.68	1.90	2.93	1.33
VP-30min	4.31	1.56	2.81	1.11
VP-60min	3.56	1.44	2.55	1.05

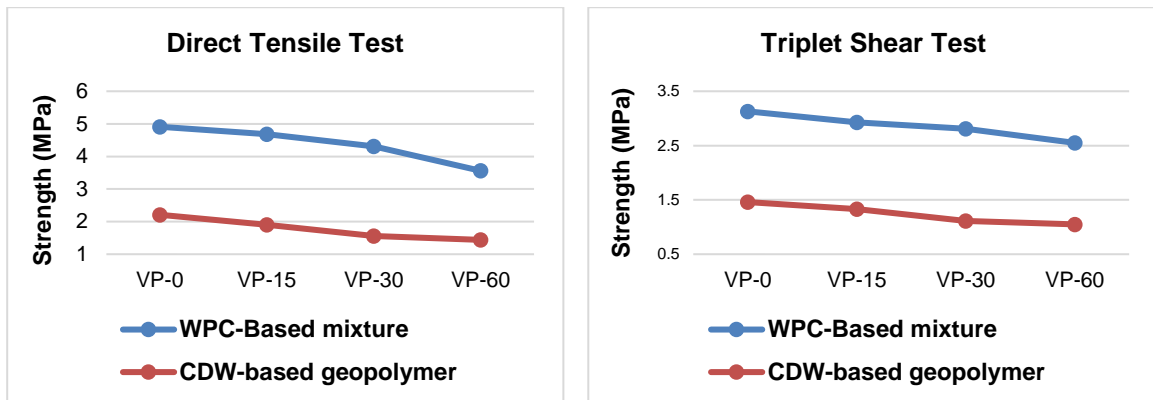


Figure 4.14. Graphical interpretation of direct tensile and triplet shear test results.

To investigate the impact of material age and manufacturing methodology on bond strength, samples prepared with different mixtures underwent two distinct tests: diagonal tension and triplet shear tests. In this regard, cast (0-min), horizontally printed (0-min) and vertically printed (0-min) samples were prepared to scrutinize the impact of manufacturing methodology on both mixtures for the diagonal tension test. Additionally, to assess the effect

of material age, vertically printed samples were produced with material ages of 0, 30 and 60-min. In the triplet shear test, horizontal (0-min) and vertical printed (0-min) samples were created in both mixtures to determine the impact of manufacturing methodology on strength. To observe the effect of material age, vertically printed samples were produced with material ages of 0, 30 and 60-min. Considering the extended open time of the geopolymer material, samples with 120-min material aging were also produced specifically for this material.

Regarding the impact of material age on the WPC-based mixture, consistent performance trends were observed based on the material's age in both tests, showcasing a decline in strength with increasing aging time. The reduction in strength of the 30-min aging period was relatively lower compared to the 60-min aging period because of the development of inadequately formed hydration elements, and for the 60-min aging period, the loss of strength was more evident due to ongoing hydration and evaporation (the loss in the triplet shear test was more pronounced than in the diagonal tension test). In addition, the effect of the shear stress applied by the auger feed screw was more evident in the 30-min interval compared to the 60-min interval. Upon comparing the triplet shear test results of samples produced at different time intervals and aging times, it was evident that the impact of material aging time on bond strength was more significant.

In the CDW-based geopolymer mixture, comparable strength values were obtained at 0 and 30-min aging periods, attributed to the compensating effect of the auger feed screw on moisture loss and ongoing geopolymerization in both tests. Nevertheless, there was a noteworthy decline in strength during the 60-min aging time due to ongoing geopolymerization and evaporation, with reduced auger feed screw effects (the loss in the triplet shear test was more pronounced than in the diagonal tension test). There was no significant decrease observed in the 120-min aging time, attributed to the decrease in evaporation and slow geopolymerization. When the triplet shear test results of samples produced with different time intervals and different aging times were compared, it was determined that the impact of the printing time interval on bond strength was more important.

When assessing the impact of manufacturing methodology on both mixtures, it was noted that the strength values of the vertically printed samples (applied pumping pressure, weight of upper layers and uniform pore structures enhance the strength) were higher than the

horizontally printed samples (less uniform pore structure cause weak interlayer bonding), and it was observed that the cast samples (homogenous and compact structures) produced in the diagonal tension test showed similar performance to the vertically printed samples. Additionally, while the diagonal tension test results indicated a more significant decrease in the CDW-based mixture, the triplet shear test outcomes demonstrated a more pronounced decrease in the WPC-based mixture.

Furthermore, derived from the diagonal tension test outcomes, the strength values of the samples produced with the WPC-based mixture are, on average, approximately 2.47 times higher than those produced with the CDW-based geopolymer mixture. Similarly, a 1.9-fold difference is observed in accordance with the triplet shear test outcomes. The strength results of specimens subjected to diagonal tension and triplet shear test in different manufacturing methodology and at different printing time intervals are shown in the Table 4.3, and graphical interpretation of test results presented in Figure 4.15.

Table 4.3. Comparison of diagonal tension and triplet shear test results (HP: Horizontal-printed specimen, VP: Vertical-printed specimen).

Sample	Diagonal Tension Test		Triplet Shear Test	
	WPC-Based mixture (MPa)	CDW-Based Geopolymer mixture (MPa)	WPC-Based mixture (MPa)	CDW-Based Geopolymer mixture (MPa)
Cast	8.00	3.15	-	-
HP-0min	7.42	2.91	2.78	1.39
VP-0min	8.11	3.13	3.13	1.46
VP-30min	7.44	3.09	2.67	1.41
VP-60min	6.63	2.90	1.86	1.20
VP-120min	-	2.77	-	1.13

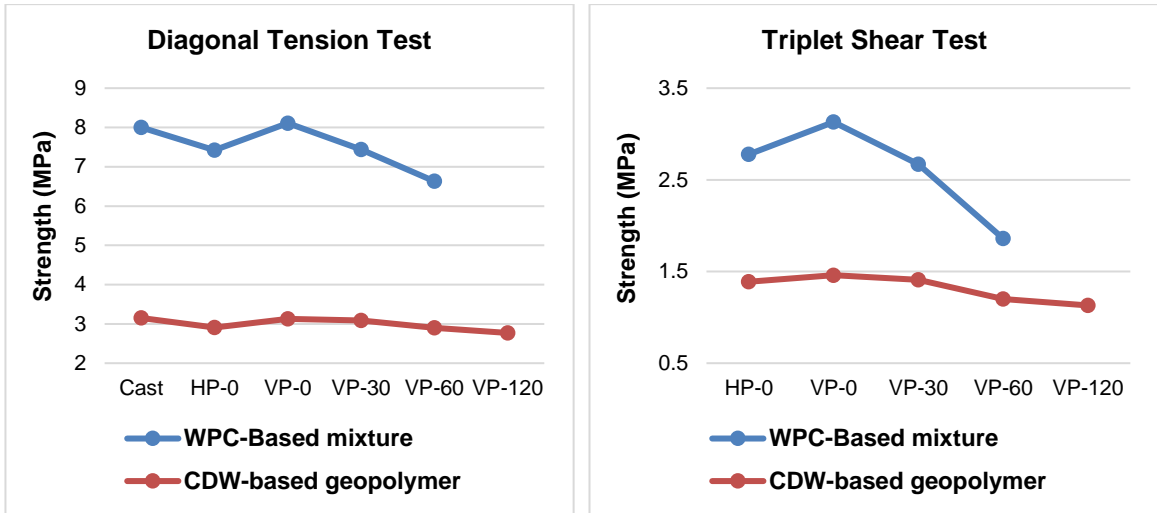


Figure 4.15. Graphical interpretation of diagonal tension and triplet shear test results.

5. CONCLUSION

Developments in 3D printing technology are observed in many different areas, and the technology in question is increasingly becoming the subject of research activities in the construction sector. In addition, the rapid consumption of the world's resources to meet the needs of the increasing population and the non-ecological nature of traditional production mechanisms necessitate a sustainable construction approach. Under these circumstances, in this thesis study, the usability of mixtures obtained using two different mixtures in the 3D-AM method, whose many benefits compared to the traditional construction method have been revealed in the literature, has been investigated. The first material is WPC-based cementitious composites, representing as in the conventional PC category (SP, VM and R admixtures were used to obtain a printable mixture), and the second one is geopolymer binder, derived from the activation of CDW (RCB, HB, RT, G and C) with alkali activators (NaOH and Ca(OH)₂).

Four different test approaches were used to determine the mechanical characteristics of these mixtures, considered many different parameters. To observe the anisotropy, called being directional dependent, the samples prepared at 4 different printing time intervals (0, 15, 30 and 60-min) were exposed to compression tests in 3 various orientation (perpendicular, parallel and lateral to printing aspect). Direct tensile and triplet shear tests were preferred to measure bond strength, samples prepared at 4 different printing time intervals (0, 15, 30 and 60-min) were subjected to 2 different tests and the data obtained were compared. For the manufacturing methodology, diagonal tension and triplet shear tests were applied on samples prepared in different ways (cast, horizontal- and vertical-printed) at 4 different material ages (0, 30, 60-min for both mixtures, and 120-min for CDW-based geopolymer).

Among these tests, the introduction of diagonal tension and triplet shear tests, specifically tailored for masonry structures, to 3D-CP samples due to their analogous nature stands as a noteworthy innovation in the literature. It is also considered an important output to conduct experiments on samples prepared at 4 different printing time intervals (0, 15, 30 and 60-min) and at 4 different material ages (0, 30, 60-min for both mixture, also 120-min for CDW-based geopolymer) which were determined meticulously by examining previous studies, and to evaluate the results obtained on 2 different parameters.

In the conducted studies, alongside the evaluation of the same parameters and the use of the same tests with both mixtures, examinations have also been carried out on specific aspects unique to each mixture. For instance, in the WPC-based mixture, samples produced at two different printing time intervals (0 and 60-min) were three-dimensionally analyzed through a specialized image processing software to observe the impact of the printing time interval on the fracture mechanism. In the CDW-based mixture, the effect of different manufacturing methodologies (cast, horizontal- and vertical-printed) was assessed using the load-displacement graph obtained with LVDT. An attempt was made to formulate the strength loss occurring with increasing printing time intervals. Furthermore, correlations were established between the results of compression tests conducted from various aspects (perpendicular, parallel and lateral) and the bond strength values obtained from triplet shear and direct tensile tests for samples produced at various printing time intervals (0, 15, 30 and 60-min).

The following outcomes were obtained from the predefined experimental researches;

- The established mechanical tests, commonly employed for appraising masonry structures such as diagonal tension and triplet shear test, are transferrable and effectively applicable to 3D-printed structures.
- Regardless of printing time intervals, the maximum compressive strength values were noticed in the perpendicular loading direction, while the compressive strength values decreased in the order of loading for the parallel and lateral directions. Prolonged printing time intervals adversely affect the compressive strength of cementitious systems. Moreover, the printing time interval exerted a more pronounced influence on compressive strength compared to the loading directions for CDW-based geopolymer mixture. However, in the WPC-based mixture, the loading directions had a greater effect than the printing time interval.
- The bond strength of both WPC-based mixture and CDW-based geopolymer mixture decreased with longer printing time intervals. As material aging time increased, the bond strength of the specimens decreased. Printing time intervals exerted a more significant influence compared to the material aging of the CDW-based geopolymer mixture. But for

the WPC-based mixture when evaluating the outcomes of the triplet shear test performed to observe the effect of material aging with printing time intervals, it was determined that material aging had a greater impact on the mixture.

- Vertical-printed specimens demonstrated robust mechanical performance under pumping pressure and top layer weight, which closely resembled the performance of cast specimens. In contrast, horizontal-printed specimens exhibited slightly weaker performance for both the WPC-based mixture and CDW-based geopolymer mixture.
- Based on the parameters, the fracture mechanisms of the 3D-printed samples may vary, and the mechanic characteristics of the 3D-printed specimens can be significantly affected.
- Upon surface examination, irregularities and a recessed rupture interface were detected on the surface of the WPC-based cementitious specimen produced without any waiting time (0-min). In contrast, a smooth and flat rupture interface was observed in the sample produced with a 60-min printing time interval. This visual observation aligns with the notion of achieving lower bond strength with an increasing printing time interval.
- In the CDW-based mixture utilized in this study, the formula derived from the results of direct tensile and triplet shear tests enabled the prediction of potential strength losses. This anticipation takes into account the printing process time limitations and unpredictable delays that may occur during the printing phase for samples produced at different time intervals.
- CDW-based geopolymer composite used in this thesis study showed a linear correlation between bond strength and compressive strength, and diagonal tension and bond strength.
- When comparing the performance of the CDW-based mixture with the WPC-based mixture, it was observed that the test results obtained with the WPC-based mixture were more than 2 times higher than those obtained with the CDW-based mixture. Moreover, the trends of the evaluated parameters for both mixtures were largely similar.

6. REFERENCES

- Abu-Tair, A.I., Rigden, S.R. and Burley, E., Testing the bond between repair materials and concrete substrate, *Materials Journal*, 93 (1996) 553–558.
- AECOM, People’s Republic of China: Construction and Demolition Waste Management and Recycling, Asian Development Bank, (2018).
- Agustí-Juan, I., Müller, F., Hack, N., Wangler, T. and Habert, G., Potential benefits of digital fabrication for complex structures: environmental assessment of a robotically fabricated concrete wall, *Journal of Cleaner Production*, 154 (2017) 330–340.
- Alecci, V., Fagone, M., Rotunno, T., Stefano, M.D., Shear strength of brick masonry walls assembled with different types of mortar, *Construction and Building Materials*, 40 (2013) 1038-1045.
- Alghamdi, H., Nair, S.A. and Neithalath, N., Insights into material design, extrusion rheology, and properties of 3D-printable alkali-activated fly ash-based binders, *Materials and Design*, 167 (2019) 107634.
- Alhawat, M., Ashour, A., Yildirim, G., Aldemir, A. and Sahmaran, M., Properties of geopolymers sourced from construction and demolition waste: A review, *Journal of Building Engineering*, 50 (2022) 104104.
- Allahverdi, A. and Kani, E.N., Construction wastes as raw materials for geopolymer binders, *International Journal of Civil Engineering*, 7(3) (2009) 154-160.
- Al-Qutaifi, S., Nazari, A. and Bagheri, A., Mechanical properties of layered geopolymer structures applicable in concrete 3D-printing, *Construction and Building Materials*, 176 (2018) 690-699.
- Amran, M., Abdelgader, H.S., Onaizi, A.M., Fediuk, R., Ozbakkaloglu, T., Rashid, R.S.M. and Murali, G., 3D-printable alkali-activated concretes for building applications: a critical review, *Construction and Building Materials*, 319 (2022) 126126.
- Annapareddy, A., Panda, B., Ting, A., Li, M. and Tan, M.J., Flow and mechanical properties of 3D printed cementitious material with recycled glass aggregates. In *Proceedings of the 3rd International Conference on Progress in Additive Manufacturing (Pro-AM 2018)*, Singapore, (2018) 14-17.
- Anonymous, Global Cement Production and Concrete Consumption in 2020, <https://gccassociation.org/concretetfuture/cement-concrete-around-the-world/> (Access date: 17th of September 2023).
- Arunothayan, A.R., Nematollahi B., Ranade R., Bong S.H. and Sanjayan, J., Development of 3D-printable ultra-high performance fiber-reinforced concrete for digital construction, *Construction and Building Materials*, 257 (2020) 119546.

- ASTM E 519-02, Standard Test Method for Diagonal Tension (Shear) in Masonry Assemblages, American Society for Testing and Materials, **2002**.
- Austin, S.A., Robins, P.J. and Goodier, C.I., The performance of hardened wet-process sprayed mortars, *Magazine of Concrete Research*, 52(3), (**2000**) 195–208.
- Babafemi, A.J., Kolawole, J. T., Miah, M.J., Paul, S.C. and Panda, B., A Concise Review on Interlayer Bond Strength in 3D Concrete Printing, *Sustainability*, 13(13) (**2021**).
- Banias, G., Achillas, C., Vlachokostas, C., Moussiopoulos, N. and Tarsenis, S., Assessing multiple criteria for the optimal location of a construction and demolition waste management facility, *Building and Environment* 45 (**2010**) 2317-2326.
- Batikha, M., Jotangia, R., Baaj, M.Y. and Mousleh, I., 3D concrete printing for sustainable and economical construction: a comparative study, *Automation in Construction*, 134 (**2022**) 104087.
- Beersaerts, G., Lucas, S.S. and Pontikes, Y., An Fe-Rich Slag-Based Mortar for 3D Printing, *Second RILEM International Conference on Concrete and Digital Fabrication*, RILEM Bookseries, (**2020**), pp.3-12.
- Beushausen, H. and Alexander, M.G., Bond strength development between concretes of different ages, *Magazine of Concrete Research*, 60 (**2008**) 65–74.
- Beyer C., Strategic implications of current trends in Additive Manufacturing, *Journal of Manufacturing Science and Engineering*, 136 (**2014**) 1-8.
- Biernacki, J.J., Bullard, J.W., Sant, G., Brown, K., Glasser, F.P., Jones, S., Ley, T., Livingston, R., Nicoleau, L., Olek, J., Sanchez, F., Shahsavari, R., Stutzman, P.E., Sobolev, K. and Prater, T., *Cements in the 21st century: Challenges, perspectives, and opportunities*. *Journal of the American Ceramic Society*, 100 (**2017**) 2746-2773.
- Bolhassani, M., Hamid, A., Lau, A.C. and Moon, F., Simplified micro modeling of partially grouted masonry assemblages, *Construction and Building Materials*, 83 (**2015**) 159-173.
- Bong, S., Nematollahi, B., Nazari, A., Xia, M. and Sanjayan, J., Fresh and hardened properties of 3D printable geopolymers cured in ambient temperature, *RILEM International Conference on Concrete and Digital Fabrication* (p. 3-11), Springer, **2018**.
- Bong, S.H., Xia, M., Nematollahi, B. and Shi, C., Ambient temperature cured ‘just-add-water’geopolymer for 3D concrete printing applications, *Cement and Concrete Composites*, 121 (**2021**) 104060.
- Bos, F., Wolfs, R., Ahmed, Z. and Salet, T., Additive manufacturing of concrete in construction: potentials and challenges of 3D concrete printing, *Virtual Physical Prototyping*, 11 (**2016**) 209-225.
- Bosscher, P., Williams, R.L., Bryson, L.S. and Castro-Lacouture, D., Cable-suspended robotic contour crafting system, *Automation in Construction*, 17 (**2007**) 45-55.

- Buswell, R.A., Leal de Silva, W.R., Jones, S.Z. and Dirrenberger, J., 3D printing using concrete extrusion: a roadmap for research, *Cement and Concrete Research*, 112 (2018) 37-49.
- Buswell, R.A., Thorpe, A., Soar, R.C. and Gibb, A.G.F., Design data and process issues for mega-scale rapid manufacturing machines used for construction, *Automation in Construction*, 17 (2008) 923–929.
- Buswell, R.A., Soar, R., Gibb, A.G.F. and Thorpe, A., Freeform Construction: Mega-Scale Rapid Manufacturing for Construction, *Automation in Construction*, 16 (2007) 224–231.
- Cachim, P., Velosa, A. and Ferraz, E., Substitution materials for sustainable concrete production in Portugal, *The KSCE Journal of Civil Engineering*, (2013) 60-66.
- Chanh, N.V., Trung, B.D. and Tuan, D.V., Recent research geopolymers concrete. The 3rd ACF International Conference-ACF/VCA, HoChiMinh, (2008).
- Chen, Y., Jansen, K., Zhang, H., Rodriguez, C.R., Gan, Y., Çopuroğlu, O. and Schlangen, E., Effect of printing parameters on interlayer bond strength of 3D printed limestone-calcined clay-based cementitious materials: An experimental and numerical study, *Construction and Building Materials*, 262 (2020) 120094.
- Chougan, M., Ghaffar, S.H., Jahanzat, M., Albar, A., Mujaddedi, N. and Swash, R., The influence of nano-additives in strengthening mechanical performance of 3D printed multi-binder geopolymer composites, *Construction and Building Materials*, 250 (2020) 118928.
- Chougan, M., Ghaffar, S.H., Sikora, P., Chung, S.Y., Rucinska, T., Stephan, D., Albar, A. and Swash, M.R., Investigation of additive incorporation on rheological, microstructural and mechanical properties of 3D printable alkali-activated materials, *Materials and Design*, 202 (2021) 109574.
- Chu, S.H., Li, L.G. and Kwan, A.K.H., Development of extrudable high strength fiber reinforced concrete incorporating nano calcium carbonate, *Additive Manufacturing*, 37 (2021) 101617.
- Corinaldesi, V., Mechanical behavior of masonry assemblages manufactured with recycled-aggregate mortars, *Cement and Concrete Composites*, 31 (2009) 505-510.
- Dadsetan, S., Siad, H., Lachemi, M. and Sahmaran, M., Construction and demolition waste in geopolymer concrete technology: a review, *Magazine of Concrete Research*, 71 (2019) 1232-1252.
- Davidovits, J., Geopolymers: inorganic polymeric new materials, *Journal of Materials Education*, 16 (1994), 91-139.
- Demiral, N.C., Ekinçi, M.O., Sahin, O., Ilcan, H., Kul, A., Yildirim, G. and Sahmaran, M., Mechanical anisotropy evaluation and bonding properties of 3D-printable construction

- and demolition waste-based geopolymer mortars, *Cement and Concrete Composites*, 134 (2022) 104814.
- Ding, T., Xiao, J. and Mechtcherine, V., Microstructure and mechanical properties of interlayer regions in extrusion-based 3D printed concrete: A critical review, *Cement and Concrete Composites*, 141 (2023) 105154
- Ding, T., Xiao, J., Zou, S. and Zhou, X., Anisotropic behavior in bending of 3D printed concrete reinforced with fibers, *Composite Structures*, 254 (2020) 112808
- Dizhur, D. and Ingham, J.M., Diagonal tension strength of vintage unreinforced clay brick masonry wall panels, *Construction and Building Materials*, 43 (2013) 418-427.
- Duan H., Miller T.R., Liu G. and Tam, V.W.Y., Construction debris becomes growing concerns of growing cities, *Waste Management*, 83 (2019) 1-5.
- Federowicz, K., Kaszyńska, M., Zieliński, A. and Hoffmann, M., Effect of curing methods on shrinkage development in 3D-printed concrete, *Materials*, 13 (2020).
- Feng, P., Meng, X., Chen, J.-F. and Ye, L., Mechanical properties of structures 3D printed with cementitious powders, *Construction and Building Materials*, 93 (2015) 486–497.
- Figliola, B., Brudny, K., Lin, W.T. and Korniejenko, K., Investigation of Mechanical Properties and Microstructure of Construction- and Demolition-Waste-Based Geopolymers, *Journal of Composites Sciences*, 6(7) (2022) 191.
- Gonçalves Rapazote, J., Laginhas, C. and Teixeira-Pinto, A., Development of building materials through alkaline activation of construction and demolition waste (CDW)-Resistance to acid attack, In *Advances in Science and Technology*, 69 (2010) 156-163.
- Gosselin, C., Duballet, R., Roux, P., Gaudilliere, N., Dirrenberger, J. and Morel, P., Large-scale 3D printing of ultra-high performance concrete - a new processing route for architects and builders, *Materials and Design*, 100 (2016) 102-109.
- Grampeix, G., Roussel, N. and Dupoirier, J., Internal vibration and viscous concrete: application and prediction of the radius of action, *Rheology and processing of construction materials. RILEM Proceedings PRO*, 2013, pp.123-130.
- Helsel, M.A., Popovics, J.S., Stynoski, P.B. and Kreiger, E., Non-destructive testing to characterize interlayer bonds of idealized concrete additive manufacturing products, *NDT and E International*, 121 (2021) 102443.
- Huang, X., Yang, W., Song, F. and Zou, J., Study on the mechanical properties of 3D printing concrete layers and the mechanism of influence of printing parameters, *Construction and Building Materials*, 335 (2022).
- Hwang, C.L., Yehualaw, M.D., Vo, D.H. and Huynh, T.P., Development of high-strength alkali-activated pastes containing high volumes of waste brick and ceramic powders, *Construction and Building Materials*, 218 (2019) 519-529.

- Ilcan, H., Şahin, O., Kul, A., Yıldırım, G., Özçelikçi, E. and Şahmaran, M., Rheological property and extrudability performance assessment of construction and demolition waste-based geopolymer mortars with varied testing protocols, *Cement and Concrete Composites*, 136 (2023) 104891.
- Ilcan, H., Şahin, O., Kul, A., Yıldırım, G. and Şahmaran, M., Rheological properties and compressive strength of construction and demolition waste-based geopolymer mortars for 3D-Printing, *Construction and Building Materials*, 328 (2022) 127114.
- Jianchao, Z., Zhang, T., Faried, M. and Wengang, C., 3D printing cement based ink, and it's application within the construction industry, in: *MATEC Web of Conferences*, 120-02003, EDP Sciences, 2017.
- Kahramanmaraş and Hatay Eartquake's Report, Republic of Türkiye Strategy and Budget Presidency, (2023).
- Kashani, A. and Ngo, T.D., Optimisation of mixture properties for 3D printing of geopolymer concrete, 2018 Proceedings of the 35th International Symposium on Automation and Robotics in Construction, July 20-25, Berlin, 2018.
- Kazemian, A., Yuan, X., Cochran, E. and Khoshnevis, B., Cementitious materials for construction-scale 3D printing: laboratory testing of fresh printing mixture, *Construction and Building Materials*, 145 (2017) 639–647.
- Keita, E., Bessaies-Bey, H., Zuo, W., Belin, P. and Roussel, N., Weak bond strength between successive layers in extrusion-based additive manufacturing: measurement and physical origin, *Cement and Concrete Research*, 123 (2019) 105787.
- Khan, S.A., Jassim, M., Ilcan, H., Sahin, O., Bayer, İ.R., Sahmaran, M. and Koc, M., 3D printing of circular materials: Comparative environmental analysis of materials and construction techniques, *Case Studies in Construction Materials*, 18 (2023a) e02059.
- Khan, S.A., Ilcan, H., Aminipour, E., Sahin, O., Rashid, A.A., Sahmaran, M. and Koc, M., Buildability analysis on effect of structural design in 3D concrete printing (3DCP): An experimental and numerical study, *Case Studies in Construction Materials*, 19 (2023b) e02295.
- Khater, H.M., Effect of calcium on geopolymerization of aluminosilicate wastes, *Journal of materials in civil engineering*, 24(1) (2012) 92-101.
- Khater, H.M., El Nagar, A.M. and Ezzat, M., Optimization of alkali activated grog/ceramic wastes geopolymer bricks, *Optimization*, 5(1) (2016).
- Khoshnevis, B., Automated construction by contour crafting-related robotics and information technologies, *Automation in Construction*, 13 (2004) 5–19.
- Kim, Y.J. and Choi, Y.W., Utilization of waste concrete powder as a substitution material for cement, *Construction and Building Materials*, 30 (2012) 500-504.
- Kloft, H., Krauss, H-W., Hack, N., Herrmann, E., Neudecker, S., Varady, P.A. and Lowke, D., Influence of process parameters on the interlayer bond strength of concrete

elements additive manufactured by Shotcrete 3D Printing (SC3DP), *Cement and Concrete Research*, 134 (2020) 106078.

- Komnitsas, K., Zaharaki, D., Vlachou, A., Bartzas, G. and Galetakis, M., Effect of synthesis parameters on the quality of construction and demolition wastes (CDW) geopolymers, *Advanced Powder Technology*, 26 (2) (2015) 368-376.
- Labonnote, N., Rønquist, A., Manum, B. and Rüter, P., Additive construction: state-of-the-art, challenges and opportunities - a review, *Automation in Construction*, 72 (2016) 347–366.
- Lan, G., Wang, Y., Xin, L. and Liu, Y., Shear test method analysis of earth block masonry mortar joints, *Construction and Building Materials*, 264 (2020) 119997.
- Le, T.T., Austin, S.A., Lim, S., Buswell, R.A., Law, R., Gibb, A.G.F. and Thorpe, T., Hardened properties of high-performance printing concrete, *Cement and Concrete Research*, 42(3) (2012) 558-566.
- Lee, H., Kim, J-H. J., Moon, J-H., Kim, W-W. and Seo, E-A., Evaluation of the Mechanical Properties of a 3D-Printed Mortar, *Materials* 12(24) (2019).
- Lim, J.H., Panda, B. and Pham, Q.C., Improving flexural characteristics of 3D printed geopolymer composites with in-process steel cable reinforcement, *Construction and Building Materials*, 178 (2018) 37-41.
- Lim, S., Buswell, R.A., Le, T.T., Austin, S.A., Gibb, A.G.F. and Thorpe, T., Developments in construction-scale additive manufacturing processes, *Automation in Construction*, 21 (2012) 262-268.
- Liu, Z., Wang, Z., Wang, L. and Zhao, X., Interlayer bond strength of 3D printing cement paste by cross-bonded method, *Journal of Chinese Ceramic Society*, 47 (2019) 648–652.
- Lloret, E., Shahab, A.R., Linus, M., Flatt, R.J., Gramazio, F., Kohler, M. and Langenberg, S., Complex concrete structures: Merging existing casting techniques with digital fabrication, *CAD Computer Aided Design*, 60 (2015) 40-49.
- Lu, B., Weng, Y.W., Li, M.Y., Qian, Y., Leong, K.F., Tan, M.J. and Qian, S.Z., A systematical review of 3D printable cementitious materials, *Construction and Building Materials*, 207 (2019) 477-490.
- Ma, G., Wang, L. and Ju, Y., State-of-the-art of 3D printing technology of cementitious material-an emerging technique for construction, *Science China Technological Science*, 61 (2018) 475-495.
- Ma, G., Li, Z., Wang, L., Wang, F. and Sanjayan, J., Mechanical anisotropy of aligned fiber reinforced composite for extrusion-based 3D printing, *Construction and Building Materials*, 202 (2019) 770–783.

- Ma, G., Salman, N.M., Wang, L. and Wang, F., A novel additive mortar leveraging internal curing for enhancing interlayer bonding of cementitious composite for 3D printing, *Construction and Building Materials*, 244 (2020) 118305.
- Madloul, N., Saidur, R., Hossain, M. and Rahim, N., A critical review on energy use and savings in the cement industries, *Renewable and Sustainable Energy Reviews*, (2011) 2042-2060.
- Marchment, T., Sanjayan, J. and Xia, M., Method of enhancing interlayer bond strength in construction scale 3D printing with mortar by effective bond area amplification, *Materials and Design*, 169 (2019) 107684.
- Maskuriy, R., Selamat, A., Maresova, P., Krejcar, O. and David, O.O., Industry 4.0 for the construction industry: Review of management perspective, *Economies*, 7 (3) (2019).
- McKelvey, D., Sivakumar, V., Bell, A. and McLaverty, G., Shear strength of recycled construction materials intended for use in vibro ground improvement, *Ground Improvement*, 6 (2002) 59-68.
- Mir, N., Khan, S.A., Kul, A., Sahin, O., Sahmaran, M. and Koç, M., Construction and demolition waste-based geopolymers for built-environment: An environmental sustainability assessment, *Proceedings*, 70 (2022a) 358-362.
- Mir, N., Khan, S.A., Kul, A., Sahin, O., Sahmaran, M. and Koç, M., Life cycle assessment of construction and demolition waste-based geopolymers suited for use in 3-dimensional additive manufacturing, *Cleaner Engineering and Technology*, 10 (2022b) 100553.
- Mir, N., Khan, S.A., Kul, A., Sahin, O., Ozcelikli E., Sahmaran, M. and Koc, M., Construction and demolition waste-based self-healing geopolymer composites for the built environment: An environmental profile assessment and optimization, *Construction and Building Materials*, 369 (2023) 130520.
- Moelich, G.M., Kruger, J. and Combrinck, R., Plastic shrinkage cracking in 3D printed concrete, *Composites Part B: Engineering*, 200 (2020) 108313.
- Mohammad, M., Masad, E. and Al-Ghamdi S.G., 3d concrete printing sustainability: A comparative life cycle assessment of four construction method scenarios, *Buildings*, 10 (12) (2020).
- Momayez, A., Ehsani, M.R., Ramezaniyanpour, A.A. and Rajaie, H., Comparison of methods for evaluating bond strength between concrete substrate and repair materials, *Cement and Concrete Research*, 35 (2005) 748-757.
- Monteiro, P.J.M., Miller, S.A. and Horvath, A., Towards sustainable concrete, *Nature Materials*, 16 (2017) 698–699.
- Moini, M., Buildability and Mechanical Performance of Architected Cement-Based Materials Fabricated Using a Direct-Ink-Writing Process, PhD Thesis, Princeton University, 2020.

- Moini, R., Baghaie, A., Rodriguez, F.B., Zavattieri, P.D., Youngblood, J.P. and Olek, J., Quantitative microstructural investigation of 3D-printed and cast cement pastes using micro-computed tomography and image analysis, *Cement and Concrete Research*, 147 (2021) 106493.
- Munir, Q., Afshariantorghabeh, S. and Karki, T., Industrial Waste Pretreatment Approach for 3D Printing of Sustainable Building Materials, *Urban Science*, 6(3) (2022) 50.
- Murcia, D.H., Genedy, M. and Taha, M.M.R., Examining the significance of infill printing pattern on the anisotropy of 3D printed concrete, *Construction and Building Materials*, 262 (2020) 120559.
- Mustafa, M., Bakri, A., Mohammed, H., Kamarudin, H., Niza, I.K. and Zarina, Y., Review on fly ash-based geopolymer concrete without Portland Cement, *Journal of Engineering and Technology Research*, 3 (2011) 1-4.
- Muthukrishnan, S., Ramakrishnan, S. and Sanjayan, J., Effect of alkali reactions on the rheology of one-part 3D printable geopolymer concrete, *Cement and Concrete Composites*, 116 (2021) 103899.
- Muthukrishnan, S., Ramakrishnan, S. and Sanjayan, J., Effect of microwave heating on interlayer bonding and buildability of geopolymer 3D concrete printing, *Construction and Building Materials*, 265 (2020) 120786.
- Nagapan, S., Abdul Rahman, I. and Asmi, A., Factors Contributing to Physical and Non-Physical Waste Generation in Construction Industry, *International Journal of Advances in Applied Sciences*, 1 (2012) 1-10.
- Nematollahi, B., Xia, M., Bong, S.H. and Sanjayan J., Hardened properties of 3D printable ‘One-Part’ Geopolymer for construction applications, in: *RILEM Bookseries*, 190-199, 2019a.
- Nematollahi, B., Xia, M., Vijay, P. and Sanjayan, J.G., Properties of Extrusion-Based 3D Printable Geopolymers for Digital Construction Applications, *3D Concrete Printing Technology*, Sanjayan, J.G., Nazari, A., Nematollahi, B., (Eds.), Elsevier, 371-388, 2019b.
- Nematollahi, B., Vijay, P., Sanjayan, J., Nazari, A., Xia, M., Nerella, V.N. and Mechtcherine, V., Effect of polypropylene fibre addition on properties of geopolymers made by 3D printing for digital construction, *Materials*, 11(12) (2018a) 2352.
- Nematollahi, B., Xia, M., Bong, S.H. and Sanjayan, J., Hardened properties of 3D printable ‘one-part’geopolymer for construction applications. In *RILEM International Conference on Concrete and Digital Fabrication*. Springer, Cham, (2018b) 190-199.
- Nematollahi, B., Xia, M., Sanjayan, J. and Vijay, P., Effect of type of fiber on inter-layer bond and flexural strengths of extrusion-based 3D printed geopolymer, In *Materials science forum*. Trans Tech Publications Ltd., 939 (2018c) 155-162.

- Nerella, V.N., Hempel, S. and Mechtcherine, V., Effects of layer-interface properties on mechanical performance of concrete elements produced by extrusion-based 3D-printing, *Construction and Building Materials*, 205 (2019) 586-601.
- Nuaklong, P., Jongvivatsakul, P., Pothisiri, T., Sata, V. and Chindapasirt, P., Influence of rice husk ash on mechanical properties and fire resistance of recycled aggregate high-calcium fly ash geopolymer concrete, *Journal of Cleaner Production*, 252(5) (2019).
- Ouda, A.S. and Gharieb, M., Development the properties of brick geopolymer pastes using concrete waste incorporating dolomite aggregate, *Journal of Building Engineering*, 27 (2020) 100919.
- Özçelikçi, E., Kul, A., Günal, M.F., Özel B.F., Yıldırım, G., Ashour, A. and Şahmaran, M., A comprehensive study on the compressive strength, durability-related parameters and microstructure of geopolymer mortars based on mixed construction and demolition waste, *Journal of Cleaner Production*, 396 (2023) 136522.
- Özkılıç, H., Ilcan H., Aminipour, E., Tuğluca, M.S., Aldemir, A. and Şahmaran, M., Bond properties and anisotropy performance of 3D-printed construction and demolition waste-based geopolymers: Effect of operational- and material-oriented parameters, *Journal of Building Engineering*, 78 (2023) 107688.
- Pan, T., Jiang, Y., He, H., Wang, Y. and Yin, K., Effect of Structural Build-Up on Interlayer Bond Strength of 3D Printed Cement Mortars, *Materials*, 14 (2) (2021).
- Panda, B., Mohamed, N.A.N. and Tan, M.J., Effect of 3d printing on mechanical properties of fly ash-based inorganic geopolymer, *International Congress on Polymers in Concrete (ICPIC 2018)*, Springer, Cham, (2018) 509-515.
- Panda, B., Paul, S., Mohamed, N.A.N., Tay, Y. and Tan, M.J., Measurement of tensile bond strength of 3D printed geopolymer mortar, *Measurement*, 113 (2018a) 108-116.
- Panda, B., Mohamed, N.A.N., Tay, Y.W.D. and Tan, M.J., Bond strength in 3D printed geopolymer mortar. In *RILEM International Conference on Concrete and Digital Fabrication*, Springer, Cham, (2018b), 200-206.
- Panda, B., Mohamed, N.A.N., Paul, S.C., Singh, G.V.P.B., Tan, M.J. and Šavija B., The effect of material fresh properties and process parameters on buildability and interlayer adhesion of 3D printed concrete, *Materials*, 12 (13) (2019a) 2149.
- Panda, B., Unluer, C. and Tan, M.J., Extrusion and rheology characterization of geopolymer nanocomposites used in 3D printing, *Composites Part B: Engineering*, 176 (2019) 107290.
- Panda, B., Singh, G., Unluer, C. and Tan, M.J., Synthesis and characterization of one-part geopolymers for extrusion based 3D concrete printing, *Journal of Cleaner Production*, 220 (2019b) 610-619.

- Panda, B., Unluer, C. and Tan, M.J., Investigation of the rheology and strength of geopolymer mixtures for extrusion-based 3D printing, *Cement and Concrete Composites*, 94 (2018) 307-314.
- Panda, B. and Tan, M.J., Experimental study on mix proportion and fresh properties of fly ash based geopolymer for 3D concrete printing, *Ceramics International*, 44 (2018) 10258-10265.
- Panda, B., Paul, S.C., Hui, L.J., Tay, Y.W.D. and Tan, M.J., Additive manufacturing of geopolymer for sustainable built environment, *Journal of Cleaner Production*, 167 (2017) 281-288.
- Panda, B., Paul, S.C. and Tan, M.J., Anisotropic mechanical performance of 3D printed fiber reinforced sustainable construction material, *Materials Letters*, 209 (2017) 146-149.
- Papachristoforou, M., Mitsopoulos, V. and Stefanidou, M., Evaluation of workability parameters in 3D printing concrete, *Procedia Structural Integrity*, 10 (2018) 155-162.
- Pham, L., Tran, P. and Sanjayan, J., Steel fibres reinforced 3D printed concrete: Influence of fibre sizes on mechanical performance, *Construction and Building Materials*, 250 (2020) 118785.
- Plessis, A., Babafemi, A.J., Paul, S.C., Panda, B., Tran, J.P. and Broeckhoven, C., Biomimicry for 3D concrete printing: A review and perspective, *Additive Manufacturing*, 38 (2021) 101823
- Provis, J. and Deventer, J.V. (Eds), *Alkali Activated Materials, State of the art report, RILEM TC 224-AA*, Springer, 2014.
- Rahul, A.V., Santhanam, M., Meena, H. and Ghani, Z., 3D printable concrete: mixture design and test methods, *Cement and Concrete Composites*, 97 (2019a) 13-23.
- Rahul, A.V., Santhanam, M., Meena, H. and Ghani, Z., Mechanical characterization of 3D printable concrete, *Construction and Building Materials*, 227 (2019b) 116710.
- Rehman, A.U. and Kim, J.H., 3D concrete printing: A systematic review of rheology, mix designs, mechanical, microstructural, and durability characteristics, *Materials*, 14 (14) (2021) 3800.
- Reig, L., Tashima, M.M., Borrachero, M.V., Monzó, J., Cheeseman, C.R. and Payá, J., Properties and microstructure of alkali-activated red clay brick waste, *Construction and Building Materials*, 43 (2013a) 98-106.
- Reig, L., Tashima, M., Soriano, L., Borrachero, M.V., Monzó, J. and Payá, J., Alkaline activation of ceramic waste materials, *Waste Biomass Valoriz*, 4(4) (2013b) 729-736.
- Robayo-Salazar, R, Gutiérrez, R.M., Villaquirán-Caicedo, M.A. and Arjona, S.D., 3D printing with cementitious materials: Challenges and opportunities for the construction sector, *Automation in Construction*, 146 (2023) 104693.

- Robayo-Salazar, R.A., Rivera, J.F. and Gutiérrez, R.M., Alkali-activated building materials made with recycled construction and demolition wastes, *Construction and Building Materials*, 149 (2017) 130-138.
- Roussel, N., Rheological requirements for printable concretes, *Cement and Concrete Research*, 112 (2018) 76-85.
- Roussel, N. and Cussigh, F., Distinct-layer casting of SCC: the mechanical consequences of thixotropy, *Cement and Concrete Research*, 38 (2008) 624–632.
- Rovnaník, P., Rovnanikova, P., Vyšvařil, M., Grzeszczyk, S. and Janowska-Renkas, E., Rheological properties and microstructure of binary waste red brick powder/metakaolin geopolymer, *Construction and Building Materials*, 188 (2018) 924-933.
- Sabir, B.B., Wild, S. and Bai, J., Metakaolin and calcined clays as pozzolans for concrete: a review, *Cement and concrete composites*, 23 (2001) 441-454.
- Sahin, O., Ilcan, H., Ateşli, A., Kul, A., Yıldırım, G. and Şahmaran, M., Construction and demolition waste-based geopolymers suited for use in 3-dimensional additive manufacturing, *Cement and Concrete Composites*, 121 (2021) 104088.
- Sahmaran, M., Al-Emam, M., Yildirim, G., Simsek, Y., Erdem, T. and Lachemi, M., High-early-strength ductile cementitious composites with characteristics of low early-age shrinkage for repair of infrastructures, *Materials and Structures*, (2015) 1389-1403.
- Sanjayan, J.G., Nematollahi, B., Xia, M. and Marchment, T., Effect of surface moisture on inter-layer strength of 3D printed concrete, *Construction and Building Materials*, 172 (2018) 468-475.
- Sata, V., Chindaprasirt, P., Use of construction and demolition waste (CDW) for alkali-activated or geopolymer concrete, *Advances in Construction and Demolition Waste Recycling*, Elsevier, 385-403, 2020.
- Scrivener, K., John, V. and Gartner, E., Eco-efficient cements: potential economically viable solutions for a low-CO₂ cement-based materials industry, *Cement and Concrete Research*, 114 (2018) 2-26.
- Sedira, N., Castro-Gomes, J. and Magrinho, M., Red clay brick and tungsten mining waste-based alkali-activated binder: Microstructural and mechanical properties, *Construction and Building Materials*, 190 (2018) 1034-1048.
- She, W., Zhao, G., Cai, D., Jiang, J. and Cao, X., Numerical study on the effect of pore shapes on the thermal behaviors of cellular concrete, *Construction and Building Materials*, 163 (2018) 113–121.
- Silfwerbrand, J., Shear bond strength in repaired concrete structures, *Materials and Structures*, 36 (2003) 419-424.
- Silva, G., Castañeda, D., Kim, S., Castañeda, A., Bertolotti, B., Ortega-San-Martin, L., Nakamatsu, J. and Aguilar, R., Analysis of the production conditions of geopolymer

matrices from natural pozzolana and fired clay brick wastes, *Construction and Building Materials*, 215 (2019) 633-643.

- Sun, Z., Cui, H., An, H., Tao, D., Xu, Y., Zhai, J. and Li, Q., Synthesis and thermal behavior of geopolymer-type material from waste ceramic, *Construction and Building Materials*, 49 (2013) 281-287.
- Tan, J., Cizer, Ö., De Vlieger, J., Dan, H. and Li, J., Impacts of milling duration on construction and demolition waste (CDW) based precursor and resulting geopolymer: Reactivity, geopolymerization and sustainability, *Resources, Conservation and Recycling*, 184 (2022) 106433.
- Tay, Y.W.D., Ting, G.H.A., Qian, Y., Panda, B., He, L. and Tan, M.J., Time gap effect on bond strength of 3D-printed concrete, *Virtual and Physical Prototyping*, 14 (1) (2019) 104-113.
- Temuujin, J.V., Van Riessen, A. and Williams, R., Influence of calcium compounds on the mechanical properties of fly ash geopolymer pastes, *Journal of hazardous materials*, 167 (1-3) (2009) 82-88.
- Torres-Carrasco, M. and Puertas, F., Waste glass in the geopolymer preparation, Mechanical and microstructural characterisation, *Journal of Cleaner Production*, 90 (2015) 397-408.
- Tschegg, E.K. and Stanzl, S.E., Adhesive power measurements of bonds between old and new concrete, *Journal of Materials Science*, 26 (1991) 5189-5194.
- TS EN 1052-3/A1:2008, Methods of test for masonry - Part 3: Determination of initial shear strength, Turkish Standards Institution, 2008.
- Ulugol, H., Kul, A., Yıldırım, G., Sahmaran, M., Aldemir, A., Figueira, D. and Ashour, A., Mechanical and microstructural characterization of geopolymers from assorted construction and demolition waste-based masonry and glass, *Journal of Cleaner Production*, 280 (2021) 124358.
- United Nations Environment Programme, Global Alliance for Building and Construction 2020-2050, Paris (2020)
- Vafaei, M. and Allahverdi, A., Durability of geopolymer mortar based on waste-glass powder and calcium aluminate cement in acid solutions, *Journal of Materials in Civil Engineering*, 29 (10) (2017a) 04017196.
- Vafaei, M. and Allahverdi, A., High strength geopolymer binder based on waste-glass powder, *Advanced Powder Technology*, 28 (1) (2017b) 215-222.
- Valencia-Saavedra, W., Robayo-Salazar, R. and Mejía de Gutiérrez, R., Alkali-activated hybrid cements based on Fly ash and construction and demolition wastes using sodium sulfate and sodium carbonate, *Molecules*, 26 (2021) 7572.
- Van Damme, H., Concrete material science: past, present, and future innovations, *Cement and Concrete Research*, 112 (2018) 5–24.

- Van Den Heever, M., Plessis, A. Du, Kruger, J. and Van Zijl, G., Evaluating the effects of porosity on the mechanical properties of extrusion-based 3D printed concrete, *Cement and Concrete Researches*, 153 (2022).
- Van Der Putten, J., De Schutter, G. and Van Tittelboom, K., The effect of print parameters on the (micro) structure of 3D printed cementitious materials, *RILEM Bookseries*, 2019, p. 234-244.
- Van Der Putten, J., Deprez, M., Cnudde, V., De Schutter, G. and Van Tittelboom, K., Microstructural characterization of 3D printed cementitious materials, *Materials*. 12 (18) (2019) 2993.
- Van Jaarsveld, J.G.S., Van Deventer, J.S.J. and Lorenzen, L., The potential use of geopolymeric materials to immobilise toxic metals: Part I. Theory and applications, *Minerals Engineering*, 10 (7) (1997), 659-669.
- Van Jaarsveld, J.G.S., Van Deventer, J.S.J. and Schwartzman, A., The potential use of geopolymeric materials to immobilise toxic metals: Part II. Material and leaching characteristics, *Minerals Engineering*, 12 (1) (1999), 75-91.
- Vásquez, A., Cárdenas, V., Robayo, R.A. and Mejía de Gutiérrez, R., Geopolymer based on concrete demolition waste, *Advanced Powder Technology*, 27 (2016) 1173-1179.
- Vergara, E.C., Aguirregabiria, B.L., Pérez, J.M.L. and Vacarezza, G.O., Innovative free-form glass fiber reinforced concrete (GRC) panel. *Revista de la construcción*, 16 (2017) 479–488.
- Wang, H., Shao, J., Zhang, J., Zou, D. and Sun, X., Bond shear performances and constitutive model of interfaces between vertical and horizontal filaments of 3D printed concrete, *Construction and Building Materials*, 316 (2022) 125819.
- Wang, L., Tian, Z., Ma, G. and Zhang, M., Interlayer bonding improvement of 3D printed concrete with polymer modified mortar: Experiments and molecular dynamics studies, *Cement and Concrete Composites*, 110 (2020) 103571.
- Weng, Y., Li, M., Zhang, D., Tan, M.J. and Qian, S., Investigation of interlayer adhesion of 3D printable cementitious material from the aspect of printing process, *Cement and Concrete Research*, 143 (2021) 106386.
- WASP, Concrete beam created with 3D printing, <http://www.wasproject.it/w/en/concrete-beam-created-with-3d-printing/> (date of access:6th August 2021)
- Wei, J. and Cen, K., Empirical assessing cement CO₂ emissions based on China's economic and social development during 2001–2030, *Science of the Total Environment*, (2019) 200-211.
- Weng, Y., Li, M., Ruan, S., Wong, T.N., Tan, M.J., Ow Yeong, K.L. and Qian, S., Comparative economic, environmental and productivity assessment of a concrete bathroom unit fabricated through 3D printing and a precast approach, *Journal of Cleaner Production*, 261 (2020) 121245.

- Wolfs, R.J.M., Bos, F.P. and Salet, T.A.M., Early age mechanical behaviour of 3D printed concrete: Numerical modelling and experimental testing, *Cement and Concrete Research*, 106 (2019) 103-116.
- Wolfs, R.J.M., Bos, F.P. and Salet, T.A.M., Hardened properties of 3D printed concrete: The influence of process parameters on interlayer adhesion, *Cement and Concrete Research*, 119 (2019) 132–140.
- Wu, H., Zuo, J., Yuan, H., Zillante, G. and Wang, J., A review of performance assessment methods for construction and demolition waste management, *Resources, Conservation and Recycling*, 150 (2019) 104407.
- Wu, Z., Yu, A.T.W. and Shen, L., Investigating the determinants of contractor's construction and demolition waste management behavior in Mainland China, *Waste Management*, 60 (2017) 290-300.
- Xiao, J., Liu, H. and Ding, H., Finite element analysis on the anisotropic behavior of 3D printed concrete under compression and flexure, *Additive Manufacturing*, 39 (2021) 101712.
- Xiao, J., Zou, S., Yu, Y., Wang, Y., Ding, T., Zhu, Y., Yu, J., Li, S., Duan, Z., Wu, Y. and Li, L., 3D recycled mortar printing: System development, process design, material properties and on-site printing, *Journal of Building Engineering*, 32 (2020) 101779.
- Xu, H. and Van Deventer, V., The geopolymerisation of alumino-silicate minerals, *International Journal of Mineral Processing*, 59 (2000) 247,266.
- Xu, Y., Yuan, Q., Li, Z., Shi, C., Wu, Q. and Huang, Y., Correlation of interlayer properties and rheological behaviors of 3DPC with various printing time intervals, *Additive Manufacturing*, 47 (2021) 102327.
- Yıldırım, G., Kul, A., Özçelikci, E., Sahmaran, M., Aldemir, A., Figueira, D. and Ashour, A., Development of alkali-activated binders from recycled mixed masonry-originated waste, *Journal of Building Engineering*, 33 (2021) (101690).
- Ye, J., Cui, C., Yu, J., Yu, K. and Xiao, J., Fresh and anisotropic-mechanical properties of 3D printable ultra-high ductile concrete with crumb rubber, *Composites Part B: Engineering* (2021) 108639.
- Yu, K., McGee, W., Ng, T.Y., Zhu, H. and Li, V.C., 3D-printable engineered cementitious composites (3DP-ECC): Fresh and hardened properties, *Cement and Concrete Research*, 143 (2021) 106388.
- Yu, S., Du, H. and Sanjayan, J., Aggregate-bed 3D concrete printing with cement paste binder, *Cement and Concrete Research*, 136 (2020) 106169.
- Zaharaki, D., Galetakis, M. and Komnitsas, K., Valorization of construction and demolition (C&D) and industrial wastes through alkali activation, *Construction and Building Materials*, 121 (2016) 686-693.

- Zareiyani, B. and Khoshnevis, B., Effects of interlocking on interlayer adhesion and strength of structures in 3D printing of concrete, *Automation in Construction*, 83 (2017a) 212–221.
- Zareiyani, B. and Khoshnevis, B., Interlayer adhesion and strength of structures in contour crafting-effects of aggregate size, extrusion rate, and layer thickness. *Automation in Construction*, 81 (2017b) 112–121.
- Zheng, L., Wu, H., Zhang, H., Duan, H., Wang, J. and Jiang, W., Characterizing the generation and flows of construction and demolition waste in China, *Construction and Building Materials*, (2017) 405-413.
- Zhang, J., Wang, J., Dong, S., Yu, X. and Han, B., A review of the current progress and application of 3D printed concrete, *Composites Part A: Applied Science and Manufacturing*, 125 (2019a) 105533.
- Zhang, Y., Zhang, Y., She, W., Yang, L., Liu, G. and Yang, Y., Rheological and harden properties of the high-thixotropy 3D printing concrete, *Construction and Building Materials*, 201 (2019b) 278–285.
- Zhong, H. and Zhang, M., 3D printing geopolymers: a review, *Cement and Concrete Composites*, 128 (2022) 104455.